Journal of Hazardous Materials 424 (2022) 127612

Contents lists available at ScienceDirect

Journal of Hazardous Materials

journal homepage: www.elsevier.com/locate/jhazmat

Review

# Layered double hydroxide based materials applied in persulfate based advanced oxidation processes: Property, mechanism, application and perspectives

Lin Ge [1], Binbin Shao [1], Qinghua Liang [1], Danlian Huang [1], Zhifeng Liu *, Qingyun He, Ting Wu, Songhao Luo, Yuan Pan, Chenhui Zhao, Jinhui Huang, Yumeng Hu

*College of Environmental Science and Engineering, Hunan University and Key Laboratory of Environmental Biology and Pollution Control (Hunan University), Ministry of Education, Changsha 410082, P.R. China*

ARTICLE INFO

<Editor: Sungjun Bae>

*Keywords:*
Layered double hydroxides (LDHs) catalysts
Persulfate activation mechanism
Advanced oxidation processes (AOPs)
Environmental remediation

ABSTRACT

Recently, persulfate-based advanced oxidation processes (persulfate-AOPs) are booming rapidly due to their promising potential in treating refractory contaminants. As a type of popular two-dimensional material, layered double hydroxides (LDHs) are widely used in energy conversion, medicine, environment remediation and other fields for the advantages of high specific surface area (SSA), good tunability, biocompatibility and facile fabrication. These excellent physicochemical characteristics may enable LDH-based materials to be promising catalysts in persulfate-AOPs. In this work, we make a summary of LDHs and their composites in persulfate-AOPs from different aspects. Firstly, we introduce different structure and important properties of LDH-based materials briefly. Secondly, various LDH-based materials are classified according to the type of foreign materials (metal or carbonaceous materials, mainly). Latterly, we discuss the mechanisms of persulfate activation (including radical pathway and nonradical pathway) by these catalysts in detail, which involve (i) bimetallic synergism for radical generation, (ii) the role of carbonaceous materials in radical generation, (iii) singlet oxygen ($^1O_2$) production and several special nonradical mechanisms. In addition, the catalytic performance of LDH-based catalysts for contaminants are also summarized. Finally, challenges and future prospects of LDH-based composites in environmental remediation are proposed. We expect this review could bring new insights for the development of LDH-based catalyst and exploration of reaction mechanism.

## 1. Introduction

As the rapid progress of modern technologies, abundant chemical products have been manufactured, which greatly improve the living standard of people and promote progress of the society. But in the manufacture process of industrial products, numerous refractory contaminants such as pharmaceuticals, benzene derivatives, organic dyes and resin precursor have been discharged into environment. These contaminants tend to exhibit ecotoxicity, mutagenicity and even carcinogenicity and can cause irreversible damage to both human and the ecosystem (Zhou et al., 2019; Zeng et al., 2018; Lu et al., 2019; Gorini et al., 2020a; Singh et al., 2019). Traditional measures such as adsorption, flocculation and membrane treatment cannot solve the pollution by these contaminants fundamentally (Pan et al., 2020; Dai et al., 2020). Recently, AOPs have raised intensive concerns of researchers because of their great potential for the effective decomposition of refractory pollutants. The activation process of some oxidants like ozone, hydrogen peroxide ($H_2O_2$) and persulfate can generate reactive

---

*Abbreviations:* LDH, layered double hydroxide; AOPs, advanced oxidation processes; persulfate-AOPs, persulfate-based advanced oxidation processes; PMS, peroxymonosulfate; PDS, peroxydisulfate; OER, oxygen evaluation reaction; SSA, specific surface area; LDOs, layered double oxides; UV–vis DRS, UV–vis diffuse reflectance spectra; ATZ, atrazine; rGO, reduced graphene oxide; CNTs, carbon nanotubes; MWCNTs, multi-walled CNTs; ROS, reactive oxygen species; AC, activated carbon; BC, biochar; g-$C_3N_4$, graphitic carbon nitride; EIS, electrochemical impedance spectroscopy; PAN, Polyacrylonitrile; rGA, reduced graphene aerogel; PVDF, polyvinylidene fluoride; SMX, sulfamethoxazole; CIP, ciprofloxacin; TC, tetracycline; CBZ, carbamazepine.

* Corresponding author.

*E-mail address:* zhifengliu@hnu.edu.cn (Z. Liu).

[1] The authors contribute equally to this paper

https://doi.org/10.1016/j.jhazmat.2021.127612
Received 23 July 2021; Received in revised form 6 October 2021; Accepted 24 October 2021

species with strong oxidation capacity, which can effectively degrade refractory contaminants into small molecule substances with low toxicity or even the nontoxic $CO_2$ and $H_2O$ (M'Arimi et al., 2020; W. Wang et al., 2021; J. Wang et al., 2021; Li et al., 2019). Originally, hydrogen peroxide ($H_2O_2$) was selected as the precursor of ·OH to degrade organic contaminants. But $H_2O_2$-AOPs have some intrinsic drawbacks like short life and low selectivity of ·OH, narrow working pH range, and unfriendly cost. In order to overcome limitations of $H_2O_2$, persulfate-AOPs are developed for the following reasons: (i) strong oxidation potential, $E_0(SO_4^{\bullet-}/SO_4^{2-})= 2.6–3.1\ V_{NHE}$ (Oh et al., 2016), (ii) the higher generation rate of radical (Anipsitakis and Dionysiou, 2004; Lee et al., 2020; Zhiyong et al., 2013; Ling et al., 2010), (iii) diverse activation methods for persulfate (Oh et al., 2016; Wang and Wang, 2018), (iv) lower requirements of reaction conditions (Ahn et al., 2016; Luo et al., 2015; Zhang et al., 2016), (v) easy storage and convenient transportation.

Persulfate, including peroxymonosulfate (PMS) and peroxydisulfate (PDS/PS), can be activated by external energy (e.g., thermal, ultraviolet, ultrasound), chemical activator (e.g., alkaline, phenol, quinone), transition metals (both metal ions and heterogeneous catalysts) and carbonaceous materials (such as biochar and graphene oxide) (Chen et al., 2018; Wang and Wang, 2018). Among the aforementioned methods, transition metal-based heterogeneous catalysts are always given attention for satisfying catalytic effectiveness , low cost and easy recyclability. However, single metal catalysts tend to lose their activity due to the ineffective conversion from $M^{(n+1)+}$ to $M^{n+}$. Despite the coupling of different metals can effectively improve this problem (e.g., $CuFe_2O_4$, $CuCo_2O_4$), the toxic metal leaching caused by the unstable crystalline structure has become a huge roadblock to the practical application of these transition metal catalysts (Zhang et al., 2013; Feng et al., 2015). Thus, to meet requirements of actual application, catalysts must simultaneously have enough activation effectiveness, stability, low toxicity, and affordable cost.

LDHs, also known as hydrotalcite-like compounds, are a type of 2D anionic clays with significant features such as resistance to thermal changes and pH variations, tunable interior architecture, high surface area, and great anion-exchange capacity. LDHs have been widely used as supercapacitors (Liu et al., 2017), batteries (Liu et al., 2016), drug carrier (Shahabadi et al., 2019), and catalysts of oxygen evaluation reaction (OER) (Lv et al., 2019). In addition, LDHs were usually employed as effective adsorbent for the elimination of heavy metal (Ma et al., 2016), radioactive element (Guo et al., 2020), and other toxic pollutants in wastewater (Zou et al., 2016). In recent years, as shown in Fig. 1, articles concerning applications of LDHs in persulfate-AOPs have gradually increased in recent years, which indicates the potential of LDHs and their derivatives in persulfate-AOPs have raised the concentration of researchers. LDHs and their derivatives may become a promising activator of persulfate because of the following merits: (i) low cost and simple process of production; (ii) flexible chemical composition. A variety of transition metals and functional anions could be employed to prepare LDHs to enhance the catalytic performance; (iii) favorable fixation effect for toxic metal ions due to stabilized structure of LDHs (Jawad et al., 2015); (iv) diversity of morphology. The morphology of LDHs can be easily altered by calcination and other tailoring methods, which will expose more active sites and provide properties that can improve the catalytic performance (Boccalon et al., 2020; Hong et al., 2020); (v) LDHs can be integrated with catalysts which possess different properties. The synergistic effect between "metal-metal" or "metal-carbon" in composites can significantly improve the redox cycle, reduce metal leaching and strengthen stability (Boccalon et al., 2020; Ma et al., 2020a).

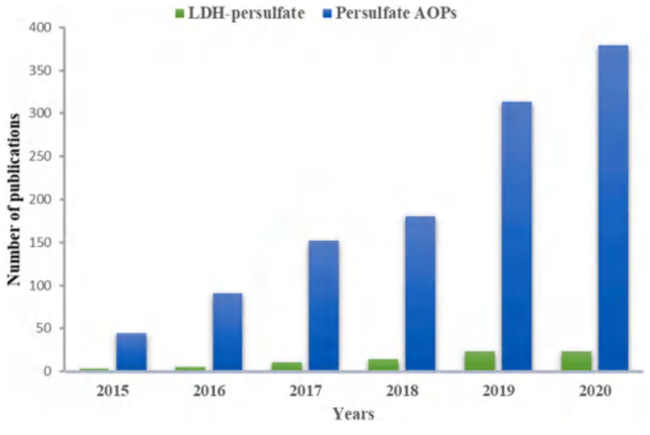

**Fig. 1.** Recent scientific publications using "Layered double hydroxide persulfate", "Persulfate advanced oxidation process" respectively as keywords based on the database to Web of science

Certainly, LDH-based materials seem relatively unpopular in persulfate-AOPs when compared with some "hot materials" such as Fe/Co/Cu/Mn oxides, nano zero-valent iron (nZVI) and biochar. But considering the excellent catalytic performance of LDH-based materials, we can believe that the exploration on them is quite promising despite there are some problems such as agglomeration and slight metal leaching.

Accordingly, it is essential to make a timely review of the latest development of LDH-based catalysts in persulfate-AOPs to help researchers understand the intrinsic relationship between characteristics of LDHs and catalytic performance, realize current challenges and promote further development of LDH-based materials. At present, some reviews tended to discuss the universal mechanism of persulfate activation while ignored the unique properties of LDHs ( Wang and Wang, 2018). Other articles were more concentrated on synthesis, properties and various applications of LDHs but did not focus on persulfate-AOPs (Mallakpour et al., 2020a; Mishra et al., 2018). Among them, few works have paid special attention to application and catalytic mechanism of LDH-based materials in persulfate-AOPs at the same time. Thus, we systematically summarize these catalysts from basic properties, classification and catalytic mechanisms in persulfate-AOPs. At the beginning, synthesis, structure and some important properties of LDHs are introduced. Secondly, we classify LDH-based composites into LDH-metal and LDH-carbonaceous catalysts. The unique advantages of coupling LDHs with different metallic and carbonaceous materials are discussed in this part. Moreover, mechanisms of persulfate activation catalyzed by LDH-based materials are summarized in detail. Finally, four types of representative refractory contaminants are selected to explain the catalytic performance of LDH-based materials in persulfate-AOPs. These contaminants are often used as target pollutants in the degradation experiments because they are widely presented in industrial production and human's daily life. Some challenges as well as future perspectives are also discussed in brief in the end. It is hoped that this review could bring some different perspectives to researchers ploughing in persulfate-AOPs and raise concern to extend the application of LDH-based materials in environmental remediation or wider fields concerning human health.

## 2. Synthesis, structure and important properties of LDHs

LDHs are a kind of ionic lamellar materials composed of positively charged brucite-like layers. There are charge compensating anions and solvation molecules inside the interlayer. The metal cations occupy the centers of edge sharing octahedra, whose vertexes contain hydroxide ions that connect to form 2D plates (Wang and O'Hare, 2012). Generally, the following formula can describe the composition of LDHs:

$$\left[M^{2+}_{1-x}M^{3+}_{x}(OH)_2\right]^{x+}\cdot A^{n-}_{x/n}\cdot mH_2O$$

In this formula, $M^{2+}$ are divalent metals ions (e.g., $Mg^{2+}$, $Zn^{2+}$, $Cu^{2+}$, $Co^{2+}$, etc.) while $M^{3+}$ are trivalent ions (e.g., $Al^{3+}$, $Fe^{3+}$, $Mn^{3+}$, $Cr^{3+}$, etc.). A is an exchangeable interlayer gallery anion (including $CO_3^{2-}$, $NO_3^{2-}$, $Cl^-$, etc.); x refers to the molar ratio of $M^{2+}/(M^{2+}+M^{3+})$ (Mallakpour et al., 2020b).

### 2.1. Synthesis of LDHs

In general, researchers have developed a series of methods to synthesize LDHs with different properties, involving co-precipitation, anion exchange, hydrothermal, reconstruction, calcination, etc. Mishra et al. (2018). Currently, co-precipitation and hydrothermal method are widely used in the synthesis of LDH-based materials due to their facile operation, low cost and reliability (Mallakpour et al., 2020c). In co-precipitation method, an alkaline solution (usually NaOH and $Na_2CO_3$) with guest anions is slowly added to a solution containing metal ions and stirred under the protection of inert gas. Finally, the mixed solution will be thermally aged (60–70 °C) to enhance the crystallinity. In hydrothermal method, metal salts and urea are mixed in an autoclave and heated at high temperature and pressure. LDHs fabricated from this method have highly crystalline morphology than that prepared from co-precipitation (Mallakpour et al., 2020c; Yu et al., 2020). Notably, parameters such as pH, temperature, reaction time can greatly affect the crystallinity, morphology and surface area of LDHs. Thus, it is essential to choose proper synthesis conditions according to the specific situations.

Except for the above-mentioned methods, there are various modification methods which can improve the catalytic performance of pristine LDHs. For instance, the FeMgAl-$MoS_4$ LDH prepared from FeMgAl-$NO_3^-$ LDH via facile ion-exchange method can significantly improve the redox cycle and enhance the degradation performance of contaminants (Ali et al., 2020). In addition, layered double oxides (LDOs), which have larger surface area, uniformly dispersed compositions and more active sites, can be prepared by calcinating LDHs at 450–600 °C (Mallakpour et al., 2020b). Moreover, LDHs can form composites with other catalysts through hydrothermal method, ultrasonic-assisted method, electrostatic self-assembly and so on (Li et al., 2021; Shahzad et al., 2019). At present, efforts are still needed to realize facile, environment-friendly and highly controllable synthesis of LDH-based catalysts. (Fig. 2).

### 2.2. Structure of LDHs

According to different preparation strategies, LDHs can be made into products that have divergent structures (bulk form, exfoliated thin nanosheets and 3D form). The basic structure of LDHs can be depicted by Fig. 3.

#### 2.2.1. Bulk LDHs

Because of the high charge density and numerous interlayer ions, there exist strong electrostatic interactions and hydrogen bonding between laminates, which will lead to aggregation of bulk LDHs (Wang and O'Hare, 2012). This stacking problem can hinder the exposure of active sites and cause low reactivity (Huang et al., 2010).

#### 2.2.2. Exfoliated thin nanosheets

Due to the limitation of bulk LDHs, it is essential to exfoliate LDHs into single nanosheets so as to acquire higher specific surface area as well as expose more active sites (Liu et al., 2017; Yu et al., 2017). When the thickness of catalysts reduces to a molecular size, increased intrinsic electrocatalytic activities and rapid transportation of reactants will be achieved (Wan et al., 2020; Zhang, 2015). Researchers have committed numerous efforts to the synthetic methods of LDH nanosheets. Generally, two-dimensional LDH nanosheets can be prepared by "top-down" and "bottom-up" approaches.

The "top-down" pathway utilizes physical shear force or chemical intercalation to break the interaction between adjacent layers so as to acquire mono- or few-layered nanosheets from bulk LDHs. Generally, "top-down" exfoliation follows two steps: (1) anionic organic guests are intercalated into the gallery to enlarge the interlayer space of LDHs (Fig. 4a), (2) using exfoliation method (e.g., ultrasonication) to acquire delaminated nanosheets (Fig. 4b). In contrast, "bottom-up" method prepares 2D nanofilms through chemical reactions/synthetization (Lu

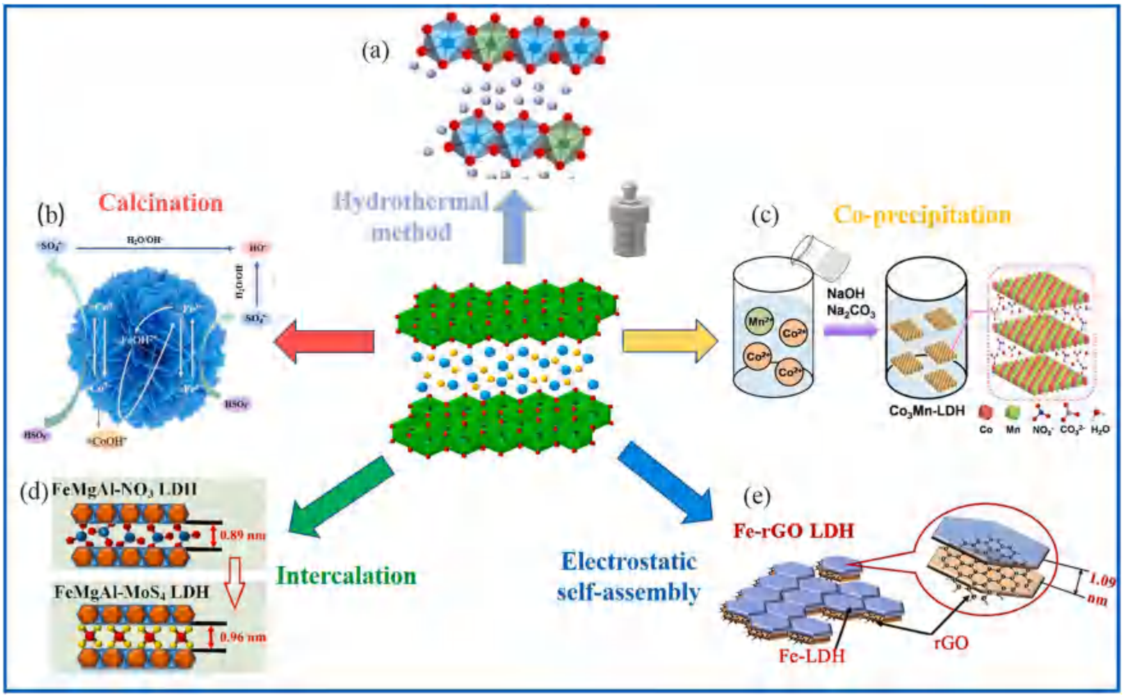

**Fig. 2.** Synthesis methods of LDH-based catalysts for persulfate-AOPs. (a) NiFe-LDH. Reproduced with permission from Yue et al. (2020). Copyright 2020 American Chemical Society. (b) CoMgFe-LDO. Reproduced with permission from Hong et al. (2020). Copyright 2020 Elsevier. (c) CoMn-LDH. Reproduced with permission from He et al. (2021). Copyright 2021 Elsevier. (d) FeMgAl-$MoS_4$-LDH. Reproduced with permission from Ali et al. (2020). Copyright 2020 Elsevier. (e) Fe-rGO LDH. Reproduced with permission from Shahzad et al. (2019). Copyright 2019 Elsevier.

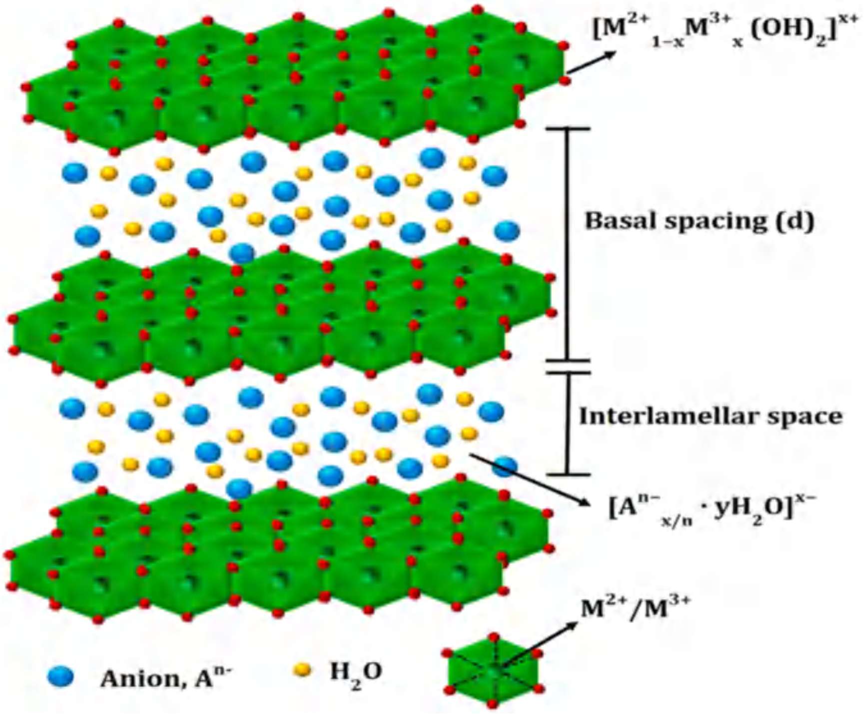

**Fig. 3.** Basic structure of LDHs (Mishra et al., 2018). Copyright 2018 Elsevier.

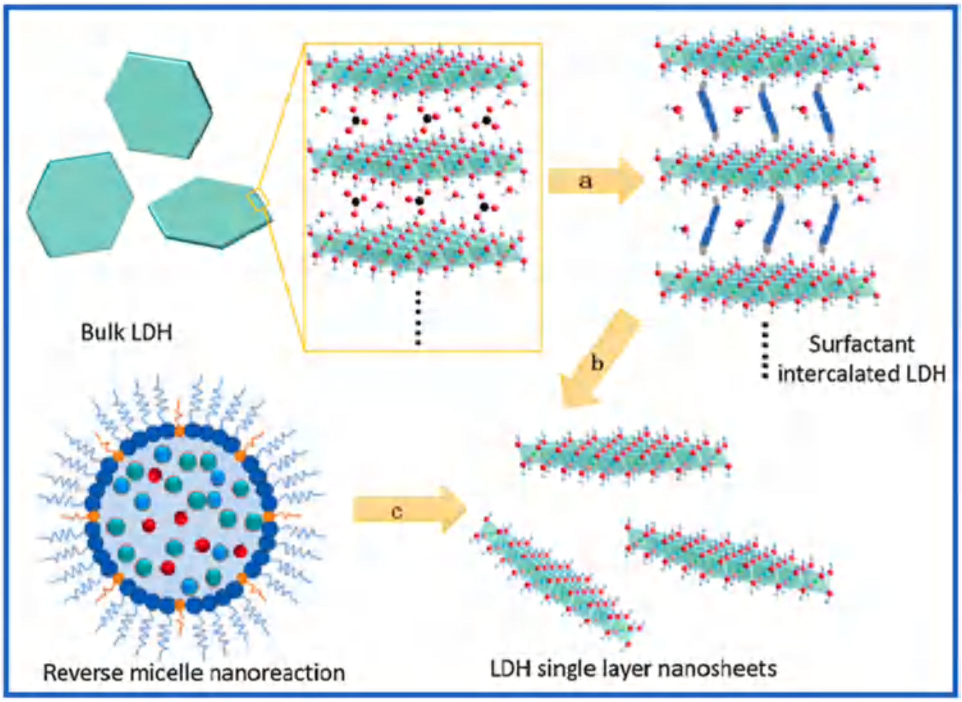

**Fig. 4.** Illustration of (a) anion exchange process; (b) exfoliating LDH into monolayer nanosheets; (c) Synthesis of LDH nanosheets via "bottom-up" method. Reproduced with permission from Long et al. (2016). Copyright 2019 Elsevier.

et al., 2020). By introducing proper precursors as nanoreactor to confine space and nutrients, LDH nanosheets can be synthesized. Previous reviews have discussed them in detail and we don't have to repeat more details (Yu et al., 2017; Chubar et al., 2017). However, the exfoliated LDH nanosheets are mainly applied in supercapacitor and OER. At present, there are few articles reporting the application of exfoliated LDH nanosheets as heterogeneous catalysts in persulfate-AOPs. Even so, LDH nanosheets without exfoliation have shown higher catalytic performance than many conventional catalysts. For instance, the NiFe LDH nanosheets exhibited higher efficiency than most Ni/Fe-based catalysts in PDS activation (Yue et al., 2020). Based on the numerous researches that proving LDH nanosheets could present significantly higher catalytic performance over their bulk counterparts. This difference is derived from the increased active sites and charge conductivity (Song and Hu, 2014). Thus, it is worthwhile to explore the catalytic performance of exfoliated LDH nanosheets in persulfate-AOPs.

### 2.2.3. 3D LDHs

Despite 2D LDHs nanosheets present good performance in different fields, there are still occasions, where a three-dimensional (3D) compound, with its ragged architecture and almost casual particle disposition, can lead to some advantages in terms of material properties and potential applications. The 3D structure can influence aspects like adsorption, diffusion, thermal stability, mechanical resistance, conductivity, and surface capacity (Boccalon et al., 2020). By changing synthetic process, the aggregation form of LDHs nanosheets could be controlled and 3D LDHs could be obtained. At present, the main processes include exfoliation-recombination, in situ growth, and template method.

Exfoliation-recombination usually follows two steps: firstly, peeling LDHs into monolayer nanosheets. Secondly, 3D-LDHs are formed via adjusting the pH of solution or adding electrical materials to make the monolayer attach to the surface of carrier. In situ growth method means that growing 3D-LDHs on the surface of matrix material by co-precipitation of metal cation and anion. This product is capable of maintaining the merits of both LDHs and matrix. The template method is the way to obtain 3D-LDHs by adding templates in the co-precipitation process to control and modify the morphology and structure of LDHs (Jenisha Barnabas et al., 2017; Nagendra et al., 2017; Jabeen et al., 2017; Gao et al., 2020). While retaining characteristics of 2D LDHs, 3D LDHs possess larger SSA and abundant pore structure, which can strengthen their catalytic performance.

The 3D LDHs have displayed great potential in different fields such as energy storage (Zhang et al., 2016), photocatalysis (Liang et al., 2019), biomedicine (Wang et al., 2018), etc. Liang et al. reported that the 3D NiAlFe LDH/rGO realized higher removal efficiency in photodegradation of ciprofloxacin than its 2D counterpart, which might be attributed to the increased active sites provided by the 3D structure (Liang et al., 2019) (Fig. 5c). However, no research has studied the performance of 3D LDHs in persulfate-AOPs. Some researchers reported that the 3D flower-like LDO could have larger SSA and more active sites. This structural change could also strengthen the interaction between persulfate and surface active sites, which is beneficial to persulfate activation (Hong et al., 2020). However, it is not entirely appropriate to discuss the influence of structure on catalytic performance of LDHs through using LDO as example. Because the conversion from LDH to LDO is not only a structural change but also a chemical transformation.

SEM and TEM images of some LDHs with different structures are presented in Fig. 5. Until now, most researchers focus on adjusting the composition of LDHs, or combining LDHs with other materials to enhance the catalytic efficiency in persulfate-AOPs. However, there is no in-depth study on the effect of regulating morphology on the persulfate activation performance of LDHs. Therefore, it is advisable for researchers to develop LDHs with different morphologies and explore the possible different catalytic performance induced by different structure.

## 2.3. Important properties of LDHs

### 2.3.1. Ability of Anion exchange

One important property of LDHs is their excellent anion change ability. Due to the relatively weak electrostatic interaction in layers, it doesn't take much effort to tune the interlayer anions of LDHs (Mishra et al., 2018; Mohapatra and Parida, 2016). The inside anions can simply substitute with the other negatively-charged molecules, and the favorite order of usual and public inorganic anions is as follows (Mallakpour et al., 2020b; Inayat et al., 2011).

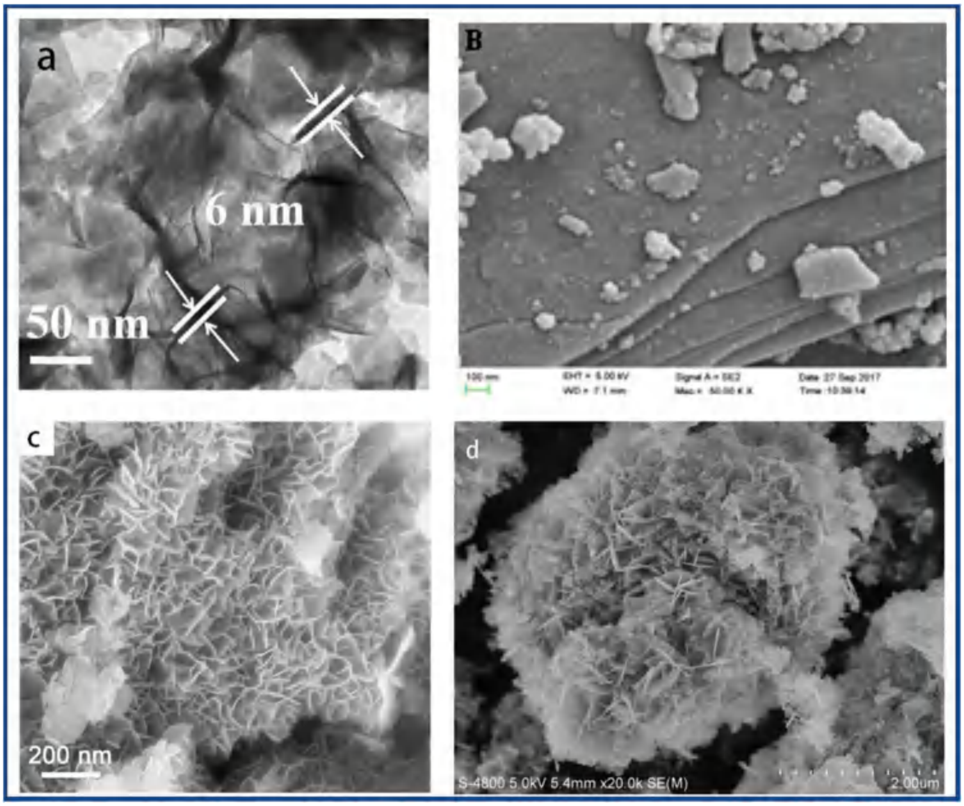

**Fig. 5.** (a) Tem image of NiFe-LDH nanosheets. Reproduced with permission from Yue et al. (2020). Copyright 2020 American Chemical Society. SEM images of (b) Bulk CuFe-LDH. Reproduced with permission from Ma et al. (2018a). Copyright 2018 Elsevier. (c) 3D NiAlFe LDH grown on rGO. Reproduced with permission from Liang et al. (2019). Copyright 2019 Elsevier. (d) Flower-like CuMgFe-LDH. Reproduced with permission from Yan et al. (2017). Copyright 2017 Elsevier.

$$NO_3^- < Br^- < Cl^- < F^- < OH^- < MoO_4^{2-} < SO_4^{2-} < CrO_4^{2-} < HPO_4^{2-} < CO_3^{2-}$$

It is difficult to exchange the $CO_3^{2-}$ because of its strong affinity with layers. In contrast, $NO_3^-$ is the preferable to be employed as a precursor to exchange with other anions (Gillman et al., 2008). Additionally, the general mechanism of anion exchange property can be indicated by the followed equation.

$$LDH.A^{m-} + X^{n-} \rightarrow LDH.X^{n-} + A^{m-} \quad (1)$$

A and X are the host and guest anions with negative charges of m and n, respectively (Rives et al., 2014). There exists the potential for the interlayer space to host additional amounts of aqueous anions, which will make LDHs a good type of anion exchanger (Chubar et al., 2017). Another unique advantage of LDHs is that both the elements of layers and interlayer anions are easily tunable. Besides, we can properly utilize the anion exchange property to synthesize or modify LDHs so as to acquire the ideal materials.

#### 2.3.2. *Thermal stability*

Thermal stability is one of the crucial properties of heterogeneous catalyst. Due to the firm covalent bond and electrostatic interaction, LDHs display thermal stability within a certain temperature range. To be specific, the physically adsorbed $H_2O$ of LDHs will lose when the temperature rises to 170 °C without the change of bulk structure. In addition, a continuous increase in temperature can lead to a series of chemical processes and generate different products (mentioned in next part). When the temperature exceeds 500 ˚C, the structure of LDHs will be destroyed completely and form stable spinels (Valente et al., 2012). The specific temperature range will change according to the type of LDHs and different processing conditions.

#### 2.3.3. *Memory effect*

The so-called “memory effect” means that when heated at high temperatures (450–600 °C), LDHs will lose their water molecules and other organic segments in their structure. As a result, they lose their layer structure and produce the metal oxides, which are known as LDOs (Mallakpour et al., 2020b). The formation of LDOs goes through four stages: dehydration, dehydroxylation, decomposition of anions and oxide reformation (Zou et al., 2017). Interestingly, when immersed in a solution containing anions, these samples will reconstruct their layer structure and produce LDHs again. Encouragingly, it is exactly due to this feature that pure LDHs can be produced (Costa et al., 2008; Deng et al., 2019). LDOs usually have larger SSA and more defects that pristine LDHs, thus exhibit better catalytic performance. However, further calcination (>600 °C) at higher temperature can destroy the structure of LDHs irreversibly and form highly dispersed metal mixed oxides (MMOs) (Zou et al., 2017; Erickson et al., 2005). Of course, not all LDHs possess memory effect. For instance, if the divalent metal ion is $Zn^{2+}$, there is no memory effect in LDHs structure; if the divalent metal ion is $Mg^{2+}$, LDHs generally have memory effect. Besides, impregnation solution, preparing procedure, and calcination temperature are all crucial factors (Hammoud et al., 2015; Rajamathi et al., 2000). Due to the similarity in crystalline structure between LDHs and MMO, it is possible to tune the exposed crystal plane and defect structure of the latter via adjusting the parameters of the topochemical conversion process ( Zhang et al., 2020Zhang et al., 2020).

#### 2.3.4. *Acid-base bifunctionality*

Due to the plentiful hydroxyl groups on the laminates, LDHs usually present alkaline. The alkalinity of different LDHs depends on the type of divalent metal hydroxides (Kagunya et al., 1996). In addition, the alkalinity of LDHs will rise after calcination due to the increased SSA. Certainly, LDHs also have acidity because of the trivalent metal hydroxide and interlayer anions (Kagunya et al., 1996). According to the acid-base bifunctionality, LDHs can be coupled with other materials and form composites with higher catalytic efficiency.

## 3. Composites of LDHs

There exist some problems when pure LDHs act alone: (1) Due to the strong hydrophilicity of LDHs, the removal performance of hydrophobic molecules is not satisfying. (2) When used in water treatment, the powdery LDHs have recovering from the solution. The problems of reusability, as well as the potential secondary pollution cannot be well addressed. (3) It is often unable to achieve high efficiency because of the limitation of a single material. Recently, modification of LDHs has raised great attention of researchers due to the intrinsic drawbacks of pure LDHs. A variety of modified LDHs and LDHs composites have been synthesized for the solvation of problems in actual application.

Substantial explorations about LDH-based materials have been committed to achieving better performance of persulfate activation (Huang et al., 2017). Herein, we will mainly focus on materials which are used for persulfate activation. As for the type of materials, we would like to divide these catalysts into metal/metal oxides introduced LDH composites, LDH-carbon materials and other complex composites.

### 3.1. *Metal/metal oxides introduced LDHs/LDOs*

#### 3.1.1. *LDHs modified by transition metals*

Previous studies have proved transition metal and metal oxides can active the persulfate (Devi et al., 2016; Ghanbari and Moradi, 2017; Hu and Long, 2016; Matzek and Carter, 2016; Wang and Wang, 2018). Transition metals are usually employed as components of cationic laminates of LDHs to activate persulfate. However, the ineffective redox from $M^{(n+1)+}$ to $M^{n+}$ will cause a drop of catalytic performance. The introduction of another transition metal may accelerate the original cycle through electron transfer between different metals (Lu et al., 2019; Wu et al., 2018). Moreover, incorporation of foreign metals can also improve the stability of heterogeneous catalysts, reducing the leaching of toxic metal ions (Zhou et al., 2020). Huang et al. prepared Ni-doped MgAl-LDH for the activation of PDS (Huang et al., 2020a). As shown by the XRD spectra, the diffraction peaks of Ni-LDHs at $2\theta = 10, 21, 35, 38$, and 60° were consistent to that of MgAl-LDH, implying that Ni doping did not affect the structure of LDHs (Fig. 6a). The SEM images also confirmed that the typical polygonal laminate structure of LDH was successfully maintained (Fig. 6b). Under the same PDS dosage, Ni-doped LDH exhibited significantly higher decomposition efficiency towards phenol in comparison with MgAl-LDH. Similarly, the doping of Fe into the Ni-LDH could enlarge the interlayer space and expose more active sites for persulfate activation (Yue et al., 2020) (Fig. 6a). Compared with pristine Ni-LDH, the as-prepared sample could fulfill more efficient degradation of various pollutants.

According to former studies (Liang et al., 2013; Lei et al., 2015a), oxidates as well as compounds of Cu and Co could activate persulfate effectively (Goh et al., 2008; Hong et al., 2019). Unfortunately, the leaching problem hinders the further application of these catalysts. CuMgFe-LDH (Yan et al., 2017), CuCoFe-LDH (Lu et al., 2019), CoFeNi-LDH (Zeng et al., 2018) were successfully synthesized to activate persulfate for contaminants decomposition. Except for the excellent removal efficiency, these modified LDHs could keep a low leaching level of metal ions during catalytic reactions. For one thing, the ample hydroxyl groups could create an alkaline condition, which has an inhibitory effect to leaching of metal ions (Lei et al., 2015b). For another, the firm bond between active sites could also control the migration of toxic ions from LDHs to the solution.

Besides the metal cations, some metallic acid anions can be incorporated into LDHs for enhancing catalytic performance. Fe-based catalysts were widely used in persulfate-AOPs, but the activity of persulfate-AOPs systems will lose gradually due to the inefficient transformation between $Fe^{3+}$ and $Fe^{2+}$. Jawad et al. Ali et al. (2020) developed a stable and effective heterogeneous catalyst by enriching $MoS_4^{2-}$ into the

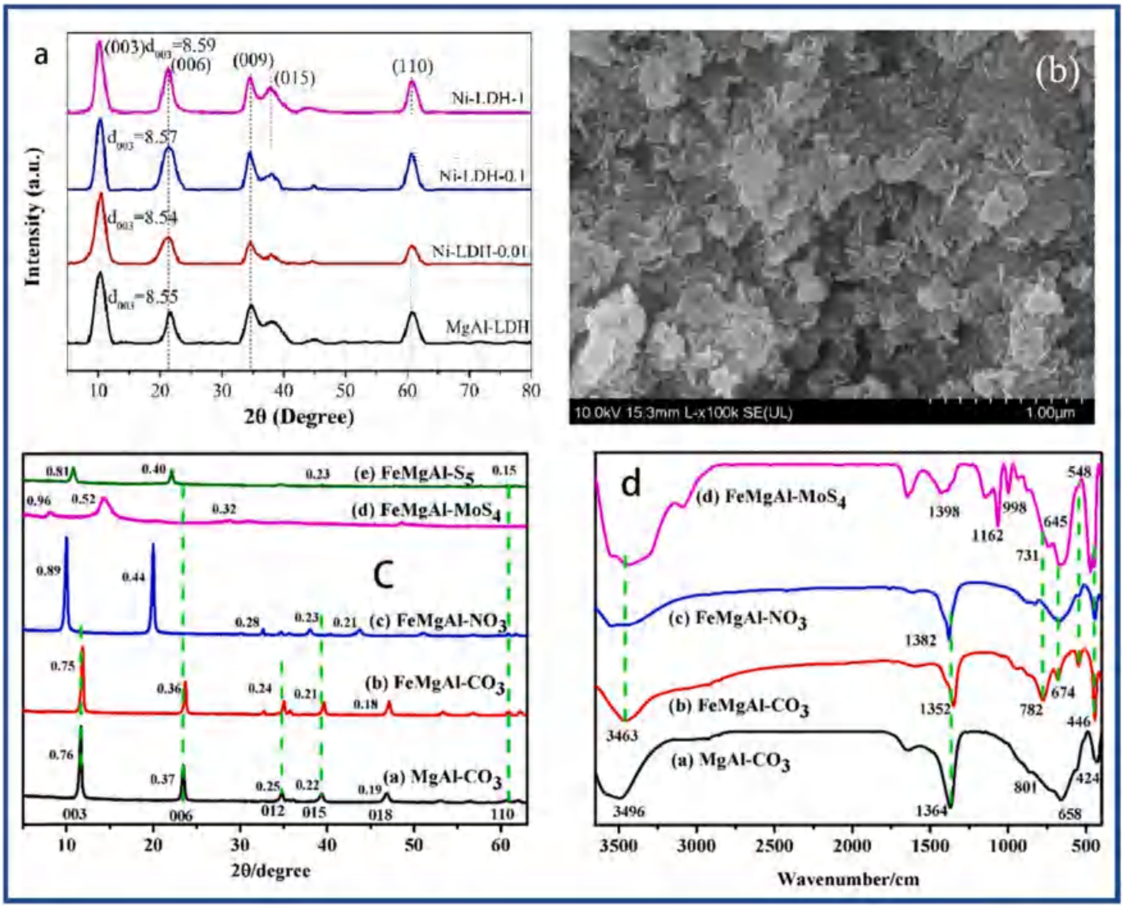

**Fig. 6.** (a) XRD pattern of MgAl-LDH and Ni-MgAl-LDHs. (b) SEM image of Ni-MgAl-LDH. Reproduced from Huang et al. (2020a). Copyright 2020 Elsevier. (c) XRD pattern and (d) FTIR spectrum of FeMgAl-LDH with different intercalated anions. Reproduced from Ali et al. (2020). Copyright 2020 Elsevier.

interlayer of FeMgAl-LDH (Fig. 7b). In order to make comparison, they also synthesized LDHs with different interlayer anions ($CO_3^{2-}$, $NO_3^-$, $S_5^{2-}$). The peak position in the XRD pattern and changes in the d-spacing indicated the successful synthesis of five types of LDHs (Fig. 6c). Furthermore, the shifting band in FTIR also confirmed that $MoS_4^{2-}$ was intercalated into the interlayer of FeMgAl-LDH (Fig. 6d). The obtained material displayed excellent catalytic activity for parahydroxy benzoic acid (PHB) degradation than other nanomaterials as well as co-catalytic systems since the $MoS_4^{2-}$ incorporation improved the "$Fe^{3+}/Fe^{2+}$" cycle greatly.

### 3.1.2. *LDHs combined with metal oxide semiconductors*

Besides the common cycle of "$M^{n+}/M^{n+1}$" for persulfate activation, there are some materials that can be used to produce $SO_4^{\bullet-}$ via photo-Fenton process (Ahmed and Chiron, 2014; Avetta et al., 2015). Former studies have reported photocatalytic activation of persulfate by LDHs (Ma et al., 2018b). But the inefficient transfer and inevitable recombination of "electron-hole" pairs in LDHs have been hindered their practical applications.

If it can be coupled with proper photocatalysts, the catalytic performance of LDHs in persulfate activation will be significantly promoted. $Bi_2O_3$, an attractive photocatalyst which is inexpensive and has favorable band gap ( Liu et al., 2019). However, pure $Bi_2O_3$ material shows relatively unsatisfying photocatalytic performance because of electron-hole recombination. $Bi_2O_3$ particles tend to agglomerate for the high surface energy (Ke et al., 2017; Sun et al., 2014). Luckily, the unique structure of LDHs is capable to facilitate electron transportation and prevent particles from aggregation to some extent (Paredes et al., 2011). Inspired by these studies, Zhang et al. Zhang et al., 2020 synthesized $Bi_2O_3$/CuNiFe LDHs as a PS activator for lomefloxacin (LOM) degradation. TEM and HRTEM founded that substantial $Bi_2O_3$ nanoparticles were distributed on the plane of CuNiFe LDHs (Fig. 8a-8b). $Bi_2O_3$ could firmly couple with CuNiFe LDHs in a unique structure, which may effectively enhance catalytic performance. Moreover, $Bi_2O_3$/CuNiFe LDHs were proved to have large surface area and mesoporous structure which could expose more active sites (compared with $Bi_2O_3$). Furthermore, in comparison with $Bi_2O_3$ and CuNiFe-LDHs, $Bi_2O_3$/CuNiFe LDHs could achieve more efficient visible light (VL) adsorption which implies the potential of the composite in photocatalysis (Fig. 8c). Yang et al. Yang et al., 2021 synthesized a direct Z-scheme $CeO_2$ @LDH heterojunction photocatalyst with a core-shell structure. As shown by TEM images (Fig. 8d-8e), the composite exhibited a three-dimensional structure, which was just like a flower and LDH nanosheets wrapped the $CeO_2$ particles. The results of UV–vis diffuses reflectance spectra (UV–vis DRS) suggested the $CeO_2$ @LDH composite possesses stronger VL adsorption than pristine $CeO_2$ (<500 nm), indicating that LDHs were of great significance in enhancing VL absorption capacity of the $CeO_2$ @LDH nanocomplex (Fig. 8f).

### 3.1.3. *LDOs coupled with transition metals*

In comparison with LDHs, LDOs display excellent properties, like large surface area, abundant active sites, and stable metals dispersion than original LDHs (Zou et al., 2016; Liu et al., 2014; Guo et al., 2018). These merits of LDOs can enhance the interaction of catalysts with persulfate, generating quantities of reactive oxygen species (ROS). Inspired by former works, Hong et al. Hong et al. (2019) synthesized ternary CoMgAl-LDOs with "flower-like" morphology through

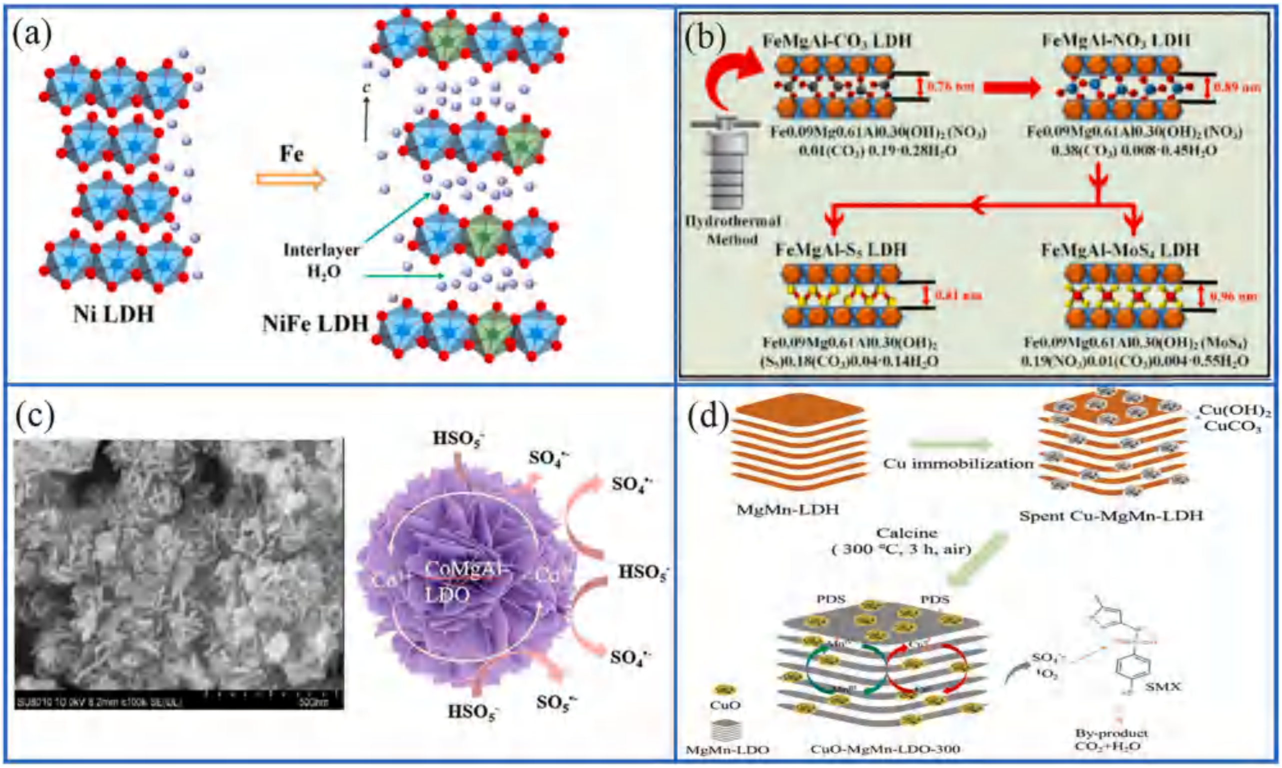

**Fig. 7.** (a) Incorporation of Fe into Ni-LDH. Reproduced from Yue et al. (2020). Copyright 2020 American Chemical Society. (b) Synthesis of FeMgAl-MoS$_4$ LDH. Reproduced from Ali et al. (2020). Copyright 2020 Elsevier. (c) SEM image and persulfate activation of CoMgAl-LDO. Reproduced from Hong et al. (2019). Copyright 2019 Elsevier. (d) Synthesis of CuO-MgMn-LDO. Reproduced from Chen et al., 2020 . Copyright 2020 Elsevier.

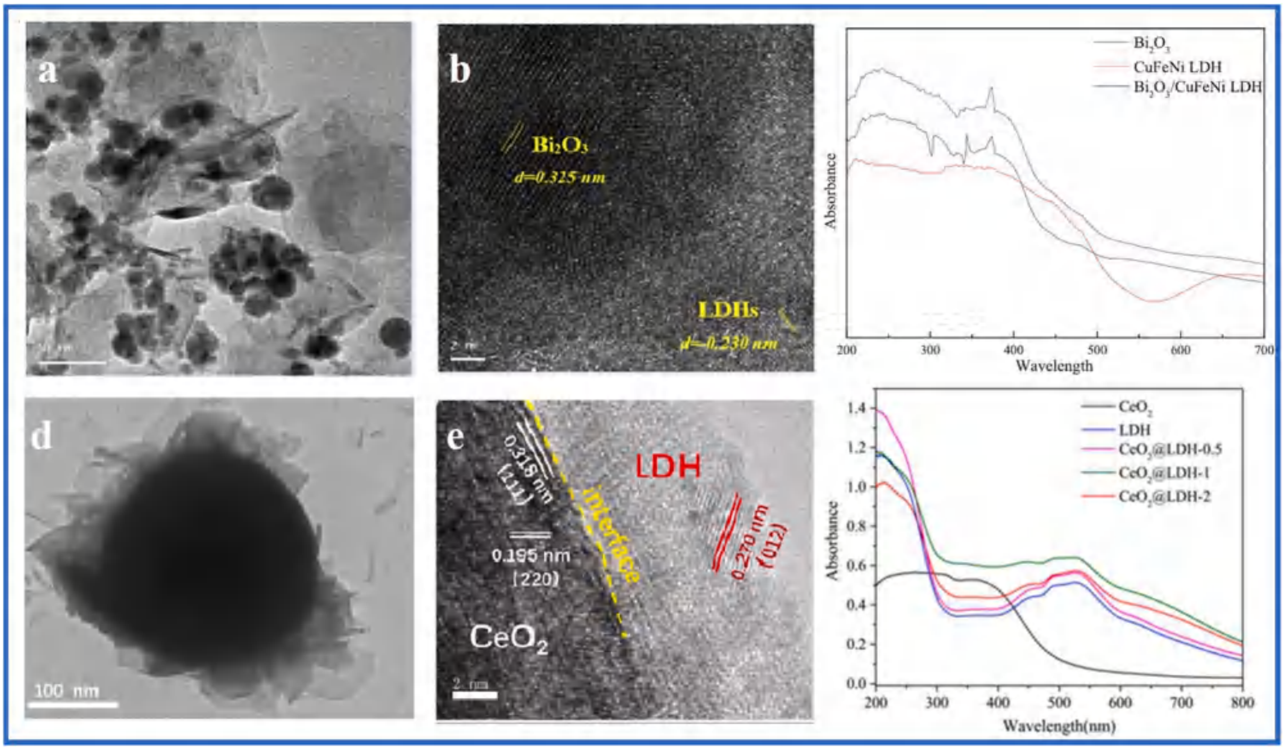

**Fig. 8.** (a) TEM and (b) HRTEM images of Bi$_2$O$_3$/CuNiFe LDHs composite. (c) UV–vis DRS of Bi$_2$O$_3$, CuNiFe LDHs and Bi$_2$O$_3$/CuNiFe LDHs composite. Reproduced from Zhang et al., 2020. Copyright 2020 Elsevier. (d) TEM image and (e) HRTEM image of CeO$_2$ @LDH. (f) UV–vis DRS of CeO$_2$, LDH and CeO$_2$ @LDH. Reproduced from Yang et al., 2021. Copyright 2020 Elsevier.

co-precipitation and calcination (Fig. 7c). The structure of $Co_1Mg_2Al_1$-LDO was not changed after the recycle experiments, which indicated the stability of this material. The CoMgAl-LDO could reach higher catalytic performance by effective PMS activation than the situation in PMS self-degradation as well as MgAl-LDO catalyzed degradation. Due to the fast circulation between Co(II) and Co(III), PMS was efficiently activated to generate $SO_4^{\bullet-}$ for atrazine (ATZ) removal. Chen et al. Chen et al., 2020 synthesized MgMn-LDH via a homogeneous co-precipitation method, then the precursor was calcined with $CuCl_2{\cdot}2H_2O$. Finally, CuO-MgMn-LDO was obtained (Fig. 7d). $Cu^{2+}$ was bonded on the homogeneous reactive sites of MgMn-LDH in the form of monolayer. This MgMn-LDH displayed excellent immobilization ability toward $Cu^{2+}$ due to the generation of $CuCO_3/Cu(OH)_2$. According to the results of nitrogen adsorption/desorption technique, CuO-MgMn-LDO had a larger SSA than that of MgMn-LDO, indicating the former might have better catalytic performance because of the increased active sites. In addition, the porous structure of CuO-MgMn-LDO could accelerate the diffusion of pollutants on the surface of catalyst. (Table 1).

Through the combination of various metal elements and different preparation methods, LDH composites with high catalytic performance can be produced. The synergistic effects between different metals are complex. For instance, interactions between Cu and Mn could facilitate the activation and transportation of active oxygen species. The construction of Z-scheme heterostructure realized rapid photogenerated electrons transfer as well as production of reactive electrons in PS activation. Since high-valent Ni cannot accumulate because of Fe introduction, the original circulation of Ni in different valent was significantly accelerated, thus the NiFe LDHs could present better catalytic efficiency. Herein, we discussed metal/metal oxide modified LDH composites that are applied in persulfate-AOPs. Metal or metal oxides have great potential in the optimization of pure LDHs. Thus, the activation mechanisms by different materials undoubtedly deserve further exploration.

### 3.2. LDH-carbon composites

During the application of metal-based materials, their drawbacks like minerals shortage, excessive cost, biotoxicity have gradually raised concern. Since the effective persulfate activation by reduced graphene oxide (rGO) was reported by Sun et al. Sun et al. (2012a), an increasing number of carbonaceous catalysts such as carbon nanotubes (CNTs), graphene, carbon nitride, activated carbon (AC), biochar (BC) have been applied in persulfate-AOPs. These materials usually possess outstanding electron conductivity, which can promote the generation of ROS. Moreover, carbonaceous materials could act as good supporting carriers for LDHs to inhibit their aggregation. However, some carbonaceous materials such as AC and BC display relatively low catalytic performance for persulfate activation when they act alone. The combination of LDHs and carbonaceous materials may overcome the drawbacks of single material while retaining their advantages, then produce composites with higher metal dispersion, electron conductivity and improved morphology.

#### 3.2.1. Composite with 1D carbonaceous material

CNTs are a kind of nanomaterials dominated by $sp^2$ hybridization and exist in the form of rolled-up graphite sheets. Due to the advantages of low mass-transfer resistance, unique electrical conductivity and good efficient adsorption capacity, CNTs have been seen as potential catalysts in persulfate-AOPs (Chen et al., 2018). On the one hand, the highly delocalized π electrons on the surface of CNTs can facilitate the electron transfer via conductive carbon tunnel, thus promoting the efficiency of persulfate activation. On the other, the surface functional groups are also in favor of the generation of $SO_4^{\bullet-}$. Li et al. fabricated a CNTs@CoMnAl-LDH composite via self-assembly of CoMnAl-LDH on the surface of CNTs (Li et al., 2015). As shown in the SEM and TEM images, the composite presented a 3D hierarchical structure, which was similar to the honeycomb. After calcination, the composite was converted to CNTs@CoMnAl-LDO while the honeycomb-like structure was maintained (Fig. 9). Compared with CoMnAl-LDO, CNTs@CoMnAl-LDO could reach high removal efficiency of BPA within a short time, which were mainly attributed to two reasons. Firstly, the morphology of LDHs was converted from 2D nanosheets converted to 3D hierarchical honeycomb after the incorporation of CNTs. The unique structure could effectively inhibit the aggregation of LDH plates and CNTs, SSA of the composite was increased and more active sites were exposed. Secondly, calcination could increase the number of defect sites in CNTs, thus improving catalytic potential of CNTs@CoMnAl-LDO in persulfate activation (Li et al., 2015).

#### 3.2.2. Heterojunction with 2D carbonaceous materials

By constructing layer-by-layer heterojunction between different 2D materials, charge transportation can be accelerated remarkably. Graphene is a kind of 2D nanomaterial which consists of carbon atoms with $sp^2$ hybridized atoms. Because of the big surface area and excellent adsorption capacity, it is often used as adsorbent for various contaminants. Additionally, GO could act as a good carrier for photocatalysts (Hu et al., 2021; Zhao et al., 2012). However, graphene which is perfectly $sp^2$-hybridized could hardly activate persulfate which may be

**Table 1**
Composition and morphology of metal/metal oxides incorporated LDHs.

| Metal elements | Anions | Preparation methods | Morphology | Calcination | Molar ratio of metals | References |
|---|---|---|---|---|---|---|
| Fe-Ni | Hydrothermal | Ultrathin nanosheet | No | 1.96 | (Yue et al., 2020) | |
| Ni-Al-Mg | $NO_3^-$ | Hydrothermal | A polygonal crystalline laminate | No | Ni-LDH-0.01 | (Huang et al., 2020a) |
| Cu-Mg-Al | $CO_3^{2-}$ | Co-precipitation | Flower shape and lamellar structure | No | $(Cu^{2+}+Mg^{2+})/Fe^{3+}$ 3.0 | (Yan et al., 2017) |
| Co-Mg-Al | $CO_3^{2-}$ | Aqueous miscible organic solvent treatment | Typical “flower-like” morphology | Yes | 1:2:1 | (Hong et al., 2019) |
| Co-Fe-Ni | $CO_3^{2-}$ | Co-precipitation | Typical lamellar structure | No | 6:3.1:1.09 | (Zeng et al., 2018) |
| Cu-Co-Fe | $CO_3^{2-}$ | Co-precipitation | Thin nanosheet | No | 1:1:1 | (Lu et al., 2019) |
| Cu-Mg-Mn | $CO_3^{2-}$ | Co-precipitation and calcination | Collapsed platelet-like shape with CuO nanoparticle adhered | Yes | Cu/Mn 0.6 Mg/Mn2.1 | |
| Fe-Mg-Al | $MoS_4^{2-}$ | Hydrothermal and ion exchange method | Typical lamellar structure | No | 0.09:0.61:0.30:0.19 | (Ali et al., 2020) |
| $Bi_2O_3$/ CuNiFe | $CO_3^{2-}$ | Co-precipitation sol–gel combustion | $Bi_2O_3$: spherical nanoparticle<br>CuNiFe LDHs: flower-shaped and layered structure | No | $Bi_2O_3$/CuNiFe1:1<br>CuNiFe 0.025:0.025:0.0625 | |
| $CeO_2$-CoAl | $CO_3^{2-}$ | Hydrothermal–calcination ($CeO_2$)<br>Co-precipitation (LDH) | 3D flower-like spherical structure | No | Co: Al 2.68<br>Co: Ce 0.81 | |

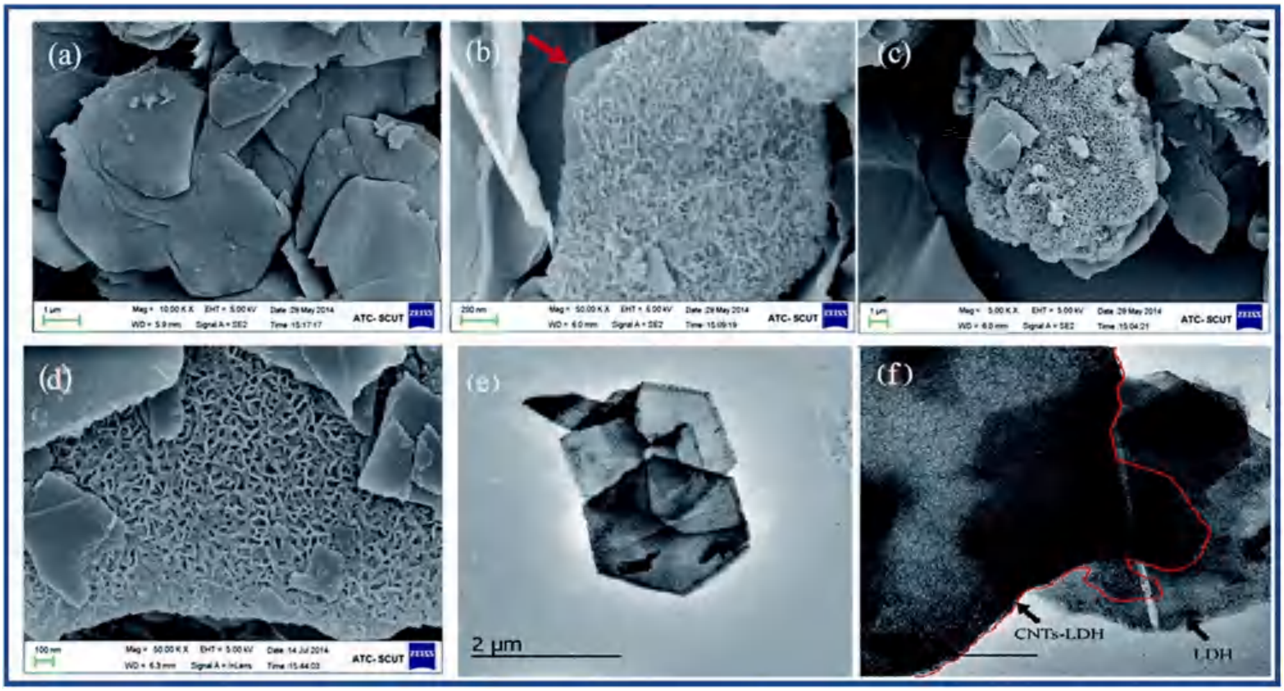

**Fig. 9.** SEM images of (a) CoMnAl-LDH, (b) and (c) CNTs–CoMnAl-LDH, (d) CNTs–CoMnAl-LDO, TEM images of (e) CoMnAl-LDH (f) CNTs–CoMnAl-LDH. Reproduced from Li et al. (2015). Copyright 2015 The Royal Society of Chemistry.

attributed to its insufficient electron giving ability by the settled π-conjugated system (Sun et al., 2012a; Oostinga et al., 2008; Kaiser and Skakalova, 2011). In fact, the graphene derivatives, including GO and rGO, usually display higher catalytic efficiency.

Shahzad et al. (2019) incorporated rGO nanosheets into the layers of LDHs, the obtained Fe-rGO LDH composite solved the agglomeration of rGO. They used two different methods to synthesize LDH-rGO composites. Single-layer rGO was intercalated into the inner space of Fe-LDH to produce Fe-rGO-LDH (Fig. 10a), while a composite with Fe-LDHs grown on multilayer rGO was made to check the effect of intercalation (Fig. 10b). As shown in SEM images (Fig. 9c-9f), the primary hexagonal morphology of LDHs was partly destroyed and nanoplates of LDHs as well as rGO were stacking orderly, which was kind of like a sandwich. The large surface area and porous structure of the novel composite may enable it to display better catalytic performance since it possesses sufficient active sites and enhanced capacity of mass transport. In their later research, Shahzad et al. (2020) synthesized a Cu-rGO LDH nanohybrid material by using similar routes and realized efficient PMS activation to decompose contaminants.

Graphitic carbon nitride (g-$C_3N_4$) has been a rising star photocatalyst due to its proper band gap, good VL response, fine chemical durability, uncomplex production and economic expenses (Mamba and Mishra, 2016; Liang et al., 2021a). But the inherent deficiencies such as small SSA, unsatisfying crystallinity, ineluctable recombination of electron-hole pairs and finite VL absorption range have restricted its photocatalytic activation efficiency towards persulfate. Interestingly, the unique oxo-bridges between metal ions in LDHs could effectively control the electron-hole recombination (Nakamura et al., 2007; Kim et al., 2014). Accordingly, LDH-g-$C_3N_4$ composites may possess great potential in photo-activation of persulfate.

Zeng et al. (2020) synthesized a CoAl-LDH/g-$C_3N_4$ heterostructure with a layer-by-layer structure. As shown in TEM images (Fig. 11a), numerous CoAl-LDH nanocrystalline were orderly interspersed on the surface of $C_3N_4$. Because of the tight connection between different components in CoAl-LDH/g-$C_3N_4$, the excited electron could shuttle rapidly between heterojunction thus increase the generation of active species. The result of photoluminescence spectra indicated that CoAl-LDH/g-$C_3N_4$ exhibited lower weaker emission intensity, proving that the incorporation of CoAl-LDH could facilitate the electron transfer and restrain the recombination of electron-hole pairs. Additionally, according to results of UV–vis DRS, the VL adsorption capacity of $C_3N_4$ was highly improved through its combination with CoAl-LDH (Fig. 11b-11d). On account of the synergistic effect in this heterojunction, sulfadiazine (SDZ) was effectively decomposed by active substances.

### 3.2.3. *Composite with 3D carbonaceous materials*

3D carbonaceous materials like BC and AC usually are featured with large surface area, unique pore structure and plentiful functional groups (White et al., 2009; Ren et al., 2020), which enable them to present good performance in persulfate activation.

Biochar could be produced from thermal-treated biomass under an oxygen-limited atmosphere (Zubair et al., 2021; Ding et al., 2020). Due to its unique characteristics such as abundant micropore or mesopore structures, rich surface functional groups, abundant mineral ingredients and extraordinary absorbability, BC has attracted widespread concern in various fields (Xiao et al., 2018). More importantly, the abundant waste biomass and facile preparation of make BC in line with the concept of sustainable development. Recently, biochar-based catalysts produced by pyrolysis have been gradually applied in persulfate-AOPs (You et al., 2021; Yang et al., 2021). However, the catalytic performance of BC was largely determined by original material and pyrolysis temperature. By optimizing the composition parameters or combining with metal catalysts, BC may have enhanced catalytic activity than its original counterpart (Qin et al., 2020). Gholami et al. (2020) incorporated the BC particles into Zn-Co-LDH nanostructures by the hydrothermal method and the composite was then used as a photocatalyst for the degradation of Gemifloxacin (GMF). From the result of UV–vis DRS, BC is of great significance in decreasing the band gap energy of this composite (Fig. 12d). As shown in SEM images, after the integration with ZnCo-LDH, BC presented a rougher surface where Zn and Co were dispersed regularly (Fig. 12a-12c). The LDH-BC/PMS system achieved high degradation efficiency towards GMF, which was higher than Co-LDH or pure BC. Due to the presence of LDH and BC, the separation

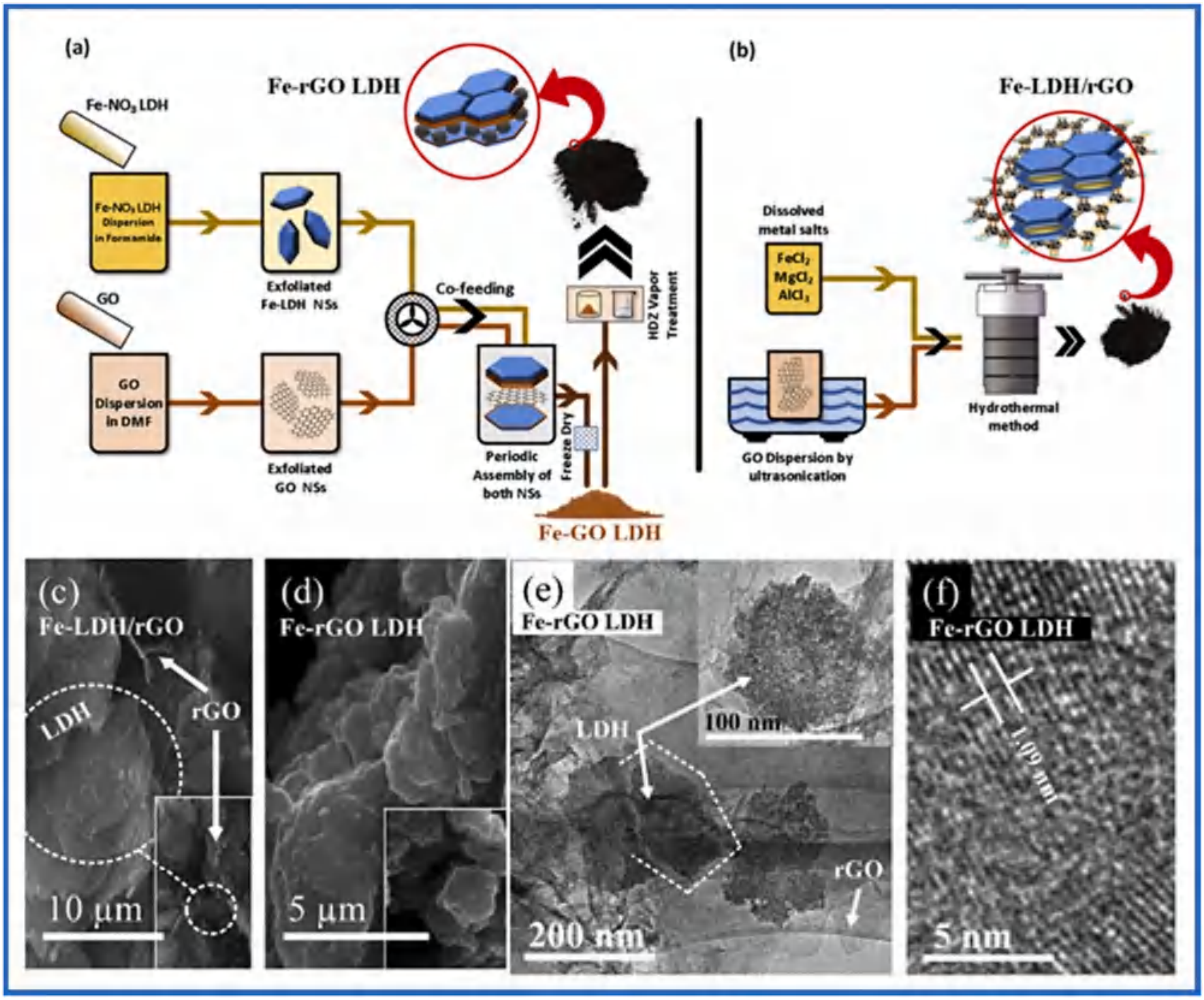

**Fig. 10.** Illustration of synthesis route for Fe-rGO LDH (a); Fe-LDH/rGO (b); SEM images of Fe-LDH/rGO (c); Fe-rGO LDH (d); TEM image (e); HRTEM images of Fe-rGO LDH (f). Reproduced with permission from (Shahzad et al., 2019). Copyright 2019 Elsevier.
((.)

efficiency of electron-hole pairs was improved. Meanwhile, the agglomeration of LDHs was availably controlled. The synergistic effect of LDH with biochar exhibited significant improvement in physico-chemical characteristics such as SSA, surface functional groups, structural heterogeneity, stability and adsorption characteristics of BC/LDH composite (Zubair et al., 2021).

Activated carbon is quite suitable for wastewater treatment due to its excellent adsorptive capability and catalytic activity (Chen et al., 2016). Despite AC have shown potential in persulfate activation (Yang et al., 2011; Saputra et al., 2013), the pure AC is still faced with problems such as relatively low catalytic activity as well as poor stability compared with carbon nanomaterials (CNTs, rGO). In most cases, AC was used as carrier in combination with metal catalytic materials (Ma et al., 2020b).

Ma et al. (2020a) synthesized the AC-supported CoFe-LDH composites (AC@CoFe-LDH) through a co-participate method and the as-prepared sample was used as a PS activator for the removal of LOM. XRD analysis confirmed the crystal structure of AC@CoFe-LDH nanocomposites. According to the SEM images, the rougher surface of AC@CoFe-LDH compared with pristine AC indicated the improvement of SSA, which might increase the active sites and therefore facilitate the catalytic efficiency (Fig. 12e-12f). Deeper characterization clearly presented the LDH plates were uniformly covered on AC surface and it was also proved to have a mesoporous structure (Fig. 12g-12h). Compared to other single catalysts (AC, AC-HCl or CoFe-LDH alone), the composite displayed higher activity for PS activation.

Moreover, 3D graphene aerogel (GA), a novel member of graphene fabricated by the self-assembly graphene nanosheets, can significantly enhance the electron transfer efficiency in catalytic process (He et al., 2021). Accordingly, it seems promising to couple graphene aerogel with LDHs to realize effective activation of persulfate. He et al. (2021) prepared a novel LDH-carbon composite (CoMn-LDH/rGA) via coupling CoMn-LDH with rGO aerogel. As shown by the SEM and TEM images, CoMn-LDH were dispersed on the 3D rGA networks which have abundant nano-scaled pores (Fig. 13a-13b). The CoMn-LDH/rGA was then used as an activator of PMS to degrade metronidazole (MTZ) under visible light irradiation. Compared with CoMn-LDH and 2D CoMn-LDH/rGO, 3D CoMn-LDH/rGA showed higher removal efficiency of MTZ. According to the results of UV–vis DRS and transient photocurrent responses (Fig. 13c-13d), the light adsorption and photocurrent response were evidently enhanced, implying that the combination of CoMn-LDH with rGA significantly improved the light response. It was the unique electron transfer channel in 3D rGA that lead to this improvement. As a result, the photogenerated electrons could effectively activate PMS to generate more ROS and realize the effective degradation of MTZ.

Besides the carbonaceous materials mentioned above, some

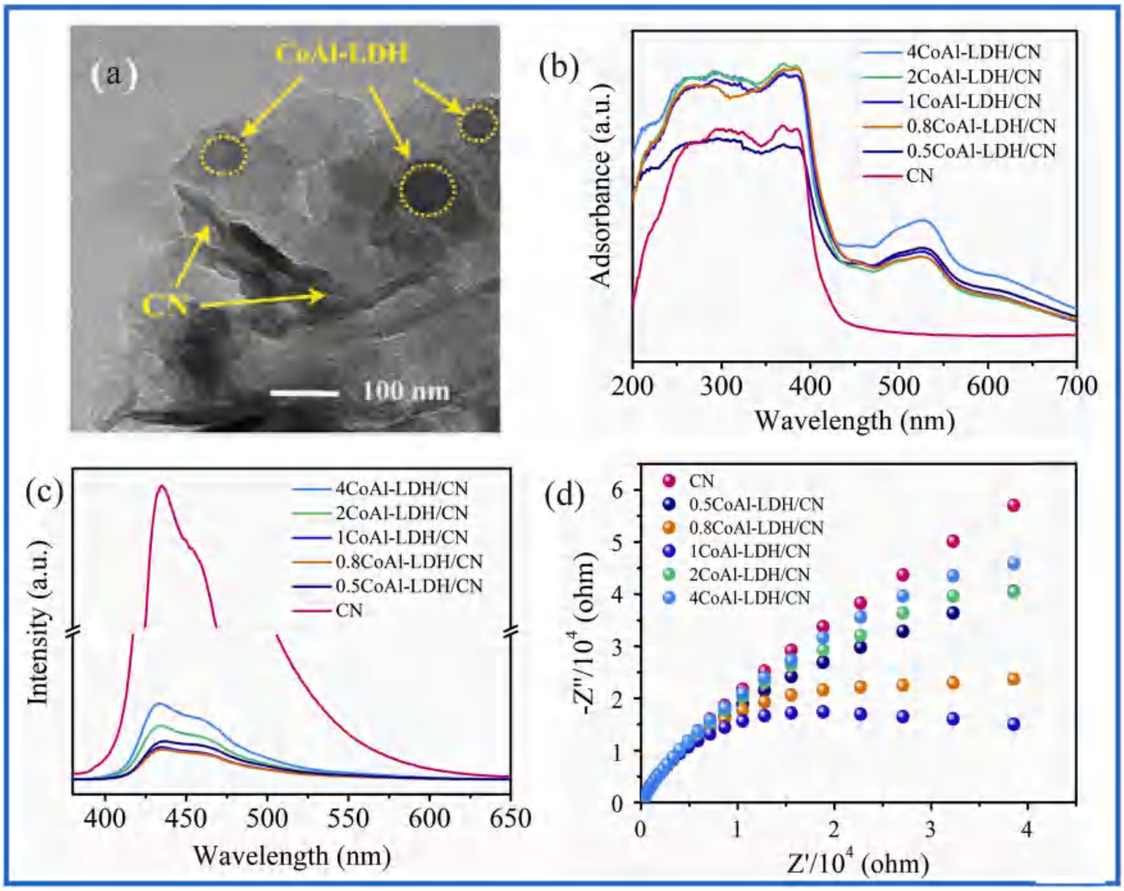

**Fig. 11.** (a) TEM image of 0.8CoAl-LDH/CN; (b) UV–vis DRS; (c) PL spectra; (d) EIS Nyquist plots of CN and CoAl-LDH/CN. Reproduced with permission from (Zeng et al., 2020). Copyright 2020 Elsevier.

materials such as fullerene, nano-diamond and ordered mesoporous carbon have been reported to activate persulfate. However, fullerene displayed low catalytic activity in persulfate-AOPs because its highly conjugated electron system is unfavorable for the capability of electron-donating and electron conductivity (Goldshleger, 2001). In addition, pristine nano-diamond with $sp^3$-hybridized structure also exhibits confined efficiency of persulfate activation. Annealing could tune the surface functional groups and degree of graphitization, improving catalytic performance of nano-diamonds (Yu et al., 2020). But the excessive cost has severely limited its development in persulfate-AOPs. Moreover, the 3D ordered mesoporous carbon is also an effective catalyst which has highly stagger, controllable and mesoporous structures. These properties are favorable for mass transfer and exposure of more active sites, thus improving the catalytic performance in persulfate-AOPs (Wang et al., 2017; Duan et al., 2015a). At present, there are only a few articles reporting the combination of LDHs with carbonaceous materials in persulfate-AOPs. Therefore, it is of potential to develop more novel LDH-carbonaceous catalysts.

### 3.3. Other composites

LDHs were usually used in the form of nanosheets for water environment remediation. Thus, the material may face the problem of recyclability as well as second pollution. It is essential to develop fixing methods for the production of LDH composites with higher catalytic performance and stability. Polyacrylonitrile (PAN), is a typical membrane basic material obtained via organic substances (Jhaveri and Murthy, 2016). The extraordinary characteristics like excellent physicochemical stability, big surface area, great flexibility and mechanical strength, the property of cost-effective make it an ideal material nanoparticles immobilization. Guo et al., 2020 synthesized LDH@fibers catalytic membrane ($Cu_1Co_1LDH@PAN$), which was utilized to activate PMS for sulfamethoxazole (SMX) degradation. The microscopic morphology of $Cu_1Co_1LDH@PAN$ was a shuttle type composed of only a few layers of nanosheets. Compared with the SEM image of PAN, some LDH particles were attached to the PAN surface evenly, making the surface of the fiber turned to be rough (Fig. 14a-14b). Besides, a 3D hierarchical structure of shuttle-like LDH nanosheets was found, which possessed a more rounded edge compared with pristine $Cu_1Co_1$-LDH sample. In comparison with $Cu_1Co_1$-LDH powder samples, $Cu_1Co_1LDH@PAN$ showed higher SMX removal efficiency. More importantly, the metal (e.g., cobalt and copper) leaching amounts were lower than that of $Cu_1Co_1LDH$ powder.

Recently, Li et al. fabricated an efficient and stable modular LDH-composite via in-situ growing CoFe-LDH nanoarrays on PVDF framework with assistance of $NH_4F$ (Li et al., 2021). As shown in Fig. 14c-14d, SEM images of CoFeLDH(F)/PVDF showed that CoFe-LDH nanosheets were uniformly grown on the surface of PVDF in the form of nanoneedle. The F doping could lead to the generation of metal fluoride, thus promoting the conversion of LDH from nanosheet to nanoneedle. Due to the 3D porous structure, superhydrophilicity, and unique wire-like nanostructure, the composite could provide more active sites and higher mass transfer efficiency. As a result, the CoFeLDH(F)/PVDF composite exhibited higher persulfate activation efficiency to degrade various organic contaminants. More importantly, this composite could keep good catalytic stability after 10 cycles of degradation tests, which was higher than the powdery catalysts, indicating that the combination with PVDF significantly improves the stability of LDHs. (Table 2).

Due to the property of flexible modification, LDHs could be integrated with other metal or non-metal materials. Methods for LDH-based

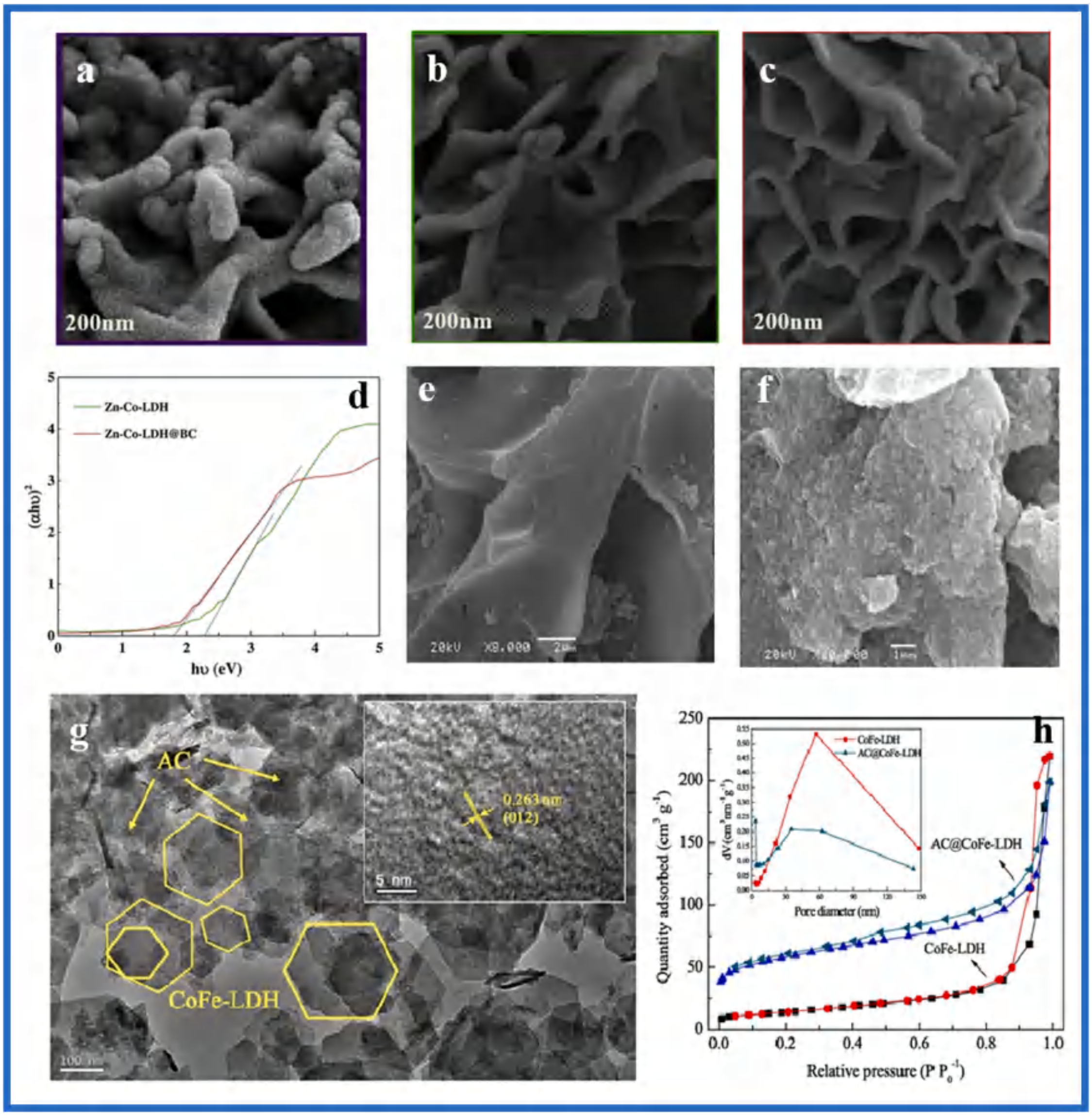

**Fig. 12.** Copyright 2020 Elsevier. (e) SEM image of AC; (f) SEM image of AC@CoFe-LDH; (g) HRTEM image of AC@CoFe-LDH; (h) Nitrogen adsorption-desorption isotherm of AC@CoFe-LDH.
(a) SEM images of (a) pure BC; (b) Zn-Co-LDH; (c) ZnCo-LDH@BC; (d) $(Ah\upsilon)^{2-h\upsilon \text{ curves of samples; Reproduced with permission from (}}$Gholami et al., 2020). (b) Reproduced with permission from (Ma et al., 2020a). Copyright 2020 Elsevier.

composite construction can mainly be divided into in situ synthesis method, anion exchange method, layer upon layer self-assembly method and calcining-annealing method,etc. LDHs can act not only as carriers but also as active substances. By changing the metallic cation and interlayer anion, adjusting pH condition, controlling atom-sphere and applying different fabrication methods, composites with various properties as well as structures could be produced. The combination between LDHs and other materials may overcome the intrinsic drawbacks of every single material, which could achieve the effect of “1 + 1 > 2”.

## 4. Mechanism of persulfate activation by LDH-based Catalysts

In persulfate-based AOPs, ROS are mainly $SO_4^{\bullet -}$, ·OH and $\bullet O_2^{-}$. By splitting the persulfate bond through energy and electron transfer reactions, sulfate radical can be in situ generated (Lee et al., 2020; Liu et al., 2020). Usually, the production process of $SO_4^{\bullet -}$ is accompanied by the generation of other free radicals. However, no $SO_4^{\bullet -}$ or ·OH was found in some persulfate-AOPs, which indicated the existence of non-radical mechanisms. Herein, we discussed radical and nonradical mechanisms in persulfate activation for the elimination of contaminants, respectively.

### 4.1. *Radical pathway*

LDHs/LDOs and their composites can provide sufficient active sites to facilitate the cleavage of peroxide bond and generation of radicals. Generally, active sites involve metal species, surface hydroxyl groups, carbonyl group (C═O), defective structure, $sp^2$-hybridized carbon and free-flowing electrons (Fig. 16).

### 4.1.1. *Bimetallic synergism for radical generation*

According to former researches, transition metals and their oxides are able to effectively active persulfate. The activation mechanism of PS and PMS by transition metals/metal oxides can be described as following equations (Eqs. (2)–(3)) (Wang and Wang, 2018; Yue et al., 2018).

$$S_2O_8^{2-} + M^{n+} \rightarrow M^{(n+1)+} + SO_4^{\bullet -} + SO_4^{2-} \tag{2}$$

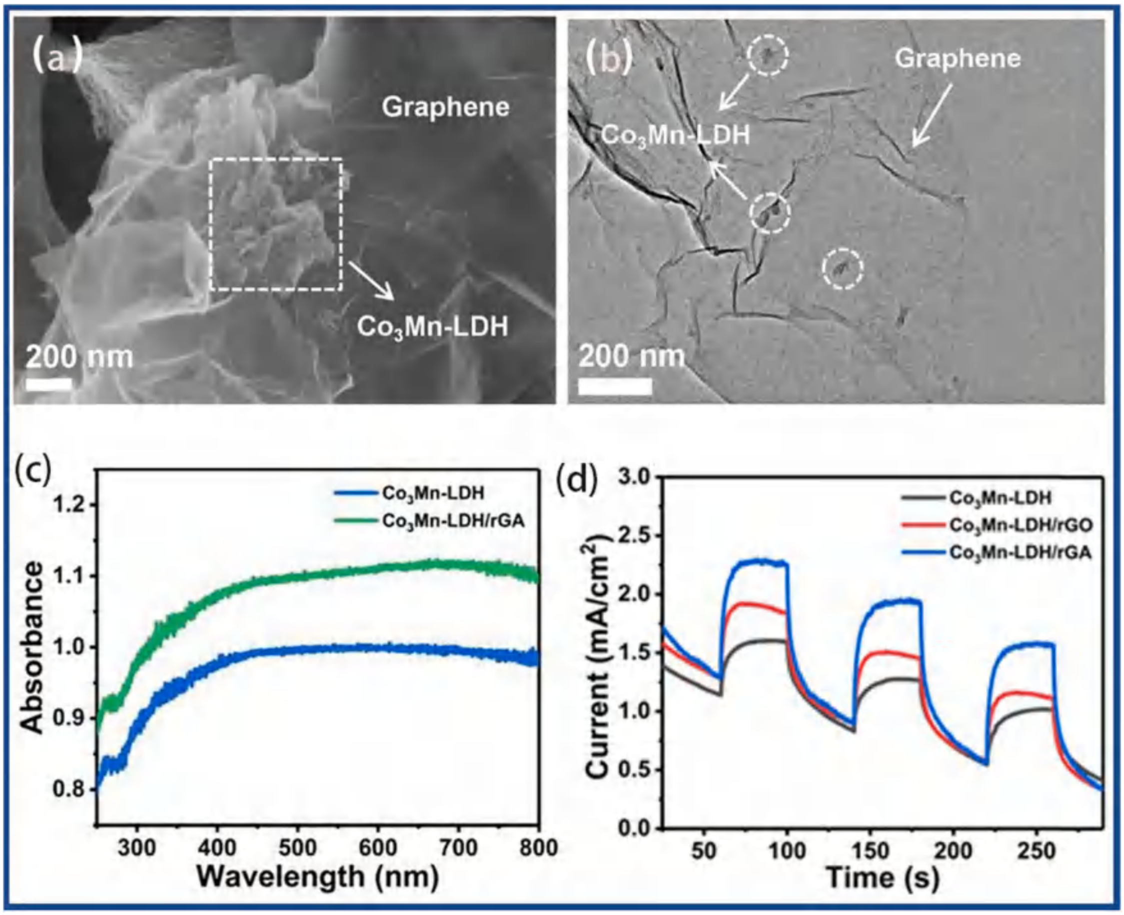

**Fig. 13.** (a) HRSEM (b) TEM images of CoMn-LDH/rGA. (c) UV–vis DRS of CoMn-LDH and CoMn-LDH/rGA. (d) Photocurrent response curves of different CoMn-LDH composites. Reproduced with permission from Ref. He et al. (2021). Copyright 2021 Elsevier.

$$HSO_5^- + M^{n+} \rightarrow M^{(n+1)+} + SO_4^{\bullet -} + OH^- \tag{3}$$

M refers to transition metals such as (Fe, Mn, Cu, Ce, Ni, Co, Ru).

Besides, $H_2O_2$ would be generated through hydrolytic process of PS as well as recombination of •OH (Monteagudo et al., 2019; Su et al., 2019).

$$S_2O_8^{2-} + 2H_2O \rightarrow 2HSO_4^- + H_2O_2 \tag{4}$$

$$\bullet OH + \bullet OH \rightarrow H_2O_2 \tag{5}$$

In persulfate-AOPs, the process from $M^{(n+1)+}$ to $M^{n+}$ usually determines the reaction rate (Yue et al., 2020). But the accumulation of metal ions in high valence state will lead to low catalytic performance. Fortunately, the combination of different metals may help to solve this problem (Zhou et al., 2020; Feng et al., 2016; Ren et al., 2015). Previous studies have proved the synergistic effects between metals could significantly improve the catalytic performance of materials. Thanks to the tunable composition of LDH composites, transition metal or metal oxides can be introduced to activate PMS/PDS with a lower leaching rate.

In CuO-MgMn-LDO/PS system, the synergistic effect between Cu and Mn greatly improved the charge transfer of this system and facilitated the activation and transportation of active oxygen species. $S_2O_8^{2-}$ initially reduced ≡Mn(IV)/≡Cu(II) to be ≡Mn(III)/≡Cu(I) and generated $S_2O_8^{\bullet -}$. Besides, the ≡Mn(III)/≡Cu(I) on the catalyst could also promote the decomposition of PS to generate $SO_4^{\bullet -}$ and ≡Mn(IV)/≡Cu(II). The reduction of ≡Mn(IV) using ≡Cu(I) to generate ≡Mn(III) could promote electron transfer in the cycle reaction of producing $SO_4^{\bullet -}$. Subsequently, ·OH would be generated from the reaction between $SO_4^{\bullet -}$ and $H_2O$. Relative reaction processes are listed in the following equations (Eqs. (6)–(10)) (Zhou et al., 2020).

$$\equiv Mn(IV) + S_2O_8^{2-} \rightarrow \equiv Mn(III) + S_2O_8^{\bullet -} \tag{6}$$

$$\equiv Cu(II) + S_2O_8^{2-} \rightarrow \equiv Cu(I) + S_2O_8^{\bullet -} \tag{7}$$

$$\equiv Mn(III) + S_2O_8^{2-} \rightarrow \equiv Mn(IV) + SO_4^{\bullet -} + SO_4^{2-} \tag{8}$$

$$\equiv Cu(I) + S_2O_8^{2-} \rightarrow \equiv Cu(II) + SO_4^{\bullet -} + SO_4^{2-} \tag{9}$$

$$SO_4^{\bullet -} + H_2O \rightarrow SO_4^{2-} + H^+ + \bullet OH \tag{10}$$

The incorporated Fe could boost the reduction conversion of $Ni^{3+}$ or $Ni^{4+}$ and keep $Ni^{2+}$ in low-valent (Yue et al., 2020). In addition, the high-valent Fe would be reduced by $S_2O_8^{2-}$, which made the NiFe-LDH@PS system work continuously. Due to the presence of a new charge transfer bridge-builder (Fe), a rapider redox cycle of Ni could be realized, which results in higher catalytic performance (Fig. 15a). Besides the reactions between Ni and $S_2O_8^{2-}$ (just like other transition metals), there also exist the following processes.

$$Fe(II) + Ni(III) \rightarrow Ni(II) + Fe(III) \tag{11}$$

$$Fe(III) + S_2O_8^{2-} \rightarrow Fe(II) + S_2O_8^{\bullet -} \tag{12}$$

$$Fe(III) + S_2O_8^{\bullet -} + H_2O \rightarrow Fe(II) + 2HSO_5^- + 2H^+ \tag{13}$$

In fact, there is also similar progress in transition metal pairs like “Co-Cu” (Lu et al., 2019; Zhou et al., 2020), “Co-Fe” (Wu et al., 2020a), “Co-Mn” (Ma et al., 2018b). We can conclude that the original redox

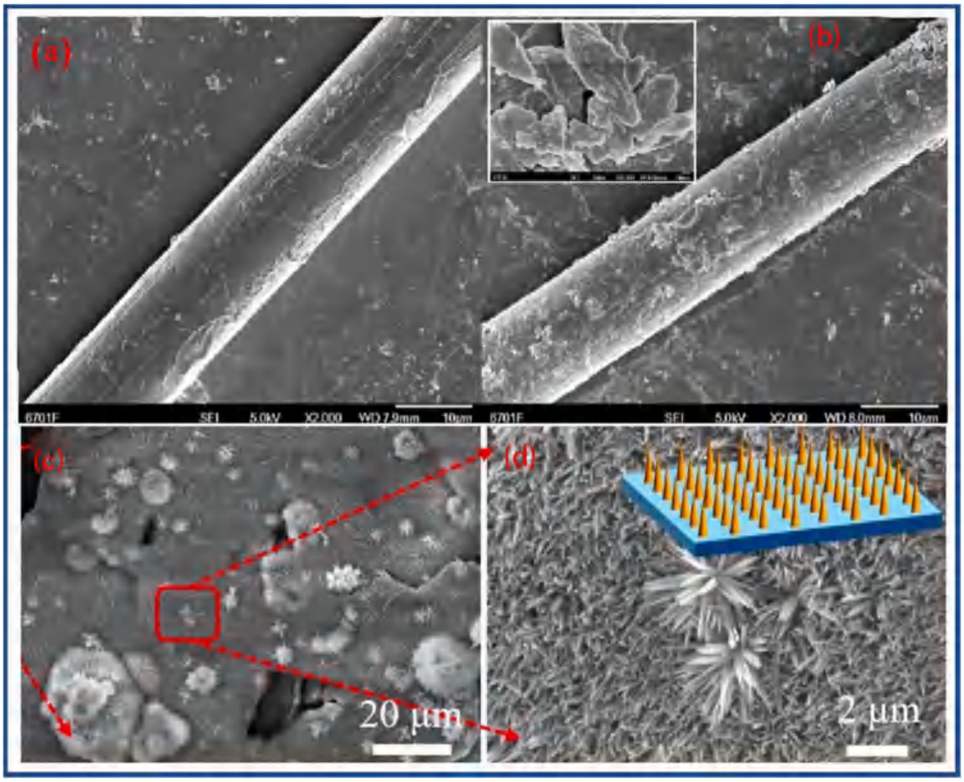

**Fig. 14.** SEM images of (a) PAN; (b) CuCo-LDH@PAN. (Inset, SEM image under 100 nm); Reproduced with permission from Guo et al. (2020). Copyright 2020 Elsevier. (c-d) SEM images of CoFeLDH(F)/PVDF. Reproduced with permission from Li et al. (2021). Copyright 2021 Elsevier.

**Table 2**
Composition and morphology of LDH-carbon composites and others.

| Metal elements | Anions | Non-metal ingredient | Preparation methods | Morphology | Calcination | References |
|---|---|---|---|---|---|---|
| Co-Mn-Al | $CO_3^{2-}$ | MWCNTs | Co-precipitation | 3D hierarchical honeycomb | Yes | (Li et al., 2015) |
| Cu-Mg-Al | $NO_3^-$ | rGO | Hydrothermal method Exfoliation-resembling | rGO intercalated nanosheet with highly mesoporous structure | No | (Shahzad et al., 2020) |
| Fe-Mg-Al | $NO_3^-$ | rGO | Hydrothermal method Exfoliation-resembling | Porous nanosheet | No | (Shahzad et al., 2019) |
| Co-Al | $NO_3^-$ | $g\text{-}C_3N_4$ | Co-precipitation and self-assembly method | multi-layered nanosheet | No | (Zeng et al., 2020) |
| Zn-Co | $NO_3^-$ | Biochar | Hydrothermal method | LDH nanosheets dispersed on BC | No | (Gholami et al., 2020) |
| Co-Fe | $CO_3^{2-}$ | Activated carbon | Co-precipitation method, ultrasonication, stirring | plate-like slices covered or wrapped with the AC surface | No | (Ma et al., 2020a) |
| CoMn | $CO_3^{2-}$ | rGA | Co-precipitation and hydrothermal method | LDH nanosheets dispersed on 3D rGA | No | (He et al., 2021) |
| Cu-Co | $CO_3^{2-}$ | PAN | Co-precipitation method | 3D LDH nanosheets attached to PAN | No | |
| Co-Fe | $CO_3^{2-}$ | PVDF | Hydrothermal method | Nanoneedle array | No | (Li et al., 2021) |

cycle will be changed after the introduction of another transition metal. The rapid charge transfer between different metal ions will significantly boost the redox process thus enhance the catalytic performance for persulfate activation. What is more, incorporation of extra metal may increase the number of hydroxyl groups on the surface of LDHs, which could react with $HSO_5^-$ to generate $SO_4^{\bullet-}$ (Zhou et al., 2020).

#### 4.1.2. Surface hydroxyl groups

It has been confirmed that surface hydroxyl groups (SHGs) can be formed via the interaction of Lewis acid sites with $H_2O$ molecules on the surface of catalysts (Khan et al., 2018). The abundant metal composition in LDH-based composites can evidently increase the L-acid sites for the generation of hydroxyl groups (Zhou et al., 2020; Wu et al., 2020a). These groups can react with the adsorbed persulfate molecules and cleave the O—O bond to produce radicals. Wu et al. Wu et al. (2020a) discovered that SHGs in FeCo-LDH could enhance the adaptability in wider pH range and become dominant persulfate activator under alkaline condition through offering abundant active sites complexation with persulfate.

#### 4.1.3. Carbonaceous materials in the generation of $SO_4^{\bullet-}$

Carbonaceous materials could act as the electron donor or mediator for persulfate activation. After accepting electrons, PMS or PDS will then generate free radicals. Generally, carbonaceous materials which possess relatively stronger electron giving and conduction ability but weak adsorbability tend to produce radicals (Yu et al., 2020).

It is believed that CNTs could realize effective persulfate activation to generate $SO_4^{\bullet-}$ (Sun et al., 2014). The surface ketonic group on CNTs might undergo electron transfer reactions with persulfate to produce free radicals (Sun et al., 2014). (Fig. 15b).

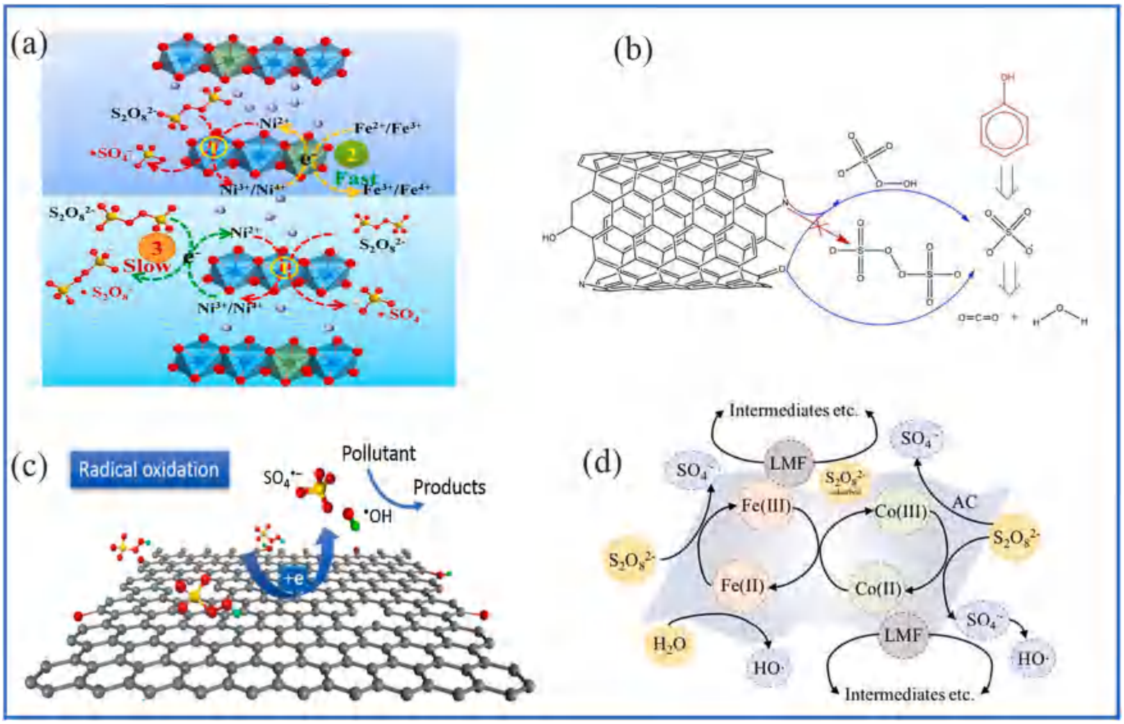

**Fig. 15.** (a) Synergism of Fe-Ni for PDS activation. Reproduced with permission from Yue et al. (2020). Copyright 2020 American Chemical Society. (b) N-CNT for activation of PMS/PDS. Reproduced with permission from (Sun et al., 2014). Copyright 2014 Elsevier. (c) radical generation on rGO. Reproduced with permission from Duan et al. (2016). Copyright 2016 Elsevier. (d) PDS activation by AC@CoFe-LDH. Reproduced with permission from Ma et al. (2020a). Copyright 2020 Elsevier.

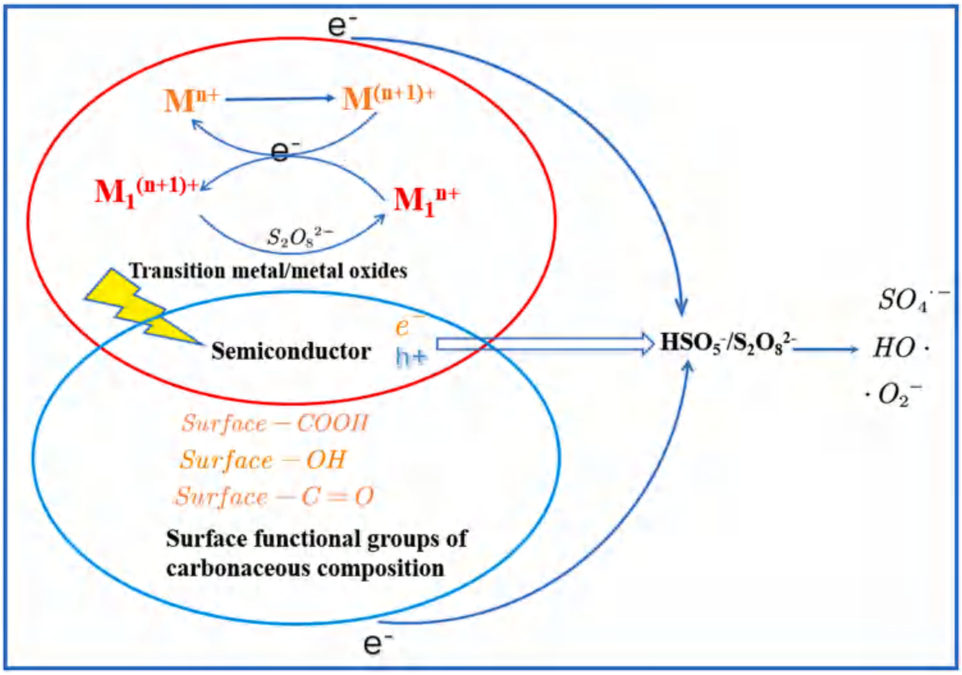

**Fig. 16.** Radical pathway in LDH/persulfate system.

$$CNT-C=O+S_2O_8^{2-}\rightarrow CNT-C-O^{*}+SO_4^{\bullet-}+SO_4^{2-} \tag{14}$$

$$CNT-C=O+HSO_5^{-}\rightarrow CNT-C-O^{*}+SO_4^{\bullet-}+OH^{-} \tag{15}$$

Li et al. (2015) integrated MWCNTs (multi-walled CNTs) with CoMnAl-LDO and the composite possessed a 3D hierarchical honeycomb nano-structure. The incorporation of MWCNTs significantly activated the PMS to generate $SO_4^{\bullet-}$, which might be attributed to distinctive structure and defects of MWCNTs.

Besides, there exist similar processes in rGO/persulfate system (Duan et al., 2016). (Fig. 15c).

$$C=C=O+HSO_5^{-}\rightarrow SO_4^{\bullet-}+C=C-O^{+}+OH^{-} \tag{16}$$

$$C = C - O^{+} + HSO_5^{-} \rightarrow C = C = O + SO_5^{\bullet -} + H^{+} \tag{17}$$

In rGO/LDH-PDS system, PDS inside LDH was successfully activated to produce $SO_4^{\bullet -}$ at the interface of rGO/LDH. The edge sites of rGO with delocalizedπelectrons could act as active sites to accelerate the generation of $SO_4^{\bullet -}$ through rapid electron transfer and the weak O—O bond. Duan et al. (2016); Huang et al. (2020b).

AC could act as a carrier for metal catalysts and its extraordinary adsorption capacity as well as rich surface functional groups may strengthen the efficiency of persulfate activation (Oh et al., 2016). In the AC@CoFe-LDH system, the *sp*$^2$ carbon and functional oxidation groups belonging to AC might participate in the PS activation reaction (Ma et al., 2020a). (Fig. 15d). Moreover, the functional groups of AC could recover through the reaction between the components of AC and $H_2O$ (Eqs. (18)–(20)). Moreover, delocalized π-electrons of AC also play an indispensable role in $SO_4^{\bullet -}$ generation (Eqs. (21)–(22)) (Oh et al., 2016).

$$AC \quad surface - COOH + \quad S_2O_8^{2-} \rightarrow AC \quad surface - COO\cdot + SO_4^{\bullet -} + HSO_4^{-} \tag{18}$$

$$AC \quad surface - OH + \quad S_2O_8^{2-} \rightarrow AC \quad surface - O\cdot + SO_4^{\bullet -} + HSO_4^{-} \tag{19}$$

$$AC \quad surface - C = O + \quad S_2O_8^{2-} \rightarrow AC \quad surface - CO\cdot + \quad SO_4^{\bullet -} + HSO_4^{-} \tag{20}$$

$$AC - \pi + HSO_5^{-} \rightarrow AC - \pi^{+} + OH^{-} + SO_4^{\bullet -} \tag{21}$$

$$AC - \pi + HSO_5^{-} \rightarrow AC - \pi^{+} + H^{+} + SO_5^{\bullet -} \tag{22}$$

A proper level of oxygenous functional groups on the surface of carbonaceous materials could accelerate the production of radicals (Ren et al., 2020; Duan et al., 2016; Sun et al., 2012b). In addition, defects generated from the breakage of C—C σ bonds also have significant influence on the catalytic performance (Duan et al., 2016). Even until now, the mechanism of persulfate activation involving carbon materials remains controversial and substantial further investigations are needed to unveil the mystery in persulfate activation concerning carbonaceous catalysts.

### 4.2. *Nonradical pathway*

Recently, researchers have found that $SO_4^{\bullet -}$ and ·OH were not the main active substances in some persulfate-based AOPs, which raised extensive discussions of nonradical mechanisms for persulfate activation. According to former researches, nonradical mechanisms mainly include $^1O_2$ (Shahzad et al., 2020; Zhu et al., 2019), mediated electron-transfer (Lee et al., 2016), generation of surface metal complex with pollutants (Chen et al., 2020) and direct oxidation (Huang et al., 2017). Unlike $H_2O_2$-based AOPs, persulfate-AOPs tend to present complicated mechanisms due to the variation of catalysts and substrates. What's more, there may exist both radial and nonradical mechanism in a system, especially those persulfate-AOPs catalyzed by composites (Huang et al., 2020a).

#### 4.2.1. *Singlet oxygen ($^1O_2$)*

$^1O_2$ is an important non-radical active specie and it can be produced by self-decay of PMS (Eq. (23)). But the process is relatively inefficient, which could not be the main pathway.

$$HSO_5^{-} + SO_5^{2-} \rightarrow HSO_4^{-} + SO_4^{2-} + {}^1O_2 \tag{23}$$

It has been reported that $^1O_2$ could be generated in photochemical process. For instance, photo-induced electron could react with dissolved oxygen to generate $\bullet O_2^{-}$, which would then react with ·OH and produce $^1O_2$ through Eq. (24) (Zeng et al., 2020; Li et al., 2013).

$$\cdot O_2^{-} + \cdot OH \rightarrow {}^1O_2 \tag{24}$$

Meanwhile, photo-induced hole ($h^+$) could react with $\bullet O_2^{-}$ to produce $^1O_2$. The presence of $^1O_2$ was also proved in degradation of SMX which used CuCo-LDH@PAN as PMS activator. According to scavenging experiments and detection of intermediate products, a degradation pathway induced by $^1O_2$ was proved but the generation approach of $^1O_2$ was unclear (Guo et al., 2020).

What is more, various carbonaceous materials (e.g., CNTs, N-doped graphene, sludge-derived biochar) could catalyze PS/PMS to produce $^1O_2$ (Duan et al., 2016; Cheng et al., 2017; Ma et al., 2019; Yin et al., 2019). Interestingly, when these carbonaceous materials are integrated with LDH-based samples, the reaction mechanism may become different. For instance, in the research of Li et al. (2015), the nonradical pathway induced by MWCNTs was not found in CNTs–LDO/PS system. Despite $\bullet O_2^{-}$ was detected in Zn-Co-LDH@BC/Persulfate system, they did not report the reaction pathway induced by $^1O_2$ (Gholami et al., 2020). Ma et al. (2020a) briefly mentioned that PS could be in-situ activated by AC@CoFe-LDH which leads to nonradical degradation of LMF. But the specific route was not proposed.

Certainly, there also exists $^1O_2$ dominated persulfate activation by hybrids of carbon-based materials and LDH. The electron-deficient copper (e.g., $Cu^{2+}$) in Cu-rGO-LDH can react with PMS to produce stable intermediates [$Cu^{2+}$-O-O-$SO_3$], which will subsequently be reduced after receiving an electron from $HSO_5^{-}$ to produce $\dot{}O_2^{-}$ (Shahzad et al., 2020).

$$\left[Cu^{2+} - OH\right]^{+} + H - O - O - SO_3^{-} \rightarrow \left[Cu^{2+} - O - O - SO_3^{-}\right] + H_2O \tag{25}$$

$$2\left[Cu^{2+} - O - O - SO_3^{-}\right] + 3H_2O + HSO_5^{-} \rightarrow 2\left[Cu^{2+} - OH\right]^{+} + 3SO_4^{2-} + 2\cdot O_2^{-} + 5H^{+} \tag{26}$$

Besides, $^1O_2$ would be produced through two different pathways (Eqs. (27)–(28)).

$$\left[Cu^{2+} - O - O - SO_3^{-}\right] + \cdot O_2^{-} + OH^{-} \rightarrow \left[Cu^{2+} - OH\right]^{+} + SO_4^{2-} + 3{}^1O_2 \tag{27}$$

$$2\cdot O_2^{-} + 2H_2O \rightarrow 2{}^1O_2 + H_2O_2 + 2OH^{-} \tag{28}$$

The route depicted by Eqs. (24)–(28) is the dominant process (Fig. 17a). Since rGO was confined in Cu-LDH layers, it wouldn't react with PMS directly, which was proved by a control experiment using rGO alone.

#### 4.2.2. *Mediated electron-transfer*

In some persulfate-AOPs, $SO_4^{\bullet -}$ and $^1O_2$ are not dominant reactive species and another persulfate activation mechanism has been proposed. In these activation processes, catalysts usually act as the electron transfer conductor, facilitating electron transfer from organic contaminants (donor) to persulfate (acceptor) (Fig. 17b). This mechanism has been proved in former studies (CuO (Zhang et al., 2014), N-CNTs (Duan et al., 2015b), N-doped graphene (Li et al., 2017)). These catalysts usually possess excellent electrical conductivity and can form charge transfer complex with persulfate for organics oxidation via electron abstraction. In the research of Zhang et al. Zhang et al. (2014), a complex of PDS with surface CuO was formed via outer-sphere interaction, then two electrons were abstracted from 2,4-DCP, resulting in the degradation of the latter. Similar nonradical process was observed in N-doped CNTs/PMS system. The activated carbon atoms could form strong interactions with PMS, forming a reactive complex and degrading phenol through electron abstraction (Duan et al., 2015b). Recently, there are studies reporting that Ni-based catalysts can induce nonradical PDS activation via generation complex with PDS molecules (Kim et al., 2020; Liu et al., 2019). The surface Ni-PDS complex can oxidize organic pollutants by electron transfer. It seems that the electron transfer usually

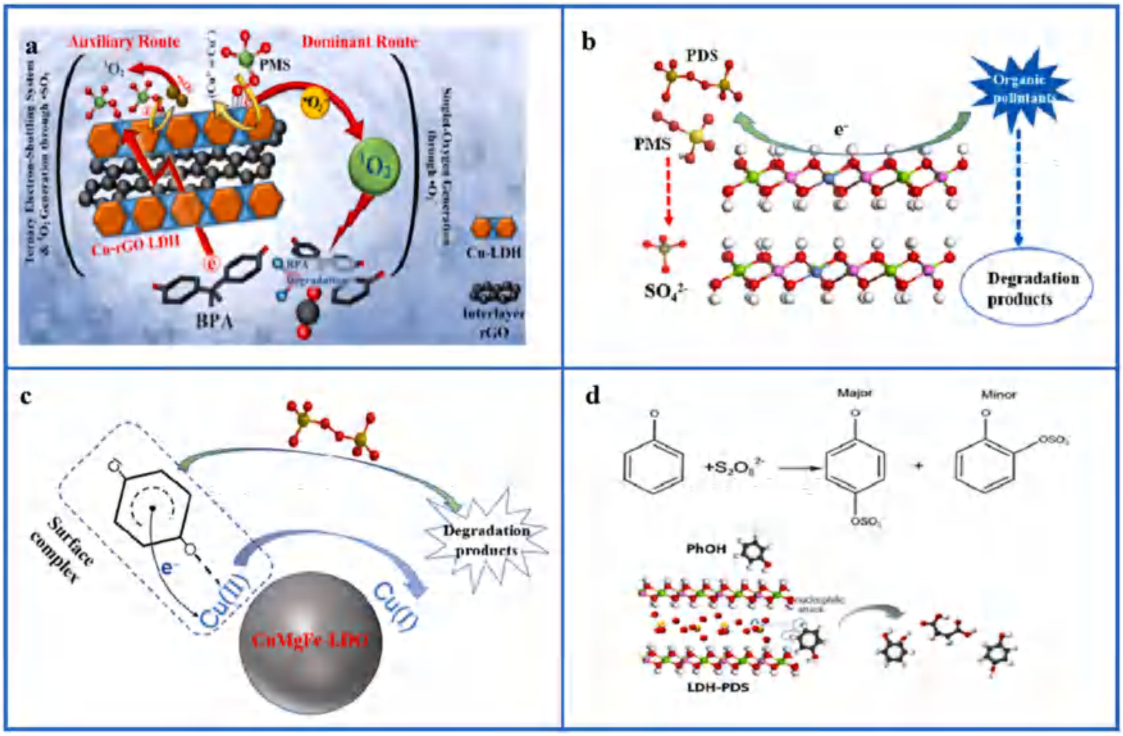

**Fig. 17.** Non-radical pathway in LDH/Persulfate system: (a) $^1O_2$ generation and mediated electron transfer. Reproduced with permission from Shahzad et al. (2020). Copyright 2020 Elsevier. (b) Mediated electron transfer. Reproduced with permission from Huang et al. (2020a). Copyright 2020 Elsevier. (c) Formation of surface complex with pollutants. Reproduced with permission from Chen et al., 2020. Copyright 2020 Elsevier. (d) Illustration of Elbs oxidation and PhOH oxidation in LDH-PDS. Reproduced with permission from (Huang et al., 2017; Behrman, 2006. Copyright 2017 Elsevier and 2006 Beilstein-Institut.

is accompanied by surface complexation of persulfate. But some researchers believed that it was not the prerequisite for this nonradical pathway (Yun et al., 2018). Until now, only a few studies point out the surface complex formation in LDHs-based catalysts/persulfate. Huang et al. mentioned a nonradical degradation pathway of phenol in Ni-LDH/PS system (Huang et al., 2020a), which could be attributed to direct oxidation by Ni(III). However, it is not clear whether the nickel on LDH surface forms a complex with phenol or with PDS. Shahzad et al. Shahzad et al. (2020) reported the existence of Cu-PMS complex in Cu-rGO LDH, but it led to the generation of $^1O_2$, instead of direct electron transfer to PMS. In addition, the interlayered rGO played the role of electron mediator which accelerated the shuttling from BPA to PMS. Thus, more studies are required to figure out mediated electron transfer mechanism for nonradical persulfate activation by LDH-based catalysts.

#### 4.2.3. *Surface metal complex with pollutants*

Unlike the complex mentioned above, active sites can react with pollutants rather than persulfate molecules to generate complex. It has been reported that CuO could form a complex with phenolic group of aromatic compounds and realize nonradical degradation of these contaminants in the presence of $H_2O_2$ (Lyu et al., 2015). Considering the similarity of $H_2O_2$ and persulfate, this mechanism might also exist in persulfate-AOPs. Chen et al. Chen et al., 2020 observed that the decomposition performance of monochlorobenzene (MCB) was lower than 4-Chlorophenol (4-CP) in a CuMgFe-LDO/PDS system. According to further experiments, they proposed the following mechanism: Initially, the surface Cu(II) could react with phenolic hydroxyl groups and a complex was formed on the surface of catalyst, where the orbital electron transfer from$\pi$to $Cu^{2+}$ would enhance the electronic polarizability of the aromatic ring (Lagutschenkov et al., 2010). Then, after accepting one electron of persulfate from Cu(II)-complex, $SO_4^{\bullet-}$ and chelated radical cations were produced. The latter would transfer one electron to Cu(II), resulting in Cu(I) production and 4-CP elimination (Fig. 17c). The formation of surface metal complex could facilitate the redox cycle of $Cu^{2+}/Cu^{+}$ and promote the catalytic performance. However, this mechanism is not observed in all copper-containing LDH@persulfate systems and the formation situation as well as degradation pathway are still worth further exploration.

#### 4.2.4. *Direct oxidation*

According to former studies (Zhu and Ford, 1991), PMS (mainly) and PDS could cause the hydroxylation of phenols via Elbs oxidation. In Elbs oxidation, the nucleophile (phenolate anion or a tautomer) will attack the peroxide oxygen of PDS and generate aromatic sulfates which will further hydrolyze to hydroxyl aromatics accompanying with S—O bond cleavage and resultant $SO_4^{2-}$ release (Behrman, 2006). The mechanism is shown in Fig. 6(d). This phenomenon was observed in the research of Huang et al. Huang et al. (2017). Due to the “intercalation effect” (latterly mentioned), the interlayer PDS will react with phenol which is adsorbed by LDH through Elbs oxidation (Fig. 17d).

### 4.3. *Interesting effects in LDH-based composites/persulfate system*

#### 4.3.1. *Synergistic effect in photo-activation of persulfate*

For the past few decades, photocatalytic technologies have become increasingly popular because of their low energy consumption, promising catalytic performance in energy conversion and environment remediation (Liang et al., 2021b; Liu et al., 2019; Luo et al., 2020; Pan et al., 2020; Shao et al., 2020a). Recently, photo-activation of persulfate has raised the concentration of researchers since photo-induced electrons can facilitate the process of persulfate activation.

Under visible light irradiation, some LDH-based catalysts will be motivated to produce photo-induced electrons and holes. Meanwhile, persulfate could act as an electron acceptor to inhibit the recombination of electron-hole pairs (Ma et al., 2018b). The electron will react with dissolved oxygen and produce $^{\cdot}O_2^-$ while holes combine with $OH^-$ and generate ·OH. Different metal ions in LDHs are connected via the medium of O and this special linkage is called oxo-bridge (Nakamura et al., 2007). The special connection can restrain the recombination of electron-hole by metal-to-metal charge transfer (Kim et al., 2014). Thus, the catalytic performance of photocatalysts for persulfate activation will be further improved by constructing heterostructures with LDHs (Zeng et al., 2020). A built-in electric field was established in the direct Z-scheme $CeO_2$ @LDH and the novel electric field could availably boost the migration of photogenerated carriers, restrain the recombination of electron-hole pairs and produce an increasing number of ROS ( Yang et al., 2021) (Fig. 18a). In $Bi_2O_3$/CuNiFe LDHs, motivated $e^-$ of $Bi_2O_3$ migrated to the CuNiFe LDHs via the interface and high-valent metal ions were reduced. Meanwhile, ·OH would be generated through the reaction between holes and $H_2O$/·OH on LDHs. Thus, effective separation of electron-hole was realized (Fig. 18b). Furthermore, $Cu^+$, $Fe^{2+}$, and $Ni^{2+}$ would then be re-oxidized to high-valent ions by PS. In the redox cycle, a large number of reactive substances would be produced, resulting in the effective decomposition of LOM. From the above discussion, we can expect that persulfate activation by photocatalysts may possess a brighter prospect compared with using other AOPs alone.

### 4.3.2. *Intercalation effect*

Because of the adjustable interior architecture, a variety of reactants could be intercalated into the inner gallery of LDH. The catalytic performance of the system will be improved evidently.

*4.3.2.1. PDS intercalation.* Huang et al. Huang et al. (2017) intercalated PDS into Mg/Al-LDH and the LDH-PDS composite exhibited high removal efficiency towards phenol. The proposed molecular structure of LDH-PDS was presented in Fig. 19a. By interacting with basic sites of LDHs, the S—O bond strength of peroxydisulfate would be weakened (Furman et al., 2010). Furthermore, molecular structure of intercalary PDS might be changed, possibly causing the adjustment of electrons as well as oxidation potential of PDS. In addition, the limited inner space of LDH protects the S—O bond from splitting then the succeeding formation of free radicals would be evaded (Zhang et al., 2014). Thus, the degradation process mainly followed a non-radical pathway (Elbs reaction). In their later researches, they utilized auxiliary activation methods (e.g., thermal activation (Huang et al., 2019)) and foreign catalysts compositing such as transition metal (Huang et al., 2020a) and rGO (Huang et al., 2020b)) to improve catalytic efficiency of persulfate-intercalated LDH. For instance, the intercalated PDS in rGO/LDH-PDS system was easier to be activated by defective edges of rGO and acquire better degradation performance of organic pollutants (Duan et al., 2016; Huang et al., 2020b). It is worthwhile that this special activation way only exists in the situation when using PDS but not PMS as the oxidant, which may be attributed to the structural differences between PMS and PDS.

*4.3.2.2. Reduced graphene oxide intercalation.* Abundant free electrons and unconfined ketone in rGO enable it to display remarkable electrical conductivity (Sun et al., 2012b). If the problem of aggregation could be avoided, the ultrathin or monolayers of rGO would significantly accelerate electron transfer to promote catalytic performance since more energy gaps were kept (Ghanbari and Moloudi, 2016). Coincidently, the inner space of LDHs could keep rGO in the form of single layer and inhibit its agglomeration. Two LDH-rGO composites with different structures were applied in PMS activation to degrade phenol (Shahzad et al., 2019). Compared with Fe-LDH/rGO composite, the Fe-rGO LDH showed higher degradation efficiency towards phenol (100% removal efficiency in 30 min) than the former (63%), which might be because the existence of monolayered rGO inside LDHs significantly accelerate the $Fe^{III}/Fe^{II}$ cycle. This improvement in catalytic performance by rGO intercalation was also observed in OER (Ma et al., 2015) and electrochemical biosensing (Asif et al., 2019). Accordingly, the periodically stacking superlattice structure of LDH nanosheets and monolayered rGO could strengthen the contact between transition metal and rGO on molecular level, thus promoting charge shuttling and substance diffusion Fig. 19b.

The excellent property of rGO-LDH credits the intercalated rGO might proceed a synergistic effect with transition metals (such as Fe, Cu) in charge transfer and redox process. Notably, the rGO-mediated specific charge transfer route of “organic pollutants-LDHs-rGO-persulfate” is still worth further investigation.

*4.3.2.3. $MoS_4^{2-}$ intercalation.* Generally, metal elements usually act as basic units of LDH laminates. But Ali et al. Ali et al. (2020) improved the Fe(III)/Fe(II) redox cycle via introducing $MoS_4^{2-}$ into inner space of Fe-LDH. According to XPS analysis, the binding energy of Fe 2p for FeMgAl-$NO_3^-$ was higher than that in $MoS_4^{2-}$ intercalated LDH, implying that $MoS_4^{2-}$ intercalation could retain Fe in low oxidation state (Fig. 19c-19d). The intercalated $MoS_4^{2-}$ established a new redox center, which remarkably accelerated the transformation of inactive ≡Fe(III)/Mo(VI) into active ≡Fe(II)/Mo(IV) via constant electron transfer. Additionally, there may exist the formation of surface complexes that promote the generation of $SO_4^{\bullet-}$. Moreover, this material could keep good catalytic performance under variation of adverse environmental conditions like pH, inorganic anions as well as organic substances, which implies its prospects in real application.

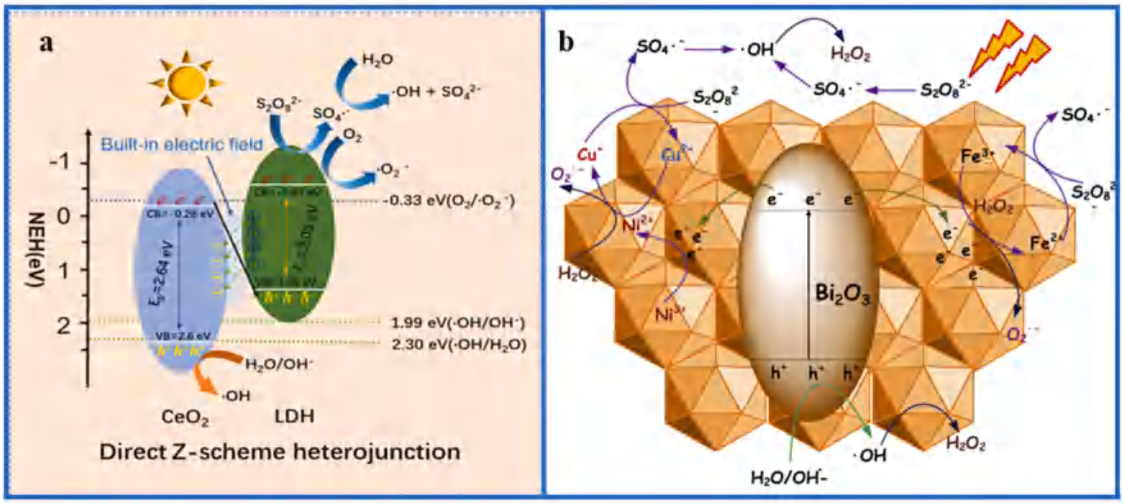

**Fig. 18.** **(a)** The electrons transfer process in $CeO_2$ @LDH. Reproduced with permission from Yang et al., 2021. Copyright 2020 Elsevier. (b) Photocatalytic activation of persulfate by $Bi_2O_3$/CuNiFe LDHs for LOM degradation. Reproduced with permission from Zhang et al., 2020 . Copyright 2020 Elsevier.

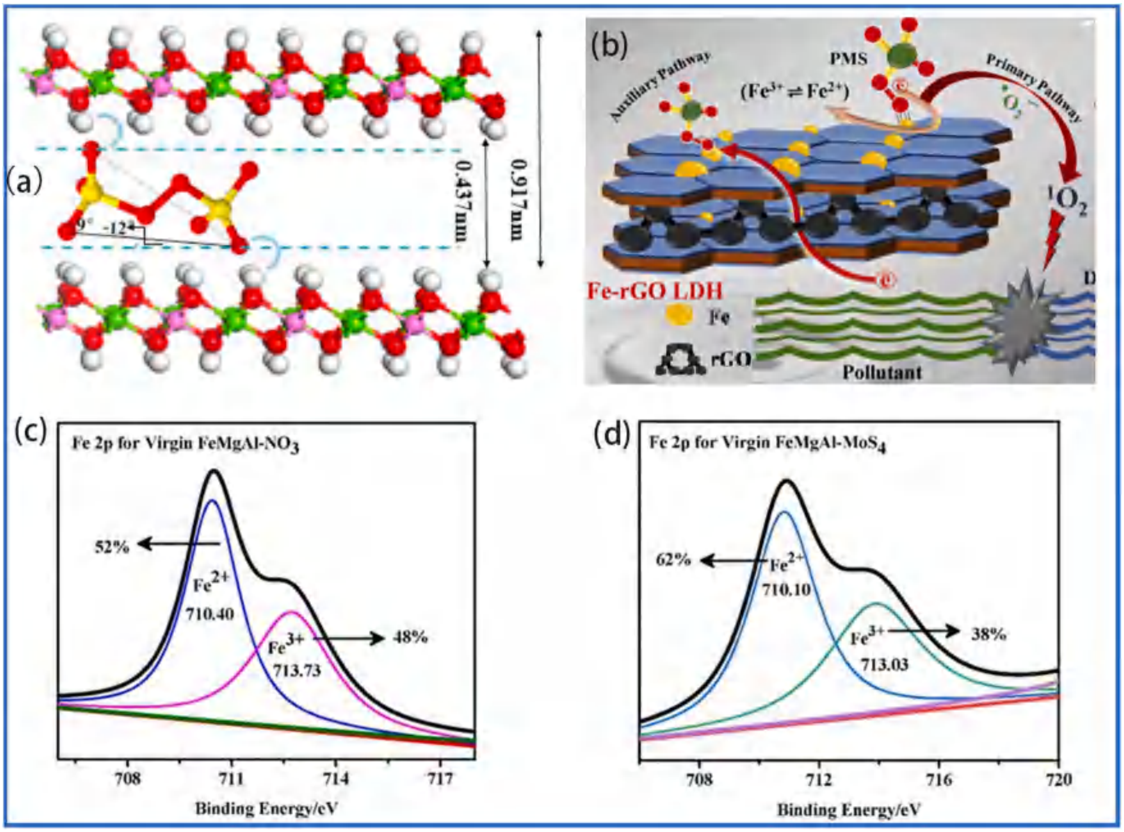

**Fig. 19.** (a) Proposed molecular structure of LDH-PDS. Reproduced with permission from Huang et al. (2017). Copyright 2017 Elsevier. (b) Different pathways of PMS activation by Fe-rGO. Reproduced with permission from Shahzad et al. (2019). Copyright 2019 Elsevier. XPS pattern showing the oxidation states of Fe (c) Fe in FeMgAl-$NO_3^-$ (d) Fe in virgin FeMgAl-$MoS_4^{2-}$. Reproduced with permission from Ali et al. (2020). Copyright 2020 Elsevier.

Base on the discussions above, whether the interlayer content was persulfate or catalyst, the magic inner space will give full play to these intercalated contents' potential. The intercalation is usually accompanied by nonradical reactions in LDH@persulfate system, which enables the LDH composites to remain effective in complex solution conditions. Of course, the intercalated LDH could also facilitate the generation of $SO_4^{\bullet-}$ (e.g., the $MoS_4^{2-}$ intercalated LDH). Moreover, the intercalated LDH exhibits a lower ion leaching rate as well as increased persulfate utilization efficiency, which makes the composite, a promising catalyst for wastewater treatment. We can consume that with the variation of intercalated matters, the reaction mechanism will present different features. Thus, it is important to figure out the reactive species and reaction pathways by combining advanced characterization and theoretical calculation.

## 5. Effect of different factors on catalytic performance

### 5.1. Intrinsic properties of catalysts

The species of metal elements, intercalated anions, structure and doped materials all have an influence on the catalytic efficiency of LDH-based materials. Catalysts containing cobalt usually have higher activation efficiency while the carcinogenic potential of cobalt is troublesome. Thus, researchers have developed various strategies to improve the activation efficiency of other metal elements. For instance, introducing new redox center (Ali et al., 2020; Yue et al., 2020), preparing 3D LDO with more active sites ( Chen et al., 2020), and coupling with carbonaceous materials are all conducive to enhance the catalytic performance of LDHs (Shahzad et al., 2020). In fact, the intrinsic properties like type of components, the ratio between different elements in composites and morphology of LDH-based catalysts are the decisive factors in persulfate activation.

### 5.2. Dosage of catalysts and persulfate

In general, increasing the concentration of LDH-based catalysts can improve the removal efficiency of contaminants since there will be more active sites for ROS production. For example, the degradation efficiency of CBZ reached 100% as the concentration of CoMgFe-LDO rose from 5 mg/L to 20 mg/L (Hong et al., 2020). However, higher concentration led to the degradation rate drop down to 92.6%, which might be attributed to the scavenger effect of the excessive metallic sites to radicals (Feng et al., 2015; Hammouda et al., 2017). In addition, the overmuch catalysts could also cause diffusion limitation and result in decreased elimination efficiency (Zhang et al., 2013; Jawad et al., 2018). Similarly, the removal efficiency is not always positively correlated with the concentration of persulfate. A moderate increase in persulfate dosage can facilitate the generation of ROS. The excessive persulfate may have slight promoting effect or even adverse effect on the catalytic performance. This phenomenon may result from the self-quenching of persulfate and the competition of persulfate and pollutants to radicals (Wu et al., 2020b; Jiang et al., 2018). Therefore, the dosage of catalysts and persulfate is not the more the better. On the one hand, adding more catalysts and persulfate means higher cost. On the other, the excessive addition may have little attributive effect or even have a negative influence on the degradation efficiency of contaminants.

### 5.3. Type of persulfate

Despite both PMS and PDS can be used to produce $SO_4^{\bullet -}$, there are differences in catalytic process due to their differences in molecular structure. PMS possesses an asymmetrical structure with a shorter peroxide bond while PDS is symmetrical with longer peroxide bond (Wang and Wang, 2018). As a result, PMS is more vulnerable to be attacked by nucleophiles such as halide ions, azide ion and bicarbonate (Lou et al., 2017; Jiang et al., 2017). Thus, PMS can be activated by some anions like $Cl^-$, $CO_3^{2-}$, $HCO_3^-$ while PDS cannot be activated by these ions. Moreover, the mechanisms of alkaline activation and phenol/quinones activation by PDS/PMS are also different. Activation of PDS by alkaline/ phenol/quinones undergoes reduction while PMS is activated through nucleophilic addition (Lee et al., 2020; Furman et al., 2010; Ahmad et al., 2013; Zhou et al., 2015). In addition, despite the dissociation energy of O—O bond in PDS is lower than that in PMS, the latter is easier to be activated by heterogeneous catalysts than the former because of the molecular asymmetry (Gao et al., 2020).

Due to the weaker O—O bond in PDS, it can be activated more effectively by external energy input (e.g., ultraviolet radiation, heating) (Luo et al., 2015; He et al., 2013; Yang et al., 2010). For instance, Huang et al. reported that the intercalation effect could decrease the activation energy of PDS and realize effective PDS activation at a relatively low temperature (Huang et al., 2019).

So far, researchers have utilized LDH-based catalysts to effectively activate PMS or PDS. But hardly has a study discussed the possible differences between PDS and PMS in activation mechanism and degradation performance when using the same kind of LDH-based catalyst.

### 5.4. pH

The influence of pH value on the degradation efficiency can be divided into three aspects. Firstly, free radicals generated from persulfates can be affected by different pH values. The excessive $H^+$ in acid solution can form strong hydrogen bonds with O—O bond in PMS, thus restraining the interaction between catalysts and PMS (Du et al., 2016). Moreover, $H^+$ can scavenge $SO_4^{\bullet -}$ and ·OH under highly acid condition (Wang and Wang, 2018). Under overly basic condition (pH>9), there will be a large number of·OH generated from the reaction between $OH^-$ and $SO_4^{\bullet -}$ (Hong et al., 2020, 2019). Additionally, the alkaline condition can also lead to the hydrolysis and self-decompose of PMS (Rastogi et al., 2009). Notably, it seems that PDS displays higher stability than PMS with the variation of pH value. It might be because that the much lower $pK_a$ value makes PDS less prone to protonation (Wu et al., 2020a).

Secondly, the pH value has some impact on the properties of LDH-based catalysts. It is generally known that the structure of LDHs would be destroyed under low pH condition and cause metal leaching (Yue et al., 2020). At higher pH, the metal ions on LDHs might turn into metallic hydroxide complexes, resulting in the decreased oxidation capacity (Hong et al., 2020, 2019; Hu and Long, 2016). Moreover, when the pH of solution exceeds the $pH_{zpc}$, there will be more negative charge on the surface of LDH, which may cause electrostatic repulsion between catalysts and persulfate.

Finally, the pH value can influence the degradation efficiency by affecting the existing state of pollutants. The degree of deprotonation of contaminants is usually positively correlated with their reactivity (Wang and Wang, 2018). For instance, the deprotonated SMX was easier to be attacked by $SO_4^{\bullet -}$ (Qi et al., 2014). Certainly, pH value may have less influence on the morphology of some pollutants (e.g., CBZ) since they can keep electroneutral within a wide pH range (Hong et al., 2020).

### 5.5. Inorganic ions and natural organic matter (NOM)

In natural water environment, there are a mass of anions and NOM, which can affect the reaction of ROS with contaminants. It has been widely reported that inorganic ions like $Cl^-$, $CO_3^{2-}$, $HCO_3^-$, $H_2PO_4^-$ and $NO_3^-$ can act as the quencher of $SO_4^{\bullet -}$ and·OH (Ghanbari and Moradi, 2017). Notably, some anions also have positive effect on persulfate activation. For example, Hong et al.Hong et al. (2019) observed that the addition of $Cl^-$ could slightly increase the degradation efficiency of ATZ, which might be attributed to the formation of reactive chlorine species (e.g., HOCl and $Cl_2^{\bullet -}$). In addition, there are also studies reporting the PMS activation by $HCO_3^-$ and $HPO_4^-$ via nucleophilic attack (Lou et al., 2017; Jiang et al., 2017). Besides the quenching effect to ROS, some inorganic ions can occupy the active sites on the surface of catalysts and cause the decrease of catalytic performance (Shahzad et al., 2020). Despite the presence of inorganic ions can facilitate persulfate activation in some specific cases, these ions often usually act as inhibitors.

Similarly, NOM in water also has inhibiting and promoting effects on the activation of persulfate. It has been confirmed that NOM can play the role of scavenger for ROS thus inhibit the degradation of pollutants. Besides, NOM may be adsorbed by LDH-based catalysts and occupy the active sites, restraining the adsorption of contaminants (Shah et al., 2019). However, some functional groups in NOM are proved to have the ability to activate persulfate. For instance, quinone, hydroquinone and phenol can form semiquinone radicals which can facilitate the activation of persulfate and generate $SO_4^{\bullet -}$ (Fang et al., 2013; Guan et al., 2013).

Until now, the inhibiting and promoting effects of inorganic ions and NOM on persulfate activation are still complicated and needing more in-depth studies.

### 5.6. Temperature

As is well known that heating can effectively accelerate the cleavage of O—O bond in persulfate and generate $SO_4^{\bullet -}$. In addition, the increase of temperature can boost the reaction kinetic according to the thermodynamic principle (Hori et al., 2008). For instance, the degradation efficiency of phenol was 69% in CuOx@Co-LDH/PS system at 25 °C while it came to 100% at 40 °C (Jawad et al., 2018). However, the high energy consumption makes it difficult to promote thermal activation in practical wastewater treatment. Furthermore, the overly high temperature can cause the recombination of free radicals and decrease the stability of catalyst (Johnson et al., 2008). Therefore, it is essential to critically evaluate the pros and cons of different temperature in persulfate/LDH system.

## 6. Application in contaminant decomposition

### 6.1. Pharmaceuticals

In recent years, various antibiotics have been developed to fight against pathogenic microorganisms. Despite these antibiotics have saved numerous lives, the consequent problem of resistance to antibiotics raised growing concern. As a matter of fact, only a small fraction was utilized and large quantities of antibiotics were released to the environment. Generally, the unused antibiotics can be easily detected in wastewater of hospitals, animal husbandry, agriculture and aquaculture. However, traditional biological processes could not degrade antibiotics efficiently. The persulfate-based AOPs with strong oxidation capacity are seen as a promising method for treating antibiotics (Ji et al., 2014).

Chen et al. Chen et al. Chen et al., 2020 prepared CuO-MgMn-LDO with excellent catalytic performance, which removed nearly 97% of SMX in 30 min. The outstanding performance of persulfate activation for SMX degradation could be attributed to the synergistic effect (Cu-Mn) as well as numerous oxygen vacancies. Under the attack of $^1O_2$ and $SO_4^{\bullet -}$, SMX was degraded to hydroxylamine derivative and other intermediates with simpler molecular structure. In the end, these intermediates would be oxidized to $CO_2$ and $H_2O$. Moreover, the composite also displayed high removal efficiency towards other antibiotics such as ciprofloxacin (CIP), tetracycline (TC) and sulfadiazine (SDZ), indicating CuO-MgMn-LDO possesses wide adaptability for the degradation of antibiotics. Encouragingly, the composite could keep a low level of Cu dissolution as well as sustained activity under varying pH condition. Despite the SMX degradation performance decreased slightly in the solution prepared from natural water, which may be related to the influence of humic acid and anion in natural water. This composite is still worth expectancy in the actual treatment of antibiotics. Zhang et al. fabricated a new $Bi_2O_3$/CuNiFe LDH composite which could degrade 84.6% of LOM under simulated sunlight ( Zhang et al., 2020). The degradation of LOM was achieved via a series of processes like hydroxylation, defluorination, decarboxylation and other complex reactions. Finally, intermediates would transform to $CO_2$, $H_2O$ and inorganic substances.

Besides antibiotics, residues of other pharmaceuticals in wastewater have raised great concern because of the potential threat to human as well as aquatic creatures. Carbamazepine (CBZ), a typical anticonvulsant medication mainly applied in the treatment of epilepsy and neuropathic pain (Jelic et al., 2012). It has been reported that CBZ could cause great harm to aquatic organisms (Moztahida et al., 2019; Ferrari et al., 2003). A CoMgFe-LDO composite with 3D flower morphology (as shown in Fig. 20a) exhibited excellent catalytic performance to activate persulfate for CBZ decomposition (Huang et al., 2020c). Due to the synergistic effect of Co/Fe, surface redox cycle was accelerated and produced highly reactive $SO_4^{\bullet-}$ and ·OH, which would degrade CBZ to transformation products through epoxidation, hydrolysis, heterocyclic ring-opening and other processes. In addition, the ZnFe-LDH/GO composite could realize elimination of phenazopyridine hydrochloride (PhP) (Motlagh et al., 2020), which is an analgesic that can relieve pain in urinary tract inflammation but may induce cancer in organisms (Khataee et al., 2016; Green et al., 1979). LDH-based catalysts usually possess flexible tunability, good adsorption capacity as well as high catalytic performance in persulfate-AOPs, which makes them display encouraging removal efficiency towards various pharmaceuticals. For dealing with the huge amount of pharmaceutical wastewater in factories, we still need more efforts to address problems of LDH-based catalysts like recyclability, stability, continuous catalytic performance and mineralization efficiency.

### 6.2. Benzene derivatives

Benzene derivatives like BTEX, nitrobenzene (NB), phenol, chlorobenzene and chlorophenol have been widely used industrial products, intermediates and solvents. Most of the benzene derivatives are difficult to degrade due to their stable structures ( Chen et al., 2020Chen et al., 2020). When exposed to these derivates in environment, the health of human and other organisms will be damaged seriously. Some benzene derivatives could increase the risk of mutagenicity and carcinogenicity even in low concentration. Huang et al. Huang et al. (2020a) employed Ni-doped MgAl-LDH to activate PDS for the treatment of phenol and 4-bromophenol. The degradation rate was nearly 100% and 74.3%, respectively. Lu et al. (2019) prepared a CuCoFe-LDH which realized complete elimination of NB in 6 min. Hydroxyl radical was produced via the reaction between PMS and metal ions on the catalyst. Latterly, NB was attacked by •OH and formed nitrophenol, p-di-produce nitrophenol, p-diphenol and other intermediates. These products would then convert to short-chain carboxylic acids and some would transform to $CO_2$ and $H_2O$ finally.

Based on these literatures, it can be concluded that LDH-based composites have the potential for degradation of benzene derivatives via effective persulfate activation. But notably, the degradation rate of some benzene derivatives was unsatisfactory relatively. For instance, compared with the high decomposition rate of phenol, 4-CP and p-nitrophenol (almost 100%), NB and MCB displayed a low elimination rate in Cu-LDO/PS system (0.7% and 31.7%) (Chen et al., 2020). It was believed benzene derivatives which have hydroxyl groups could be decomposed more rapidly in Cu-LDO/PS system, which might be attributed to the different reaction pathways (Chen et al., 2020). In

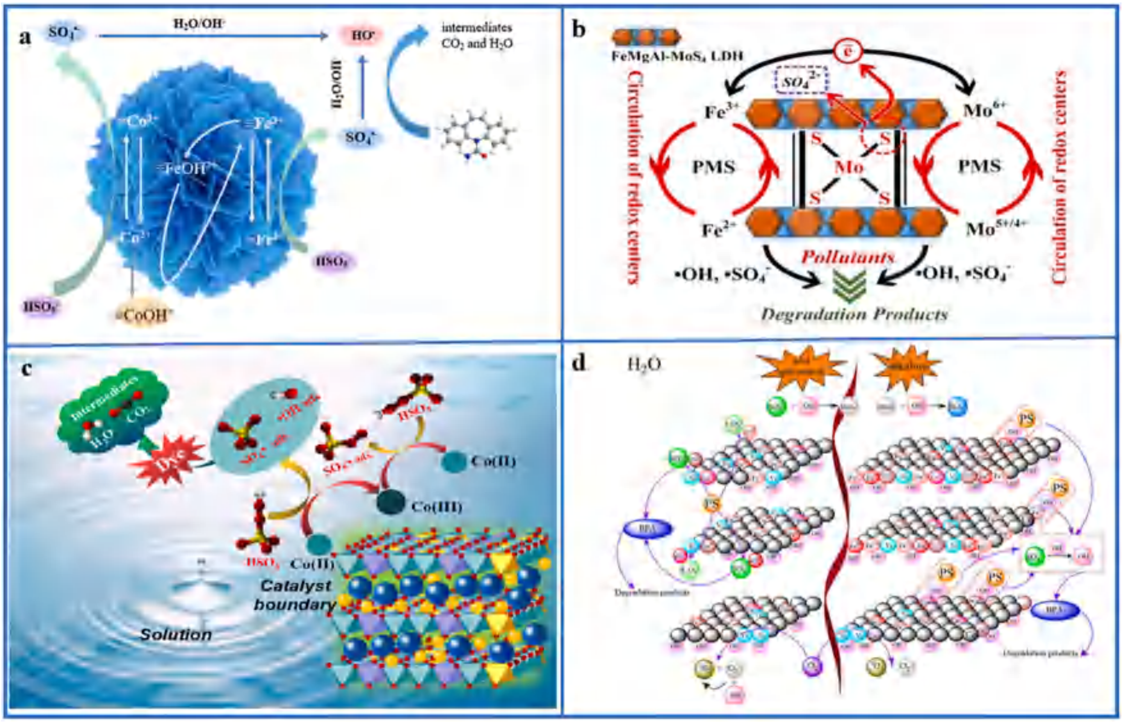

**Fig. 20.** Degradation mechanism of different organic contaminants (a) CBZ. Reproduced with permission from Huang et al. (2020c). Copyright 2020 Elsevier. (b) benzene derivatives. Reproduced with permission from Ali et al. (2020). Copyright 2020 Elsevier. (c). CR/RhB. Reproduced with permission from Zeng et al. (2018). Copyright 2020 Elsevier. (d) Copyright 2018 Elsevier. BPA Reproduced with permission from Wu et al. (2020a).

**Table 3**
Catalytic performance of LDH-based composites applied in contaminants degradation.

| Catalyst | Contaminant | Reaction Conditions | Removal efficiency | Main ROS | Metal leaching | Recyclability | Ref |
|---|---|---|---|---|---|---|---|
| **Metal/metal oxide doped LDHs** | | | | | | | |
| NiFe-LDH | TC<br>2,4,6-trichlorophenol (TCP)<br>BPA | [PDS]= 0.4 g/L<br>[TC]= 50 mg/L<br>[TCP]= 50 mg/L<br>[BPA]= 100 mg/L<br>[Cat]= 0.5 g/L | 100% in 10 min<br>100% in 20 min<br>100% in 10 min | $SO_4^{\bullet-}$ | – | 100% after 4 cycles | (Yue et al., 2020) |
| NiMgAl-LDH | Phenol<br>4-bromophenol<br>2-methylisoborneol | [PS]= 0.74 mM<br>[LOM]= 10 mg/L<br>[Cat]= 0.4 g/L | 84.6% in 40 min | $\cdot OH$, $SO_4^{\bullet-}$<br>$\cdot O_2^-$, $h^+$ | Ni: 0.098 mg·L$^{-1}$ | – | (Huang et al., 2020a) |
| CuMgFe-LDH | Ethylbenzene | [PDS] = 4 mM<br>[Cat]= 0.2 g/L<br>[Ethylbenzene] = 0.08 mM | 93.7% in 25 min | $\cdot OH$, $SO_4^{\bullet-}$ | Cu: 0.095 mg/L<br>Fe: 0.064 mg/L<br>Mg: 0.125 mg/L | 83.9% after 5 cycles | (Yan et al., 2017) |
| CoFeNi-LDH | Congo red(CR)<br>Rhodamine B(RhB) | [PMS]= 0.15 mg/L<br>[Cat]= 0.2 g/L<br>[CR]= 20 mg/L<br>[RhB]= 20 mg/L | nearly 100% in 6 min<br>nearly 100% in10 min | $SO_4^{\bullet-}$ | Co: 0.68 mg/L | 95% after 4 cycle | (Zeng et al., 2018) |
| CuCoFe-LDH | NB | [PS]= 0.5 mM<br>[NB]= 16 μM<br>[Cat]= 0.1 g/L | over 99% within 6 min | $\cdot OH$ | Co: 34 μg/L<br>Cu: 92 μg/L | 85% after 5 cycles | (Lu et al., 2019) |
| MnFe-LDH | Acid Orange 7 | [PMS]= 0.20 g/L<br>[AO7]= 20 mg/L<br>[Cat]= 0.20 g/L | 97.56% in 30 min | $SO_4^{\bullet-}$,$\cdot OH$ | Mn: 0.54 mg/L<br>Fe: not detected | over 90% after 5 runs | (Hou et al., 2019) |
| FeCo-LDH | BPA | [PS] = 4 mM<br>[BPA]= 30.0 mg/L<br>[Cat] = 0.5 g/L | 99.38% in 60 min | $SO_4^{\bullet-}$,$\cdot OH$<br>$\cdot O_2^-$,$^1O_2$ | – | 71.27% after 5 cycles | (Wu et al., 2020a) |
| FeMgAl-MoS$_4$LDH | PHB<br>4-CP<br>2,4-DCP<br>BA<br>Phenol<br>NB | [PMS]= 5 mM<br>[Pollutant]= 10 ppm<br>[Cat]= 0.25 g/L | 100% in 1 h<br>100% in 1 h<br>100% in 1 h<br>100% in 1 h<br>60%– 70% in 1 h<br>60%– 70% in 1 h | $SO_4^{\bullet-}$,$\cdot OH$ | – | 77% after 5 cycles (PHB) | (Ali et al., 2020) |
| **LDHs with metal oxide semiconductor** | | | | | | | |
| Bi$_2$O$_3$/CuNiFe | LOM | [PS]= 0.74 mM<br>[LOM]= 10 mg/L<br>[Cat]= 0.4 g/L | 84.6% in 40 min | $\cdot OH$, $SO_4^{\bullet-}$<br>$\cdot O_2^-$, $h^+$ | – | 74.3% after 4 cycles | (H. Zhang et al., 2020, W. Zhang et al., 2020) |
| Z-scheme CeO$_2$ @LDH | Rhodamine B<br>Methylene blue<br>Methyl orange<br>TC | [PMS]= 6 mM [Cat]= 0.4 g/L<br>[RhB]= 10 mg/L<br>[MB]= 5 mg/L<br>[MO]= 10 mg/L<br>[TC]= 10 mg/L | 96.9% in 30 min<br>91.7% in 30 min<br>91.2% in 30 min | $SO_4^{\bullet-}$,$\cdot OH$<br>$\cdot O_2^-$ | – | 91.6% after 4 cycles | (Yang et. al., 2021) |
| **LDOs with transition metals** | | | | | | | |
| CoMgAl-LDO | ATZ | [PMS]= 0.4Mm<br>[ATZ]= 10 mg/L<br>[Cat]= 75 mg/L | 98.7% in 15 min | $SO_4^{\bullet-}$ | Co: 0.15 mg/L | 81.1% after 4 cycles | (Hong et al., 2019) |
| CuO-MgMn-LDO | SMX | [PS]= 1.0 mM<br>[SMX]= 0.02 mM<br>[Cat]= 0.4 g/L | 97% in 30 min | $^1O_2$, $SO_4^{\bullet-}$ | Cu< 1.0 mg·L$^{-1}$<br>Mn< 1.0 mg·L$^{-1}$ | 88% after 5 cycles | (Y. Chen et al., 2020; M. Chen et al., 2020) |
| CoMgFe-LDO | CBZ | [PS]= 0.2 g/L<br>[CBZ]= 5 mg/L<br>[Cat]= 20 mg/L | 100% in 20 min | $SO_4^{\bullet-}$,$\cdot OH$ | Co:0.04 mg/L<br>Fe 0.27 mg·L$^{-1}$ | 80.9% after 3 cycles | (Hong et al., 2020) |
| CuOx@Co-LDH | Phenol | [PDS] = 2 mM<br>[Cat] = 0.3 g/L<br>[phenol] = 0.1 mM | 100% in 40 min | $\cdot OH$,<br>$SO_4^{\bullet-}$,$\cdot O_2^-$ | Co: not detected<br>Cu: 0.08 mg/L | – | (Jawad et al., 2018) |
| MgAl-Cu-LDO | Phenol | [PDS]= 0.5 g/L<br>[ Phenol]= 10 mg/L<br>[Cat]= 0.3/L | 100% in 20 min | $SO_4^{\bullet-}$,$\cdot OH$ | Cu< 0.4 mg/L | – | (Guo et al., 2018) |
| **LDH-carbonaceous composites** | | | | | | | |
| CNTs-CoMnAl-LDO | BPA | [PMS]= 0.15 g/L<br>[ Phenol]= 20 mg/L<br>[Cat]= 0.02/L | 100% in 10 min | $SO_4^{\bullet-}$ | Mn: < 0.005 mg /L<br>Co: < 0.1 mg /L | Nearly 100% after 3 cycles | (Li et al., 2015) |
| FeMgAl-rGO LDH | Phenol | [PMS]= 5 mM<br>[ Phenol]= 0.2 mM<br>[Cat]= 0.15 g/L | 100% in 10 min | $^1O_2$ | – | 88% after 3 cycles | (Shahzad et al., 2019) |
| Cu-rGO LDH | BPA | [PMS]= 3 mM<br>[BPA]= 0.09 mM<br>[Cat]= 0.25 g/L | Over 99% in 40 min | $^1O_2$ | – | 84% after 3 runs | (Shahzad et al., 2020) |
| MgAl-LDH/rGO | Phenol | | | | – | 50% after 4 cycles | (Huang et al., 2020b) |

(continued on next page)

**Table 3** (*continued*)

| Catalyst | Contaminant | Reaction Conditions | Removal efficiency | Main ROS | Metal leaching | Recyclability | Ref |
|---|---|---|---|---|---|---|---|
|  | BPA | [PDS]= 0.4 mM<br>[phenol]= 0.032 mmol/L<br>[BPA]= 0.022 mM<br>[Cat]= 1 g/L | 92.4% in 15 min<br>100% in 60 min | $SO_4^{\bullet-}$<br>Intercalated-PDS |  |  |  |
| ZnFe-LDH/GO |  | PhP | [PS]= 1 mM<br>[PhP]= 15 mg/L<br>[Cat]= 1 mg/mL | 93.95% in 150 min | $SO_4^{\bullet-}$, $\dot{}O_2^-$<br>·OH, $h^+$ | Zn:1.249 $mg{\cdot}L^{-1}$<br>Fe 0.2759 $mg{\cdot}L^{-1}$ | Nearly 82% after 5 cycles |
| (Motlagh et al., 2020) |  |  |  |  |  |  |  |
| CoAl-LDH/g-$C_3N_4$ | Sulfadiazine (SDZ) | [PS]= 0.5 g/L<br>[SDZ]= 10 μM<br>[Cat]= 0.1 g/L | 87.1% in 15 min | $h^+$,·OH,$\dot{}O_2^-$,<br>$SO_4^{\bullet-}$,$^1O_2$ | Co< 0.2 $mg{\cdot}L^{-1}$ | 80.2% after 4 cycles | (Zeng et al., 2020) |
| Zn-Co-LDH-Biochar | GMF | [PS]= 3 mM<br>[GMF]= 15–35 mg/L<br>[Cat]= 0.15–0.75 g/L | 97.7% in 130 min | ·OH, $h^+$,$\dot{}O_2^-$ | – | > 87.7% after 5 cycles | (Gholami et al., 2020) |
| AC@CoFe-LDH | LOM | [PS]= 1 g/L<br>[LOM]= 5 mg/L<br>[Cat]= 0.2 g/L | 93.2% in 60 min | $SO_4^{\bullet-}$,·OH | – | 80.9% after 4 cycles | (Ma et al., 2020a) |
| CoMn- LDH/rGA | MTZ | [PMS] = 0.15 g/L<br>[MTZ]= 0.02 g/L [Cat] = 0.5 g/L | 93.7% in 10 min | $SO_4^{\bullet-}$,$^1O_2$<br>·OH | Co:0.60 mg/L<br>Mn:0.45 mg/L | 86% after 10 cycles | (He et al., 2021) |
|  | **Other LDH composites** |  |  |  |  |  |  |
| CuCo-LDH@PAN | SMX | [PMS] = 0.24 mM<br>[SMX]= 0.032 mM<br>[Cat] = 60 mg/L | 95.2% in 30 min | $SO_4^{\bullet-}$ | – | 95% after 10 cycles |  |
| CoFe-LDHs@PVDF | MB | [PMS] = 0.5 mM<br>[MB]= 0.032 mM | 100% in 6 min | $SO_4^{\bullet-}$,$^1O_2$ | Co:4.628 mg/L<br>Fe:0.036 mg/L | 99.56% after 10 cycles(MB) | (Li et al., 2021) |
|  | TC | [TC]= 20 mg/L<br>[BPA]= 20 mg/L | 98.59% in 10 min |  |  |  |  |
|  | BPA |  | 86.65% in 10 min |  |  |  |  |

addition, some benzene derivatives such as BA and NB are seen as chemical scavengers for reactive radicals, which could result in a decrease of decomposition efficiency (Ali et al., 2020). This evident difference in degradation performance was also observed in the research of Ali et al. (2020). The degradation rate of 4-CP was much higher than NB, which might be attributed to the selectivity of $SO_4^{\bullet-}$.

### 6.3. *Synthetic organic dyes*

With the rapid development of contemporary industry involving textile industry, leather tanning industry, paper manufacturing industry, food production photoelectrochemical cells, pharmaceutical industry, etc., masses of synthetic organic dyes were discharged in effluents (Martínez-Huitle and Brillas, 2009; Brillas and Martínez-Huitle, 2015). Due to the environmental threat and wide existence, organic dyes have become hot target contaminants in AOP researches. Generally, LDH-based materials exhibit good performance in decomposition for organic dyes despite there is a little slight difference in degradation efficiency because of the structure of dyes as well as the type of catalysts. Due to the strong oxidation power of LDH/persulfate system, the original molecule of organic dyes will be destroyed and turn into small compounds. Sulfonate group, azo-group, ethyl group and other functional groups could be cleaved by ROS, forming low-molecular-weight intermediates. After a series of ring-opening and oxidation processes, some of the intermediates are converted to $CO_2$ and $H_2O$ (Hou et al., 2019; Gong et al., 2017). (Fig. 20c).

### 6.4. *Bisphenol A*

Recently, the threat of endocrine disrupting chemicals (EDCs) has raised great concern for their negative effects on organisms. Bisphenol A is a typical EDC for the manufacture of epoxy resin and polycarbonate (Gorini et al., 2020b). BPA could interact with human estrogen receptors and influence estrogen-target organs (Welshons et al., 2006). Chrono exposure to BPA may cause adverse effects such as reproductive disorders (Mínguez-Alarcón et al., 2016), cardiovascular disease (Han and Hong, 2016), obesity (Carwile and Michels, 2011) and a series of human diseases. Accordingly, BPA is often employed as a target pollutant for evaluating the catalytic capability of LDH-based catalysts. BPA could be effectively decomposed by $SO_4^{\bullet-}$ and ·OH generated by LDH@persulfate system (Fig. 20d). Both aliphatic-ring opening products and aromatics were discovered in the degradation reaction. In addition, the molecular structure of degradation products became increasingly simpler with the reaction proceeding. Finally, these compounds were degraded to $CO_2$ and $H_2O$ (Wu et al., 2020a). (Table 3).

## 7. Conclusion and outlooking

Due to the advantages of highly tunable composition, affordable cost, low toxicity and simple synthesis, the potential in persulfate-AOPs of LDH-based composites has gradually attracted concerns. Raw LDHs usually clump in bulk form and display limited catalytic performance. Thus, exfoliating bulk LDHs into mono-/few-layer nanosheets and growing 3D LDHs are of great significance to promote their catalytic efficiency since larger surface area and more active sites are exposed. In addition, calcinating LDHs to LDOs can further enhance catalytic activity. Persulfate activation mechanisms, involving radical pathway ($SO_4^{\bullet-}$,·OH) and non-radical pathway ($^1O_2$, mediated electron transfer, etc.) were summarized in detail. We also paid attention to some encouraging effects such as photocatalytic activation of persulfate and intercalation effect, which enable LDH-based materials to realize effective persulfate activation.

Despite the prospects of LDH-based catalysts in persulfate-AOPs seem bright, there are still roadblocks on the way to further industrial applications. And researchers should make more efforts to address tricky problems like toxicity, recyclability and long-term stability.

(1) Optimization of synthesis process

Structure, chemical composition, and the proportion of different ingredients will have great influence on the physical and chemical characteristics of catalysts. Since properties of catalysts and pollutants can affect the catalytic performance, researchers should design and synthesize LDH-based composites according to specific situations. In addition, the current synthesis routes have different drawbacks. The preparation methods and reaction conditions could have a significant impact on the characteristics of LDHs, which is unfavorable for industrial application. Moreover, some routes are too tedious to achieve large-scale synthesis and some may cause serious pollution. Thus, researchers still have to commit efforts to develop novel synthesis methods which are facile, efficient, economical and eco-friendly. Furthermore, except for exploring optimized design in practical experiments, computational chemistry and artificial intelligence algorithms are also advisable for researchers to confirm the structure and composition of LDHs to design catalysts with higher performance (Roberts et al., 2020).

(2) Combination with other novel materials

Because of the intrinsic drawbacks of single LDHs, the combination of LDHs with other novel materials may become the main trend in the future. We have discussed some LDH-based composites applied in persulfate-AOPs in this review. Actually, there are still various functional materials which deserve further exploration such as CNTs (Li et al., 2015; Ghasemi et al., 2020), MOFs (Ramachandran et al., 2020; Zhang et al., 2021; Wang et al., 2021), covalent organic frameworks (COFs) (Fan et al., 2020; Huang et al., 2021), Mxenes (Shao et al., 2021, 2020b), organic polymers (Guo et al., 2020; Liu et al., 2020), quantum dots (Wu et al., 2020). In the process of developing novel LDH-based composites, catalytic performance should never be the only evaluation principle. On the contrary, the facile fabrication and the potential for industrial applications need to be carefully considered. In fact, synthesis processes of some composites are overly complex and expensive, which makes it hard to apply them in industrial water treatment. Thus, later researches are recommended to design and synthesize LDH-based composites in a systematic mind rather than just focus on the catalytic performance. Some important characteristics including cost, chronic stability, toxicity, recyclability should be important evaluation criteria for novel catalysts.

(3) Deeper exploration of reaction mechanisms

With the rapid development of persulfate-AOPs, illustration of activation mechanism is increasingly important. Besides the familiar free radicals and $^1O_2$. There are some complicated pathways (e.g., surface complex and mediated electron transfer). The reaction pathways in LDH-carbon hybrids are particularly complicated and require further exploration. Notably, the persulfate-AOPs display evident substrate specificity (Lee et al., 2020), which means more organic contaminants should be checked to identify the reaction pathway. Furthermore, there exist both radical-based and nonradical pathways in some LDH-composites/persulfate systems. As generally known, the free radical pathway usually exhibits higher mineralization efficiency toward organic pollutants, while nonradical dominated system displays better resistance to the interference impurities in aqueous solutions. Current studies mainly concentrate on the identification of reaction pathways, but control of these pathways is still difficult. Thus, more innovative and insightful studies should be designed to recognize active species in LDH-composites/persulfate system and find ways to regulate the process of the reaction pathway. Finally, even in one system, there may exist differences in catalytic performance between PMS and PDS, which is worthy of particular concern.

(4) Extension of application fields

Compared with the widespread application in energy, medicine and adsorption of pollutants, the application of LDH-based composites in persulfate-AOPs seems fewer. Meanwhile, contaminants used in many studies are limited to several kinds such as organic dyes, phenols and antibiotics. It is expected that a wider variety of pollutants which are difficult to deal with will be employed in LDH composites/persulfate system. Moreover, present studies mainly focused on treatment of wastewater and contaminants in air and soil are overlooked. Despite a few researchers have made some progress, further efforts are still required to promote the wider application. In addition, to contact with the COVID-19 ranging around the world, the antimicrobial application of LDH-based materials also deserves great concern and exploration (Chen et al., 2012, 2021). Finally, no matter how fancy performance the novel material exhibits in laboratory, it must be examined by complicated conditions in field experiments.

(5) Ecological risk assessment of novel catalysts

With the rise of the concept of “Green Chemistry”, the negative environmental effects caused by the production and application of new catalysts have raised widespread attention (Lowry et al., 2012; Raja et al., 2021; Zhang et al., 2020). Presently, composites with higher catalytic performance usually contain toxic components such as Co/Cu. Besides, some poisonous reagents may be employed in the production process of LDH-based material. Furthermore, the recycle of nanomaterials remains a tricky problem (Peng et al., 2020). Hence, to drive practical application of LDH-based composites, several efforts are indispensable: Firstly, use less or no toxic ingredients in the synthesis process. If these components are necessary, keeping the lowest leaching rate is essential. Secondly, find innocuous substitutes for toxic materials and improve the catalytic performance through tailoring engineering methods. Last but not least, plenty of in vivo and in vitro experiments are needed to assess the potential hazards of new materials to living organisms. Moreover, the migration and transformation of these materials in the natural environment are also worthy of deeper investigations.

## Declaration of Competing Interest

The authors declare that they have no known competing financial interests or personal relationships that could have appeared to influence the work reported in this paper.

## Acknowledgements

The study was financially supported by the National Natural Science Foundation of China (52100181, 51979103, 51679085, 51521006, 51508177), the Program for Changjiang Scholars and Innovative Research Team in University (IRT-13R17), the Project funded by the Project funded by China Postdoctoral Science Foundation (2021T140192, 2021M690054), the Funds of Hunan Science and Technology Innovation Project (2018RS3115, 2020RC5012), the Key Research and Development Project of Hunan Province of China (2017SK2241). The authors also gratefully acknowledge the National Supercomputing Center in Changsha for providing the computing resources.

## References

Ahmad, M., Teel, A.L., Watts, R.J., 2013. Mechanism of persulfate activation by phenols. Environ. Sci. Technol. 47 (11), 5864–5871.

Ahmed, M.M., Chiron, S., 2014. Solar photo-Fenton like using persulphate for carbamazepine removal from domestic wastewater. Water Res. 48, 229–236.

Ahn, Y.-Y., Yun, E.T., Seo, J.W., Lee, C., Kim, S.H., Kim, J.H., Lee, J., 2016. Activation of peroxymonosulfate by surface-loaded noble metal nanoparticles for oxidative degradation of organic compounds. Environ. Sci. Technol. 50 (18), 10187–10197.

Ali, J., Wenli, L., Shahzad, A., Ifthikar, J., Aregay, G.G., Shahib, I.I., Elkhlifi, Z., Chen, Z., Chen, Z., 2020. Regulating the redox centers of Fe through the enrichment of Mo moiety for persulfate activation: a new strategy to achieve maximum persulfate utilization efficiency. Water Res 181, 115862.

Anipsitakis, G.P., Dionysiou, D.D., 2004. Radical generation by the interaction of transition metals with common oxidants. Environ. Sci. Technol. 38 (13), 3705–3712.

Asif, M., Aziz, A., Wang, H., Wang, Z., Wang, W., Ajmal, M., Xiao, F., Chen, X., Liu, H., 2019. Superlattice stacking by hybridizing layered double hydroxide nanosheets with layers of reduced graphene oxide for electrochemical simultaneous determination of dopamine, uric acid and ascorbic acid. Microchim. Acta 186 (2), 61.

Avetta, P., Pensato, A., Minella, M., Malandrino, M., Maurino, V., Minero, C., Hanna, K., Vione, D., 2015. Activation of persulfate by irradiated magnetite: implications for the degradation of phenol under heterogeneous photo-fenton-like conditions. Environ. Sci. Technol. 49 (2), 1043–1050.

Behrman, E.J., 2006. The Elbs and Boyland-Sims peroxydisulfate oxidations. Beilstein J. Org. Chem. 2, 22.

Boccalon, E., Gorrasi, G., Nocchetti, M., 2020. Layered double hydroxides are still out in the bloom: Syntheses, applications and advantages of three-dimensional flower-like structures. Adv. Colloid Interface Sci. 285, 102284.

Brillas, E., Martínez-Huitle, C.A., 2015. Decontamination of wastewaters containing synthetic organic dyes by electrochemical methods. An updated review. Appl. Catal. B: Environ. 166–167, 603–643.

Carwile, J.L., Michels, K.B., 2011. Urinary bisphenol A and obesity: NHANES 2003–2006. Environ. Res. 111 (6), 825–830.

Cheng, X., Guo, H., Zhang, Y., Wu, X., Liu, Y., 2017. Non-photochemical production of singlet oxygen via activation of persulfate by carbon nanotubes. Water Res. 113, 80–88.

Chen, X., Oh, W.-D., Lim, T.-T., 2018. Graphene- and CNTs-based carbocatalysts in persulfates activation: Material design and catalytic mechanisms. Chem. Eng. J. 354, 941–976.

Chen, M., Wu, P., Zhu, N., Dang, Z., Bi, Y., Pei, F., 2020. Re-utilization of spent Cu2+-immobilized MgMn-layered double hydroxide for efficient sulfamethoxazole degradation: Performance and metals synergy. Chem. Eng. J. 392, 123709.

Chen, J., Hong, W., Huang, T., Zhang, L., Li, W., Wang, Y., 2016. Activated carbon fiber for heterogeneous activation of persulfate: implication for the decolorization of azo dye. Environ. Sci. Pollut. Res Int 23 (18), 18564–18574.

Chen, Y., Ouyang, D., Zhang, W., Yan, J., Qian, L., Han, L., Chen, M., 2020. Degradation of benzene derivatives in the CuMgFe-LDO/persulfate system: The role of the interaction between the catalyst and target pollutants. J. Environ. Sci. (China) 90, 87–97.

Chen, C., Gunawan, P., Lou, X.W.D., Xu, R., 2012. Silver nanoparticles deposited layered double hydroxide nanoporous coatings with excellent antimicrobial activities. Adv. Funct. Mater. 22 (4), 780–787.

Chen, Y., Ji, Q., Zhang, G., Liu, H., Qu, J., 2021. Synergetic lipid extraction with oxidative damage amplifies cell-membrane-destructive stresses and enables rapid sterilization. Angew. Chem. Int. Ed. 60 (14), 7744–7751.

Chubar, N., Gilmour, R., Gerda, V., Mičušík, M., Omastova, M., Heister, K., Man, P., Fraissard, J., Zaitsev, V., 2017. Layered double hydroxides as the next generation inorganic anion exchangers: Synthetic methods versus applicability. Adv. Colloid Interface Sci. 245, 62–80.

Costa, F.R., Leuteritz, A., Wagenknecht, U., Jehnichen, D., Häußler, L., Heinrich, G., 2008. Intercalation of Mg–Al layered double hydroxide by anionic surfactants: preparation and characterization. Appl. Clay Sci. 38 (3), 153–164.

Dai, J., Meng, X., Zhang, Y., Huang, Y., 2020. Effects of modification and magnetization of rice straw derived biochar on adsorption of tetracycline from water. Bioresour. Technol. 311, 123455.

Deng, Y., Jiang, Y., Zhao, X., Wang, J., 2019. Recent progress in functionalized layered double hydroxides and their application in efficient electrocatalytic water oxidation. J. Energy Chem. 32, 93–104.

Devi, P., Das, U., Dalai, A.K., 2016. In-situ chemical oxidation: Principle and applications of peroxide and persulfate treatments in wastewater systems. Sci. Total Environ. 571, 643–657.

Ding, S., et al., 2020. Targeted degradation of dimethyl phthalate by activating persulfate using molecularly imprinted Fe-MOF-74. Chemosphere, 128620-128620.

Duan, X., Sun, H., Kang, J., Wang, Y., Indrawirawan, S., Wang, S., 2015a. Insights into heterogeneous catalysis of persulfate activation on dimensional-structured nanocarbons. ACS Catal. 5 (8), 4629–4636.

Duan, X., Sun, H., Ao, Z., Zhou, L., Wang, G., Wang, S., 2016. Unveiling the active sites of graphene-catalyzed peroxymonosulfate activation. Carbon 107, 371–378.

Duan, X., Sun, H., Wang, Y., Kang, J., Wang, S., 2015b. N-doping-induced nonradical reaction on single-walled carbon nanotubes for catalytic phenol oxidation. ACS Catal. 5 (2), 553–559.

Du, Y., Ma, W., Liu, P., Zou, B., Ma, J., 2016. Magnetic CoFe2O4 nanoparticles supported on titanate nanotubes (CoFe2O4/TNTs) as a novel heterogeneous catalyst for peroxymonosulfate activation and degradation of organic pollutants. J. Hazard. Mater. 308, 58–66.

Erickson, K.L., Bostrom, T.E., Frost, R.L., 2005. A study of structural memory effects in synthetic hydrotalcites using environmental SEM. Mater. Lett. 59 (2), 226–229.

Fang, G., Gao, J., Dionysiou, D.D., Liu, C., Zhou, D., 2013. Activation of persulfate by quinones: free radical reactions and implication for the degradation of PCBs. Environ. Sci. Technol. 47 (9), 4605–4611.

Fan, H., Peng, M., Strauss, I., Mundstock, A., Meng, H., Caro, J., 2020. High-flux vertically aligned 2D covalent organic framework membrane with enhanced hydrogen separation. J. Am. Chem. Soc. 142 (15), 6872–6877.

Feng, Y., Liu, J., Wu, D., Zhou, Z., Deng, Y., Zhang, T., Shih, K., 2015. Efficient degradation of sulfamethazine with CuCo2O4 spinel nanocatalysts for peroxymonosulfate activation. Chem. Eng. J. 280, 514–524.

Feng, Y., Wu, D., Deng, Y., Zhang, T., Shih, K., 2016. Sulfate radical-mediated degradation of sulfadiazine by cufeo2 rhombohedral crystal-catalyzed peroxymonosulfate: synergistic effects and mechanisms. Environ. Sci. Technol. 50 (6), 3119–3127.

Ferrari, B., Paxéus, N., Lo Giudice, R., Pollio, A., Garric, J., 2003. Ecotoxicological impact of pharmaceuticals found in treated wastewaters: study of carbamazepine, clofibric acid, and diclofenac. Ecotoxicol. Environ. Saf. 55 (3), 359–370.

Furman, O.S., Teel, A.L., Watts, R.J., 2010. Mechanism of base activation of persulfate. Environ. Sci. Technol. 44 (16), 6423–6428.

Gao, Y., Zhu, Y., Chen, Z., Zeng, Q., Hu, C., 2020. Insights into the difference in metal-free activation of peroxymonosulfate and peroxydisulfate. Chem. Eng. J. 394, 123936.

Ghanbari, K., Moloudi, M., 2016. Flower-like ZnO decorated polyaniline/reduced graphene oxide nanocomposites for simultaneous determination of dopamine and uric acid. Anal. Biochem. 512, 91–102.

Ghanbari, F., Moradi, M., 2017. Application of peroxymonosulfate and its activation methods for degradation of environmental organic pollutants: Review. Chem. Eng. J. 310, 41–62.

Ghasemi, M., Khataee, A., Gholami, P., Soltani, R., Hassani, A., Orooji, Y., 2020. In-situ electro-generation and activation of hydrogen peroxide using a CuFeNLDH-CNTs modified graphite cathode for degradation of cefazolin. J. Environ. Manag. 267, 110629.

Gholami, P., Khataee, A., Soltani, R., Dinpazhoh, L., Bhatnagar, A., 2020. Photocatalytic degradation of gemifloxacin antibiotic using Zn-Co-LDH@biochar nanocomposite. J. Hazard Mater. 382, 121070.

Gillman, G.P., Noble, M.A., Raven, M.D., 2008. Anion substitution of nitrate-saturated layered double hydroxide of Mg and Al. Appl. Clay Sci. 38 (3–4), 179–186.

Goh, K.H., Lim, T.T., Dong, Z., 2008. Application of layered double hydroxides for removal of oxyanions: a review. Water Res 42 (6–7), 1343–1368.

Goldshleger, N.F., 2001. Fullerenes and fullerene-based materials in catalysis. Fuller. Sci. Technol. 9 (3), 255–280.

Gong, C., Chen, F., Yang, Q., Luo, K., Yao, F., Wang, S., Wang, X., Wu, J., Li, X., Wang, D., Zeng, G., 2017. Heterogeneous activation of peroxymonosulfate by Fe-Co layered doubled hydroxide for efficient catalytic degradation of Rhoadmine B. Chem. Eng. J. 321, 222–232.

Gorini, F., Bustaffa, E., Coi, A., Iervasi, G., Bianchi, F., 2020a. Bisphenols as environmental triggers of thyroid dysfunction: clues and evidence. Int. J. Environ. Res. Public Health 17 (8).

Gorini, F., Bustaffa, E., Coi, A., Iervasi, G., Bianchi, F., 2020b. Bisphenols as environmental triggers of thyroid dysfunction: clues and evidence. Int J. Environ. Res Public Health 17 (8).

Green, E.D., Zimmerman, R.C., Ghurabi, W.H., Colohan, D.P., 1979. Phenazopyridine hydrochloride toxicity: a cause of drug-induced methemoglobinemia. J. Am. Coll. Emerg. Physicians 8 (10), 426–431.

Guan, Y.-H., Ma, J., Ren, Y.M., Liu, Y.L., Xiao, J.Y., Lin, L.Q., Zhang, C., 2013. Efficient degradation of atrazine by magnetic porous copper ferrite catalyzed peroxymonosulfate oxidation via the formation of hydroxyl and sulfate radicals. Water Res. 47 (14), 5431–5438.

Guo, Y., Gong, Z., Li, C., Gao, B., 2020. Efficient removal of uranium (VI) by 3D hierarchical Mg/Fe-LDH supported nanoscale hydroxyapatite: A synthetic experimental and mechanism studies. Chem. Eng. J. 392, 123682.

Guo, S., Jiang, Y., Li, L., Huang, X., Zhuang, Z., Yu, Y., 2018. Thin CuOx-based nanosheets for efficient phenol removal benefitting from structural memory and ion exchange of layered double oxides. J. Mater. Chem. A 6 (9), 4167–4178.

Liu, B., Guo, W., Wang, H., Si, Q., Ren, N., et al., 2020. Efficient degradation of sulfamethoxazole by CuCo LDH and LDH@fibers composite membrane activating peroxymonosulfate. Chem. Eng. J. 398, 125676.

Hammoud, D., Gennequin, C., Aboukaïs, A., Aad, E.A., 2015. Steam reforming of methanol over x % Cu/Zn–Al 400 500 based catalysts for production of hydrogen: Preparation by adopting memory effect of hydrotalcite and behavior evaluation. Int. J. Hydrog. Energy 40 (2), 1283–1297.

Hammouda, S.B., Zhao, F., Safaei, Z., Srivastava, V., Lakshmi Ramasamy, D., Iftekhar, S., kalliola, S., Sillanpää, M., 2017. Degradation and mineralization of phenol in aqueous medium by heterogeneous monopersulfate activation on nanostructured cobalt based-perovskite catalysts ACoO3 (A=La, Ba, Sr and Ce): Characterization, kinetics and mechanism study. Appl. Catal. B: Environ. 215, 60–73.

Han, C., Hong, Y.-C., 2016. Bisphenol A, hypertension, and cardiovascular diseases: epidemiological, laboratory, and clinical trial evidence. Curr. Hypertens. Rep. 18 (2), 11.

He, S., Yin, R., Chen, Y., Lai, T., Guo, W., Zeng, L., Zhu, M., 2021. Consolidated 3D Co3Mn-layered double hydroxide aerogel for photo-assisted peroxymonosulfate activation in metronidazole degradation. Chem. Eng. J. 423, 130172.

He, X., de la Cruz, A.A., Dionysiou, D.D., 2013. Destruction of cyanobacterial toxin cylindrospermopsin by hydroxyl radicals and sulfate radicals using UV-254nm activation of hydrogen peroxide, persulfate and peroxymonosulfate. J. Photochem. Photobiol. A: Chem. 251, 160–166.

Hong, Y., Zhou, H., Xiong, Z., Liu, Y., Yao, G., Lai, B., 2020. Heterogeneous activation of peroxymonosulfate by CoMgFe-LDO for degradation of carbamazepine: efficiency, mechanism and degradation pathways. Chem. Eng. J. 391, 123604.

Hong, Y., Peng, J., Zhao, X., Yan, Y., Lai, B., Yao, G., 2019. Efficient degradation of atrazine by CoMgAl layered double oxides catalyzed peroxymonosulfate: optimization, degradation pathways and mechanism. Chem. Eng. J. 370, 354–363.

Hori, H., Nagaoka, Y., Murayama, M., Kutsuna, S., 2008. Efficient decomposition of perfluorocarboxylic acids and alternative fluorochemical surfactants in hot water. Environ. Sci. Technol. 42 (19), 7438–7443.

Hou, L., Li, X., Yang, Q., Chen, F., Wang, S., Ma, Y., Wu, Y., Zhu, X., Huang, X., Wang, D., 2019. Heterogeneous activation of peroxymonosulfate using Mn-Fe layered double hydroxide: Performance and mechanism for organic pollutant degradation. Sci. Total Environ. 663, 453–464.

Huang, S., Peng, H., Tjiu, W.W., Yang, Z., Zhu, H., Tang, T., Liu, T., 2010. Assembling exfoliated layered double hydroxide (ldh) nanosheet/carbon nanotube (CNT) hybrids via electrostatic force and fabricating nylon nanocomposites. J. Phys. Chem. B 114 (50), 16766–16772.

Huang, X., Su, M., Zhou, J., Shu, W., Huang, Z., Gao, N., Qian, G., 2017. Novel activation of persulfate by its intercalation into Mg/Al-layered double hydroxide: Enhancement of non-radical oxidation. Chem. Eng. J. 328, 66–73.

Huang, X., Zhou, X., Han, S., Zhou, J., Qian, G., Gao, N., 2020a. Cycle of Ni(II)-Ni(III)-Ni (II) in Ni-doped layered double hydroxides for activation of intercalated peroxydisulfate. Chem. Eng. J. 386, 123937.

Huang, X., Su, Q., Han, S., Zhou, J., Qian, G., Gao, N., 2020b. Efficient activation of intercalated persulfate via a composite of reduced graphene oxide and layered double hydroxide. J. Hazard. Mater. 389, 122051.

Huang, X., Zhou, X., Su, Q., Zhou, J., Qian, G., Gao, N., Liu, J., 2019. Synergic thermal activation of peroxydisulfate intercalated Mg/Al layered double hydroxide at a low temperature. Chem. Eng. J. 363, 133–140.

Huang, X., Su, Q., Han, S., Zhou, J., Qian, G., Gao, N., 2020c. Efficient activation of intercalated persulfate via a composite of reduced graphene oxide and layered double hydroxide. J. Hazard. Mater. 389, 122051.

Huang, J., Liu, X., Zhang, W., Liu, Z., Zhong, H., Shao, B., Liang, Q., Liu, Y., Zhang, W., He, Q., 2021. Functionalization of covalent organic frameworks by metal modification: Construction, properties and applications. Chem. Eng. J. 404, 127136.

Hu, P., Long, M., 2016. Cobalt-catalyzed sulfate radical-based advanced oxidation: a review on heterogeneous catalysts and applications. Appl. Catal. B: Environ. 181, 103–117.

Hu, Y., Zhou, C., Wang, H., Chen, M., Zeng, G., Liu, Z., Liu, Y., Wang, W., Wu, T., Shao, B., Liang, Q., 2021. Recent advance of graphene/semiconductor composite nanocatalysts: Synthesis, mechanism, applications and perspectives. Chem. Eng. J. 414, 128795.

Inayat, A., Klumpp, M., Schwieger, W., 2011. The urea method for the direct synthesis of ZnAl layered double hydroxides with nitrate as the interlayer anion. Appl. Clay Sci. 51 (4), 452–459.

Jabeen, M., Ishaq, M., Song, W., Xu, L., Deng, Q., 2017. Synthesis of Ni/Co/Al-layered triple hydroxide@brominated graphene hybrid on nickel foam as electrode material for high-performance supercapacitors. RSC Adv. 7 (74), 46553–46565.

Jawad, A., Li, Y., Lu, X., Chen, Z., Liu, W., Yin, G., 2015. Controlled leaching with prolonged activity for Co–LDH supported catalyst during treatment of organic dyes using bicarbonate activation of hydrogen peroxide. J. Hazard. Mater. 289, 165–173.

Jawad, A., Lang, J., Liao, Z., Khan, A., Ifthikar, J., Lv, Z., Long, S., Chen, Z., Chen, Z., 2018. Activation of persulfate by CuOx@Co-LDH: A novel heterogeneous system for contaminant degradation with broad pH window and controlled leaching. Chem. Eng. J. 335, 548–559.

Jelic, A., Cruz-Morató, C., Marco-Urrea, E., Sarrà, M., Perez, S., Vicent, T., Petrović, M., Barcelo, D., 2012. Degradation of carbamazepine by Trametes versicolor in an air pulsed fluidized bed bioreactor and identification of intermediates. Water Res. 46 (4), 955–964.

Jenisha Barnabas, M., Parambadath, S., Ha, C.-S., 2017. Amino modified core–shell mesoporous silica based layered double hydroxide (MS-LDH) for drug delivery. J. Ind. Eng. Chem. 53, 392–403.

Jhaveri, J.H., Murthy, Z.V.P., 2016. A comprehensive review on anti-fouling nanocomposite membranes for pressure driven membrane separation processes. Desalination 379, 137–154.

Jiang, X., Guo, Y., Zhang, L., Jiang, W., Xie, R., 2018. Catalytic degradation of tetracycline hydrochloride by persulfate activated with nano Fe0 immobilized mesoporous carbon. Chem. Eng. J. 341, 392–401.

Jiang, M., Lu, J., Ji, Y., Kong, D., 2017. Bicarbonate-activated persulfate oxidation of acetaminophen. Water Res. 116, 324–331.

Ji, Y., Ferronato, C., Salvador, A., Yang, X., Chovelon, J.M., 2014. Degradation of ciprofloxacin and sulfamethoxazole by ferrous-activated persulfate: Implications for remediation of groundwater contaminated by antibiotics. Sci. Total Environ. 472, 800–808.

Johnson, R.L., Tratnyek, P.G., Johnson, R.O.B., 2008. Persulfate persistence under thermal activation conditions. Environ. Sci. Technol. 42 (24), 9350–9356.

Kagunya, W., Hassan, Z., Jones, W., 1996. Catalytic properties of layered double hydroxides and their calcined derivatives. Inorg. Chem. 35 (21), 5970–5974.

Kaiser, A.B., Skakalova, V., 2011. Electronic conduction in polymers, carbon nanotubes and graphene. Chem. Soc. Rev. 40 (7), 3786–3801.

Ke, J., Liu, J., Sun, H., Zhang, H., Duan, X., Liang, P., Li, X., Tade, M.O., Liu, S., Wang, S., 2017. Facile assembly of Bi2O3/Bi2S3/MoS2 n-p heterojunction with layered n-Bi2O3 and p-MoS2 for enhanced photocatalytic water oxidation and pollutant degradation. Appl. Catal. B: Environ. 200, 47–55.

Khan, A., Wang, H., Liu, Y., Jawad, A., Ifthikar, J., Liao, Z., Wang, T., Chen, Z., 2018. Highly efficient α-Mn2O3@α-MnO2-500 nanocomposite for peroxymonosulfate activation: comprehensive investigation of manganese oxides. J. Mater. Chem. A 6 (4), 1590–1600.

Khataee, A., Rad, T.S., Vahid, B., Khorram, S., 2016. Preparation of zeolite nanorods by corona discharge plasma for degradation of phenazopyridine by heterogeneous sono-Fenton-like process. Ultrason. Sonochem. 33, 37–46.

Kim, S.J., Lee, Y., Lee, D.K., Lee, J.W., Kang, J.K., 2014. Efficient Co–Fe layered double hydroxide photocatalysts for water oxidation under visible light. J. Mater. Chem. A 2 (12), 4136–4139.

Kim, H.-H., Lee, D., Choi, J., Lee, H., Seo, J., Kim, T., Lee, K.M., Pham, A.L., Lee, C., 2020. Nickel–Nickel oxide nanocomposite as a magnetically separable persulfate activator for the nonradical oxidation of organic contaminants. J. Hazard. Mater. 388, 121767.

Lagutschenkov, A., Sinha, R.K., Maitre, P., Dopfer, O., 2010. Structure and Infrared Spectrum of the Ag+−Phenol Ionic Complex. J. Phys. Chem. A 114 (42), 11053–11059.

Lee, J., von Gunten, U., Kim, J.H., 2020. Persulfate-based advanced oxidation: critical assessment of opportunities and roadblocks. Environ. Sci. Technol. 54 (6), 3064–3081.

Lee, H., Kim, H.I., Weon, S., Choi, W., Hwang, Y.S., Seo, J., Lee, C., Kim, J.H., 2016. Activation of persulfates by graphitized nanodiamonds for removal of organic compounds. Environ. Sci. Technol. 50 (18), 10134–10142.

Lei, Y., Chen, C.S., Tu, Y.J., Huang, Y.H., Zhang, H., 2015a. Heterogeneous degradation of organic pollutants by persulfate activated by cuo-fe3o4: mechanism, stability, and effects of pH and bicarbonate Ions. Environ. Sci. Technol. 49 (11), 6838–6845.

Lei, Y., Chen, C.S., Tu, Y.J., Huang, Y.H., Zhang, H., 2015b. Heterogeneous degradation of organic pollutants by persulfate activated by CuO-Fe3O4: mechanism, stability, and effects of pH and bicarbonate ions. Environ. Sci. Technol. 49 (11), 6838–6845.

Li, J., Li, Y., Xiong, Z., Yao, G., Lai, B., 2019. The electrochemical advanced oxidation processes coupling of oxidants for organic pollutants degradation: a mini-review. Chin. Chem. Lett. 30 (12), 2139–2146.

Liang, J., Wei, Y., Yao, Y., Zheng, X., Shen, J., He, G., Chen, H., 2019. Constructing high-efficiency photocatalyst for degrading ciprofloxacin: three-dimensional visible light driven graphene based NiAlFe LDH. J. Colloid Interface Sci. 540, 237–246.

Liang, H., Zhang, Y., Huang, S., Hussain, I., 2013. Oxidative degradation of p-chloroaniline by copper oxidate activated persulfate. Chem. Eng. J. 218, 384–391.

Liang, Q., Shao, B., Tong, S., Liu, Z., Tang, L., Liu, Y., Cheng, M., He, Q., Wu, T., Pan, Y., Huang, J., Peng, Z., 2021a. Recent advances of melamine self-assembled graphitic carbon nitride-based materials: Design, synthesis and application in energy and environment. Chem. Eng. J. 405, 126951.

Liang, Q., Liu, X., Wang, J., Liu, Y., Liu, Z., Tang, L., Shao, B., Zhang, W., Gong, S., Cheng, M., He, Q., Feng, C., 2021b. In-situ self-assembly construction of hollow tubular g-C3N4 isotype heterojunction for enhanced visible-light photocatalysis: Experiments and theories. J. Hazard. Mater. 401, 123355.

Ling, S.K., Wang, S., Peng, Y., 2010. Oxidative degradation of dyes in water using Co2+/H2O2 and Co2+/peroxymonosulfate. J. Hazard. Mater. 178 (1), 385–389.

Liu, Y., Fu, N., Zhang, G., Xu, M., Lu, W., Zhou, L., Huang, H., 2017. Design of Hierarchical Ni□Co@Ni□Co layered double hydroxide core–shell structured nanotube array for high-performance flexible all-solid-state battery-type supercapacitors. Adv. Funct. Mater. 27 (8), 1605307.

Liu, Y., Liu, Y., Shi, H., Wang, M., Cheng, S.H.S., Bian, H., Kamruzzaman, M., Cao, L., Chung, C.Y., Lu, Z., 2016. Cobalt-copper layered double hydroxide nanosheets as high performance bifunctional catalysts for rechargeable lithium-air batteries. J. Alloy. Compd. 688, 380–387.

Li, B., Guo, Z., Cui, Y., Feng, Y., Wu, C., Meng, M., 2021. LDHs-based 3D modular foam with double metal-fluorine interaction for efficiently promoting peroxymonosulfate activation in water pollutant control. Chem. Eng. J. 425, 131541.

Liu, R., Wang, Y., Liu, D., Zou, Y., Wang, S., 2017. Water-plasma-enabled exfoliation of ultrathin layered double hydroxide nanosheets with multivacancies for water oxidation. Adv. Mater. 29 (30), 1701546.

Liu, Z., Jiang, Y., Liu, X., Zeng, G., Shao, B., Liu, Y., Liu, Y., Zhang, W., Zhang, W., Yan, M., He, X., 2019. Silver chromate modified sulfur doped graphitic carbon nitride microrod composites with enhanced visible-light photoactivity towards organic pollutants degradation. Compos. Part B: Eng. 173, 106918.

Liu, Q., et al., 2014. Predicting user likes in online media based on conceptualized social network profiles. Springer International Publishing,, Cham.

Li, W., Wu, P., Yang, S., Zhu, Y., Kang, C., Tran, L.T., Zeng, B., 2015. 3D hierarchical honeycomb structured MWCNTs coupled with CoMnAl–LDO: fabrication and application for ultrafast catalytic degradation of bisphenol A. RSC Adv. 5 (12), 8859–8867.

Liu, D., Li, M., Li, X., Ren, F., Sun, P., Zhou, L., 2020. Core-shell Zn/Co MOFs derived Co3O4/CNTs as an efficient magnetic heterogeneous catalyst for persulfate activation and oxytetracycline degradation. Chem. Eng. J. 387, 124008.

Li, T., Zhao, L., He, Y., Cai, J., Luo, M., Lin, J., 2013. Synthesis of g-C3N4/SmVO4 composite photocatalyst with improved visible light photocatalytic activities in RhB degradation. Appl. Catal. B: Environ. 129, 255–263.

Li, D., Duan, X., Sun, H., Kang, J., Zhang, H., Tade, M.O., Wang, S., 2017. Facile synthesis of nitrogen-doped graphene via low-temperature pyrolysis: the effects of precursors and annealing ambience on metal-free catalytic oxidation. Carbon 115, 649–658.

Liu, L., Wang, Y., Liu, Q., Wang, W., Duan, L., Yang, X., Yi, S., Xue, X., Zhang, J., 2019. Activating peroxydisulfate by morphology-dependent NiO catalysts: structural origin of different catalytic properties. Appl. Catal. B: Environ. 256, 117806.

Liu, Y., Yi, Z., Tan, X., Dong, X.Q., Zhang, X., 2019. Metal or metal-containing nanoparticle@MOF nanocomposites as a promising type of photocatalyst. Coord. Chem. Rev. 388, 63–78.

Long, X., Wang, Z., Xiao, S., An, Y., Yang, S., 2016. Transition metal based layered double hydroxides tailored for energy conversion and storage. Mater. Today 19 (4), 213–226.

Lou, X., Fang, C., Geng, Z., Jin, Y., Xiao, D., Wang, Z., Liu, J., Guo, Y., 2017. Significantly enhanced base activation of peroxymonosulfate by polyphosphates: Kinetics and mechanism. Chemosphere 173, 529–534.

Lowry, G.V., Gregory, K.B., Apte, S.C., Lead, J.R., 2012. Transformations of nanomaterials in the environment. Environ. Sci. Technol. 46 (13), 6893–6899.

Lu, H., Sui, M., Yuan, B., Wang, J., Lv, Y., 2019. Efficient degradation of nitrobenzene by Cu-Co-Fe-LDH catalyzed peroxymonosulfate to produce hydroxyl radicals. Chem. Eng. J. 357, 140–149.

Luo, C., Ma, J., Jiang, J., Liu, Y., Song, Y., Yang, Y., Guan, Y., Wu, D., 2015. Simulation and comparative study on the oxidation kinetics of atrazine by UV/H2O2, UV/HSO5− and UV/S2O82−. Water Res. 80, 99–108.

Lu, X., Xue, H., Gong, H., Bai, M., Tang, D., Ma, R., Sasaki, T., 2020. 2D layered double hydroxide nanosheets and their derivatives toward efficient oxygen evolution reaction. Nano-Micro Lett. 12 (1), 86.

Luo, S., Zeng, Z., Zeng, G., Liu, Z., Xiao, R., Xu, P., Wang, H., Huang, D., Liu, Y., Shao, B., Liang, Q., Wang, D., He, Q., Qin, L., Fu, Y., 2020. Recent advances in conjugated microporous polymers for photocatalysis: designs, applications, and prospects. J. Mater. Chem. A 8 (14), 6434–6470.

Du, Z., Zhang, C., Wang, M., Zhang, X., Ning, J., Lv, X., Zhao, G., Xie, Z., Xu, J., Zhu, S., 2019. 2D layered double hydroxides for oxygen evolution reaction: from fundamental design to application. Adv. Energy Mater. 9 (17), 1803358.

Lyu, L., Zhang, L., Wang, Q., Nie, Y., Hu, C., 2015. Enhanced fenton catalytic efficiency of γ-Cu–Al2O3 by σ-Cu2+–ligand complexes from aromatic pollutant degradation. Environ. Sci. Technol. 49 (14), 8639–8647.

M'Arimi, M.M., Mecha, C.A., Kiprop, A.K., Ramkat, R., 2020. Recent trends in applications of advanced oxidation processes (AOPs) in bioenergy production: review. Renew. Sustain. Energy Rev. 121, 109669.

Ma, L., Wang, Q., Islam, S.M., Liu, Y., Ma, S., Kanatzidis, M.G., 2016. Highly selective and efficient removal of heavy metals by layered double hydroxide intercalated with the MoS4(2-) Ion. J. Am. Chem. Soc. 138 (8), 2858–2866.

Ma, Q., Nengzi, L., Li, B., Wang, Z., Liu, L., Cheng, X., 2020a. Heterogeneously catalyzed persulfate with activated carbon coated with CoFe layered double hydroxide (AC@CoFe-LDH) for the degradation of lomefloxacin. Sep. Purif. Technol. 235, 116204.

Mallakpour, S., Hatami, M., Hussain, C.M., 2020a. Recent innovations in functionalized layered double hydroxides: Fabrication, characterization, and industrial applications. Adv. Colloid Interface Sci. 283, 102216.

Mallakpour, S., Hatami, M., Hussain, C.M., 2020b. Recent innovations in functionalized layered double hydroxides: Fabrication, characterization, and industrial applications. Adv. Colloid Interface Sci. 283, 102216.

Mallakpour, S., Hatami, M., Hussain, C.M., 2020c. Recent innovations in functionalized layered double hydroxides: Fabrication, characterization, and industrial applications. Adv. Colloid Interface Sci. 283, 102216.

Ma, Y., Chen, F., Yang, Q., Zhong, Y., Shu, X., Yao, F., Xie, T., Li, X., Wang, D., Zeng, G., 2018a. Sulfate radical induced degradation of Methyl Violet azo dye with CuFe layered doubled hydroxide as heterogeneous photoactivator of persulfate. J. Environ. Manag. 227, 406–414.

Mamba, G., Mishra, A.K., 2016. Graphitic carbon nitride (g-C 3 N 4) nanocomposites: a new and exciting generation of visible light driven photocatalysts for environmental pollution remediation. Appl. Catal. B: Environ. 198, 347–377.

Martínez-Huitle, C.A., Brillas, E., 2009. Decontamination of wastewaters containing synthetic organic dyes by electrochemical methods: A general review. Appl. Catal. B: Environ. 87 (3–4), 105–145.

Matzek, L.W., Carter, K.E., 2016. Activated persulfate for organic chemical degradation: a review. Chemosphere 151, 178–188.

Ma, Y., Chen, F., Yang, Q., Zhong, Y., Shu, X., Yao, F., Xie, T., Li, X., Wang, D., Zeng, G., 2018b. Sulfate radical induced degradation of methyl violet azo dye with CuFe layered doubled hydroxide as heterogeneous photoactivator of persulfate. J. Environ. Manag. 227, 406–414.

Ma, Q., Nengzi, L., Zhang, X., Zhao, Z., Cheng, X., 2020b. Enhanced activation of persulfate by AC@CoFe2O4 nanocomposites for effective removal of lomefloxacin. Sep. Purif. Technol. 233, 115978.

Ma, W., Wang, N., Du, Y., Tong, T., Zhang, L., Andrew Lin, K.Y., Han, X., 2019. One-step synthesis of novel Fe3C@nitrogen-doped carbon nanotubes/graphene nanosheets for catalytic degradation of Bisphenol A in the presence of peroxymonosulfate. Chem. Eng. J. 356, 1022–1031.

Ma, W., Ma, R., Wang, C., Liang, J., Liu, X., Zhou, K., Sasaki, T., 2015. A Superlattice of alternately stacked Ni–Fe hydroxide nanosheets and graphene for efficient splitting of water. ACS Nano 9 (2), 1977–1984.

Mínguez-Alarcón, L., Hauser, R., Gaskins, A.J., 2016. Effects of bisphenol A on male and couple reproductive health: a review. Fertil. Steril. 106 (4), 864–870.

Mishra, G., Dash, B., Pandey, S., 2018. Layered double hydroxides: A brief review from fundamentals to application as evolving biomaterials. Appl. Clay Sci. 153, 172–186.

Mohapatra, L., Parida, K., 2016. A review on the recent progress, challenges and perspective of layered double hydroxides as promising photocatalysts. J. Mater. Chem. A 4 (28), 10744–10766.

Monteagudo, J.M., Durán, A., San Martín, I., Carrillo, P., 2019. Effect of sodium persulfate as electron acceptor on antipyrine degradation by solar TiO2 or TiO2/rGO photocatalysis. Chem. Eng. J. 364, 257–268.

Motlagh, P.Y., Khataee, A., Hassani, A., Sadeghi Rad, T., 2020. ZnFe-LDH/GO nanocomposite coated on the glass support as a highly efficient catalyst for visible light photodegradation of an emerging pollutant. J. Mol. Liq. 302, 112532.

Moztahida, M., Jang, J., Nawaz, M., Lim, S.R., Lee, D.S., 2019. Effect of rGO loading on Fe3O4: a visible light assisted catalyst material for carbamazepine degradation. Sci. Total Environ. 667, 741–750.

Nagendra, B., Rosely, C., Leuteritz, A., Reuter, U., Gowd, E.B., 2017. Polypropylene/layered double hydroxide nanocomposites: influence of LDH intralayer metal constituents on the properties of polypropylene. ACS Omega 2 (1), 20–31.

Nakamura, R., Okamoto, A., Osawa, H., Irie, H., Hashimoto, K., 2007. Design of all-inorganic molecular-based photocatalysts sensitive to visible light: Ti(IV)−O−Ce(III) bimetallic assemblies on mesoporous silica. J. Am. Chem. Soc. 129 (31), 9596–9597.

Oh, W.-D., Dong, Z., Lim, T.-T., 2016. Generation of sulfate radical through heterogeneous catalysis for organic contaminants removal: Current development, challenges and prospects. Appl. Catal. B: Environ. 194, 169–201.

Oostinga, J.B., Heersche, H.B., Liu, X., Morpurgo, A.F., Vandersypen, L.M., 2008. Gate-induced insulating state in bilayer graphene devices. Nat. Mater. 7 (2), 151–157.

Pan, Y., Liu, X., Zhang, W., Liu, Z., Zeng, G., Shao, B., Liang, Q., He, Q., Yuan, X., Huang, D., Chen, M., 2020. Advances in photocatalysis based on fullerene C60 and its derivatives: properties, mechanism, synthesis, and applications. Appl. Catal. B: Environ. 265, 118579.

Paredes, S.P., Valenzuela, M.A., Fetter, G., Flores, S.O., 2011. TiO2/MgAl layered double hydroxides mechanical mixtures as efficient photocatalysts in phenol degradation. J. Phys. Chem. Solids 72 (8), 914–919.

Peng, Z., Liu, X., Zhang, W., Zeng, Z., Liu, Z., Zhang, C., Liu, Y., Shao, B., Liang, Q., Tang, W., Yuan, X., 2020. Advances in the application, toxicity and degradation of carbon nanomaterials in environment: a review. Environ. Int 134, 105298.

Qin, F., Peng, Y., Song, G., Fang, Q., Wang, R., Zhang, C., Zeng, G., Huang, D., Lai, C., Zhou, Y., Tan, X., Cheng, M., Liu, S., 2020. Degradation of sulfamethazine by biochar-supported bimetallic oxide/persulfate system in natural water: Performance and reaction mechanism. J. Hazard. Mater. 398, 122816.

Qi, C., Liu, X., Lin, C., Zhang, X., Ma, J., Tan, H., Ye, W., 2014. Degradation of sulfamethoxazole by microwave-activated persulfate: Kinetics, mechanism and acute toxicity. Chem. Eng. J. 249, 6–14.

Rajamathi, M., Nataraja, G.D., Ananthamurthy, S., Kamath, P.V., 2000. Reversible thermal behavior of the layered double hydroxide of Mg with Al: mechanistic studies. J. Mater. Chem. 10 (12), 2754-2753.

Raja, I.S., Lee, J.H., Hong, S.W., Shin, D.M., Lee, J.H., Han, D.W., 2021. A critical review on genotoxicity potential of low dimensional nanomaterials. J. Hazard. Mater. 409, 124915.

Ramachandran, R., Thangavel, S., Minzhang, Li, Haiquan, S., Zong-Xiang, Xu, Wang, F., 2020. Efficient degradation of organic dye using Ni-MOF derived NiCo-LDH as peroxymonosulfate activator. Chemosphere 271, 128509.

Rastogi, A., Al-Abed, S.R., Dionysiou, D.D., 2009. Sulfate radical-based ferrous–peroxymonosulfate oxidative system for PCBs degradation in aqueous and sediment systems. Appl. Catal. B: Environ. 85 (3), 171–179.

Ren, Y., Lin, L., Ma, J., Yang, J., Feng, J., Fan, Z., 2015. Sulfate radicals induced from peroxymonosulfate by magnetic ferrospinel MFe2O4 (M = Co, Cu, Mn, and Zn) as heterogeneous catalysts in the water. Appl. Catal. B: Environ. 165, 572–578.

Rives, V., del Arco, M., Martín, C., 2014. Intercalation of drugs in layered double hydroxides and their controlled release: A review. Appl. Clay Sci. 88–89, 239–269.

Roberts, J., Song, Y., Crocker, M., Risko, C., 2020. A genetic algorithmic approach to determine the structure of Li-Al layered double hydroxides. J. Chem. Inf. Model 60 (10), 4845–4855.

Saputra, E., Muhammad, S., Sun, H., Wang, S., 2013. Activated carbons as green and effective catalysts for generation of reactive radicals in degradation of aqueous phenol. RSC Adv. 3 (44), 21905–21910.

Shahabadi, N., Razlansari, M., Zhaleh, H., Mansouri, K., 2019. Antiproliferative effects of new magnetic pH-responsive drug delivery system composed of Fe3O4, CaAl layered double hydroxide and levodopa on melanoma cancer cells. Mater. Sci. Eng.: C. 101, 472–486.

Shahzad, A., Jawad, A., Ifthikar, J., Chen, Z., Chen, Z., 2019. The hetero-assembly of reduced graphene oxide and hydroxide nanosheets as superlattice materials in PMS activation. Carbon 155, 740–755.

Shahzad, A., Ali, J., Ifthikar, J., Aregay, G.G., Zhu, J., Chen, Z., Chen, Z., 2020. Non-radical PMS activation by the nanohybrid material with periodic confinement of reduced graphene oxide (rGO) and Cu hydroxides. J. Hazard Mater. 392, 122316.

Shah, N.S., Ali Khan, J., Sayed, M., Ul Haq Khan, Z., Sajid Ali, H., Murtaza, B., Khan, H. M., Imran, M., Muhammad, N., 2019. Hydroxyl and sulfate radical mediated degradation of ciprofloxacin using nano zerovalent manganese catalyzed S2O82−. Chem. Eng. J. 356, 199–209.

Shao, B., Wang, J., Liu, Z., Zeng, G., Tang, L., Liang, Q., He, Q., Wu, T., Liu, Y., Yuan, X., 2020a. Ti3C2Tx MXene decorated black phosphorus nanosheets with improved visible-light photocatalytic activity: experimental and theoretical studies. J. Mater. Chem. A 8 (10), 5171–5185.

Shao, B., Liu, Z., Zeng, G., Liu, Y., Liang, Q., He, Q., Wu, T., Pan, Y., Huang, J., Peng, Z., Luo, S., Liang, C., Liu, X., Tong, S., Liang, J., 2021. Synthesis of 2D/2D CoAl-LDHs/Ti3C2Tx Schottky-junction with enhanced interfacial charge transfer and visible-light photocatalytic performance. Appl. Catal. B: Environ. 286, 119867.

Shao, B., Liu, Z., Zeng, G., Wang, H., Liang, Q., He, Q., Cheng, M., Zhou, C., Jiang, L., Song, B., 2020b. Two-dimensional transition metal carbide and nitride (MXene) derived quantum dots (QDs): synthesis, properties, applications and prospects. J. Mater. Chem. A 8 (16), 7508–7535.

Singh, R., Singh, A.P., Kumar, S., Giri, B.S., Kim, K.H., 2019. Antibiotic resistance in major rivers in the world: a systematic review on occurrence, emergence, and management strategies. J. Clean. Prod. 234, 1484–1505.

Song, F., Hu, X., 2014. Exfoliation of layered double hydroxides for enhanced oxygen evolution catalysis. Nat. Commun. 5 (1), 4477.

Sun, W., Zhang, H., Lin, J., 2014. Surface Modification of Bi2O3 with Fe(III) Clusters toward efficient photocatalysis in a broader visible light region: implications of the interfacial charge transfer. J. Phys. Chem. C. 118 (31), 17626–17632.

Sun, H., Liu, S., Zhou, G., Ang, H.M., Tadé, M.O., Wang, S., 2012a. Reduced graphene oxide for catalytic oxidation of aqueous organic pollutants. ACS Appl. Mater. Interfaces 4 (10), 5466–5471.

Su, S., Cao, C., Zhao, Y., Dionysiou, D.D., 2019. Efficient transformation and elimination of roxarsone and its metabolites by a new α-FeOOH@GCA activating persulfate system under UV irradiation with subsequent As(V) recovery. Appl. Catal. B: Environ. 245, 207–219.

Sun, H., Kwan, C., Suvorova, A., Ang, H.M., Tadé, M.O., Wang, S., 2014. Catalytic oxidation of organic pollutants on pristine and surface nitrogen-modified carbon nanotubes with sulfate radicals. Appl. Catal. B: Environ. 154–155, 134–141.

Sun, H., Liu, S., Zhou, G., Ang, H.M., Tadé, M.O., Wang, S., 2012b. Reduced graphene oxide for catalytic oxidation of aqueous organic pollutants. ACS Appl. Mater. Interfaces 4 (10), 5466–5471.

Valente, J.S., Rodriguez-Gattorno, G., Valle-Orta, M., Torres-Garcia, E., 2012. Thermal decomposition kinetics of MgAl layered double hydroxides. Mater. Chem. Phys. 133 (2), 621–629.

Wang, J., Liu, H., Ma, D., Wang, Y., Yao, G., Yue, Q., Gao, B., Wang, S., Xu, X., 2021. Degradation of organic pollutants by ultraviolet/ozone in high salinity condition: Non-radical pathway dominated by singlet oxygen. Chemosphere 268, 128796.

Wang, Q., O'Hare, D., 2012. Recent advances in the synthesis and application of layered double hydroxide (LDH) nanosheets. Chem. Rev. 112 (7), 4124–4155.

Wang, J., Wang, S., 2018. Activation of persulfate (PS) and peroxymonosulfate (PMS) and application for the degradation of emerging contaminants. Chem. Eng. J. 334, 1502–1517.

Wan, H., Chen, F., Ma, W., Liu, X., Ma, R., 2020. Advanced electrocatalysts based on two-dimensional transition metal hydroxides and their composites for alkaline oxygen reduction reaction. Nanoscale 12 (42), 21479–21496.

Wang, Z., Yu, H., Ma, K., Chen, Y., Zhang, X., Wang, T., Li, S., Zhu, X., Wang, X., 2018. Flower-like surface of three-metal-component layered double hydroxide composites for improved antibacterial activity of lysozyme. Bioconjugate Chem. 29 (6), 2090–2099.

Wang, J., Tang, L., Somasundaran, P., Fan, W., Zeng, G., Deng, Y., Zhou, Y., Wang, J., Shen, Y., 2017. Highly effective antibacterial activity by the synergistic effect of three dimensional ordered mesoporous carbon-lysozyme composite. J. Colloid Interface Sci. 503, 131–141.

Wang, W., Yan, H., Anand, U., Mirsaidov, U., 2021. Visualizing the conversion of metal–organic framework nanoparticles into hollow layered double hydroxide nanocages. J. Am. Chem. Soc. 143 (4), 1854–1862.

Welshons, W.V., Nagel, S.C., vom Saal, F.S., 2006. Large effects from small exposures. iii. endocrine mechanisms mediating effects of bisphenol a at levels of human exposure. Endocrinology 147 (6), s56–s69.

White, R.J., Budarin, V., Luque, R., Clark, J.H., Macquarrie, D.J., 2009. Tuneable porous carbonaceous materials from renewable resources. Chem. Soc. Rev. 38 (12), 3401–3418.

Wu, X., Luo, B., Chen, F., Yang, F., 2018. Heterogeneous Fenton degradation of azo dye 4BS over Co–Mn–Fe ternary hydrotalcites. Chem. Pap. 72 (10), 2433–2441.

Wu, L., Hong, J., Zhang, Q., Chen, B.Y., Wang, J., Dong, Z., 2020a. Deciphering highly resistant characteristics to different pHs of oxygen vacancy-rich Fe2Co1-LDH/PS system for bisphenol A degradation. Chem. Eng. J. 385, 123620.

Wu, L., Hong, J., Zhang, Q., Chen, B.Y., Wang, J., Dong, Z., 2020b. Deciphering highly resistant characteristics to different pHs of oxygen vacancy-rich Fe2Co1-LDH/PS system for bisphenol A degradation. Chem. Eng. J. 385, 123620.

Wu, T., Liu, X., Liu, Y., Cheng, M., Liu, Z., Zeng, G., Shao, B., Liang, Q., Zhang, W., He, Q., Zhang, W., 2020. Application of QD-MOF composites for photocatalysis: Energy production and environmental remediation. Coord. Chem. Rev. 403, 213097.

Xiao, X., Chen, B., Chen, Z., Zhu, L., Schnoor, J.L., 2018. Insight into multiple and multilevel structures of biochars and their potential environmental applications: a critical review. Environ. Sci. Technol. 52 (9), 5027–5047.

Yan, J., Chen, Y., Qian, L., Gao, W., Ouyang, D., Chen, M., 2017. Heterogeneously catalyzed persulfate with a CuMgFe layered double hydroxide for the degradation of ethylbenzene. J. Hazard. Mater. 338, 372–380.

Yang, C., Zhang, G., Meng, Y., Pan, G., Ni, Z., Xia, S., 2021. Direct Z-scheme CeO2@LDH core–shell heterostructure for photodegradation of Rhodamine B by synergistic persulfate activation. J. Hazard. Mater. 408, 124908.

Yang, X., et al., 2021. Recent advances in photodegradation of antibiotic residues in water. In: Chemical engineering journal (Lausanne, Switzerland: 1996), 405, 126806-126806.

Yang, S., Yang, X., Shao, X., Niu, R., Wang, L., 2011. Activated carbon catalyzed persulfate oxidation of Azo dye acid orange 7 at ambient temperature. J. Hazard. Mater. 186 (1), 659–666.

Yang, S., Wang, P., Yang, X., Shan, L., Zhang, W., Shao, X., Niu, R., 2010. Degradation efficiencies of azo dye Acid Orange 7 by the interaction of heat, UV and anions with common oxidants: Persulfate, peroxymonosulfate and hydrogen peroxide. J. Hazard. Mater. 179 (1), 552–558.

Yin, R., Guo, W., Wang, H., Du, J., Wu, Q., Chang, J.S., Ren, N., 2019. Singlet oxygen-dominated peroxydisulfate activation by sludge-derived biochar for sulfamethoxazole degradation through a nonradical oxidation pathway: Performance and mechanism. Chem. Eng. J. 357, 589–599.

You, Y., Shi, Z., Li, Y., Zhao, Z., He, B., Cheng, X., 2021. Magnetic cobalt ferrite biochar composite as peroxymonosulfate activator for removal of lomefloxacin hydrochloride. Sep. Purif. Technol. 272, 118889.

Yu, I.K.M., Hanif, A., Tsang, D.C.W., Shang, J., Su, Z., Song, H., Ok, Y.S., Poon, C.S., 2020. Tuneable functionalities in layered double hydroxide catalysts for thermochemical conversion of biomass-derived glucose to fructose. Chem. Eng. J. 383, 122914.

Yue, D., Yan, X., Guo, C., Qian, X., Zhao, Y., 2020. NiFe layered double hydroxide (LDH) nanosheet catalysts with Fe as electron transfer mediator for enhanced persulfate activation. J. Phys. Chem. Lett. 11 (3), 968–973.

Yu, J., Wang, Q., O'Hare, D., Sun, L., 2017. Preparation of two dimensional layered double hydroxide nanosheets and their applications. Chem. Soc. Rev. 46 (19), 5950–5974.

Ren, N., Feng, Z., Liang, N., Xie, J., Wang, A., Sun, C., Yu, X., 2020. Metal-free carbon materials for persulfate-based advanced oxidation process: microstructure, property and tailoring. Prog. Mater. Sci. 111, 100654.

Yue, D., Qian, X., Ren, M., Fang, M., Jia, J., Zhao, Y., 2018. Secondary battery inspired α-nickel hydroxide as an efficient Ni-based heterogeneous catalyst for sulfate radical activation. Sci. Bull. 63 (5), 278–281.

Yun, E.-T., Lee, J.H., Kim, J., Park, H.D., Lee, J., 2018. Identifying the nonradical mechanism in the peroxymonosulfate activation process: singlet oxygenation versus mediated electron transfer. Environ. Sci. Technol. 52 (12), 7032–7042.

Zeng, H., Zhang, W., Deng, L., Luo, J., Zhou, S., Liu, X., Pei, Y., Shi, Z., Crittenden, J., 2018. Degradation of dyes by peroxymonosulfate activated by ternary CoFeNi-layered double hydroxide: Catalytic performance, mechanism and kinetic modeling. J. Colloid Interface Sci. 515, 92–100.

Zeng, H., Zhang, H., Deng, L., Shi, Z., 2020. Peroxymonosulfate-assisted photocatalytic degradation of sulfadiazine using self-assembled multi-layered CoAl-LDH/g-C3N4 heterostructures: Performance, mechanism and eco-toxicity evaluation. J. Water Process Eng. 33, 101084.

Zhang, Y., Zhang, J., Xiao, Y., Chang, V.W.C., Lim, T.T., 2016. Kinetic and mechanistic investigation of azathioprine degradation in water by UV, UV/H2O2 and UV/persulfate. Chem. Eng. J. 302, 526–534.

Zhang, T., Zhu, H., Croué, J.-P., 2013. Production of sulfate radical from peroxymonosulfate induced by a magnetically separable CuFe2O4 spinel in water: efficiency, stability, and mechanism. Environ. Sci. Technol. 47 (6), 2784–2791.

Zhang, H., Nengzi, L.C., Wang, Z., Zhang, X., Li, B., Cheng, X., 2020. Construction of Bi2O3/CuNiFe LDHs composite and its enhanced photocatalytic degradation of lomefloxacin with persulfate under simulated sunlight. J. Hazard Mater. 383, 121236.

Zhang, H., 2015. Ultrathin Two-Dimensional Nanomaterials. ACS Nano 9 (10), 9451–9469.

Gao, J., Liu, M., Song, H., Zhang, S., Qian, Y., Li, A., 2016. High-performance hybrid supercapacitor with 3D hierarchical porous flower-like layered double hydroxide grown on nickel foam as binder-free electrode. J. Power Sources 318, 76–85.

Zhang, Q., Peng, W., Li, Y., Zhang, F., Fan, X., 2020. Topochemical synthesis of low-dimensional nanomaterials. Nanoscale 12 (43), 21971–21987.

Zhang, T., Chen, Y., Wang, Y., Le Roux, J., Yang, Y., Croué, J.P., 2014. Efficient Peroxydisulfate Activation Process Not Relying on Sulfate Radical Generation for Water Pollutant Degradation. Environ. Sci. Technol. 48 (10), 5868–5875.

Zhang, W.-D., Hu, Q.T., Wang, L.L., Gao, J., Zhu, H.Y., Yan, X., Gu, Z.G., 2021. In-situ generated Ni-MOF/LDH heterostructures with abundant phase interfaces for enhanced oxygen evolution reaction. Appl. Catal. B: Environ. 286, 119906.

Zhang, W., Zeng, Z., Liu, Z., Huang, J., Xiao, R., Shao, B., Liu, Y., Liu, Y., Tang, W., Zeng, G., Gong, J., He, Q., 2020. Effects of carbon nanotubes on biodegradation of pollutants: Positive or negative? Ecotoxicol. Environ. Saf. 189, 109914.

Zhao, G., Wen, T., Chen, C., Wang, X., 2012. Synthesis of graphene-based nanomaterials and their application in energy-related and environmental-related areas. RSC Adv. 2 (25), 9286–9303.

Zhiyong, Y., Wenhua, W., Lin, S., Liqin, L., Zhiyin, W., Xuanfeng, J., Chaonan, D., Ruiying, Q., 2013. Acceleration comparison between Fe2+/H2O2 and Co2+/oxone for decolouration of azo dyes in homogeneous systems. Chem. Eng. J. 234, 475–483.

Zhou, Z., Liu, X., Sun, K., Lin, C., Ma, J., He, M., Ouyang, W., 2019. Persulfate-based advanced oxidation processes (AOPs) for organic-contaminated soil remediation: A review. Chem. Eng. J. 372, 836–851.

Zhou, X., Luo, C., Luo, M., Wang, Q., Wang, J., Liao, Z., Chen, Z., Chen, Z., 2020. Understanding the synergetic effect from foreign metals in bimetallic oxides for PMS activation: A common strategy to increase the stoichiometric efficiency of oxidants. Chem. Eng. J. 381, 122587.

Zhou, Y., Jiang, J., Gao, Y., Ma, J., Pang, S.Y., Li, J., Lu, X.T., Yuan, L.P., 2015. Activation of peroxymonosulfate by benzoquinone: a novel nonradical oxidation process. Environ. Sci. Technol. 49 (21), 12941–12950.

Zhu, S., Li, X., Kang, J., Duan, X., Wang, S., 2019. Persulfate activation on crystallographic manganese oxides: mechanism of singlet oxygen evolution for nonradical selective degradation of aqueous contaminants. Environ. Sci. Technol. 53 (1), 307–315.

Zhu, W., Ford, W.T., 1991. Oxidation of alkenes with aqueous potassium peroxymonosulfate and no organic solvent. J. Org. Chem. 56 (25), 7022–7026.

Zou, Y., Wang, X., Chen, Z., Yao, W., Ai, Y., Liu, Y., Hayat, T., Alsaedi, A., Alharbi, N.S., Wang, X., 2016. Superior coagulation of graphene oxides on nanoscale layered double hydroxides and layered double oxides. Environ. Pollut. 219, 107–117.

Zou, Y., Wang, X., Wu, F., Yu, S., Hu, Y., Song, W., Liu, Y., Wang, H., Hayat, T., Wang, X., 2017. Controllable synthesis of Ca-Mg-Al layered double hydroxides and calcined layered double oxides for the efficient removal of U(VI) from wastewater solutions. ACS Sustain. Chem. Eng. 5 (1), 1173–1185.

Zubair, M., Ihsanullah, I., Abdul Aziz, H., Azmier Ahmad, M., Al-Harthi, M.A., 2021. Sustainable wastewater treatment by biochar/layered double hydroxide composites: progress, challenges, and outlook. Bioresour. Technol. 319, 124128.